# Fusion Ignition Research Experiment
-FIRE-
Engineering Status Report
For Fiscal Year 2000

Issued October, 2000
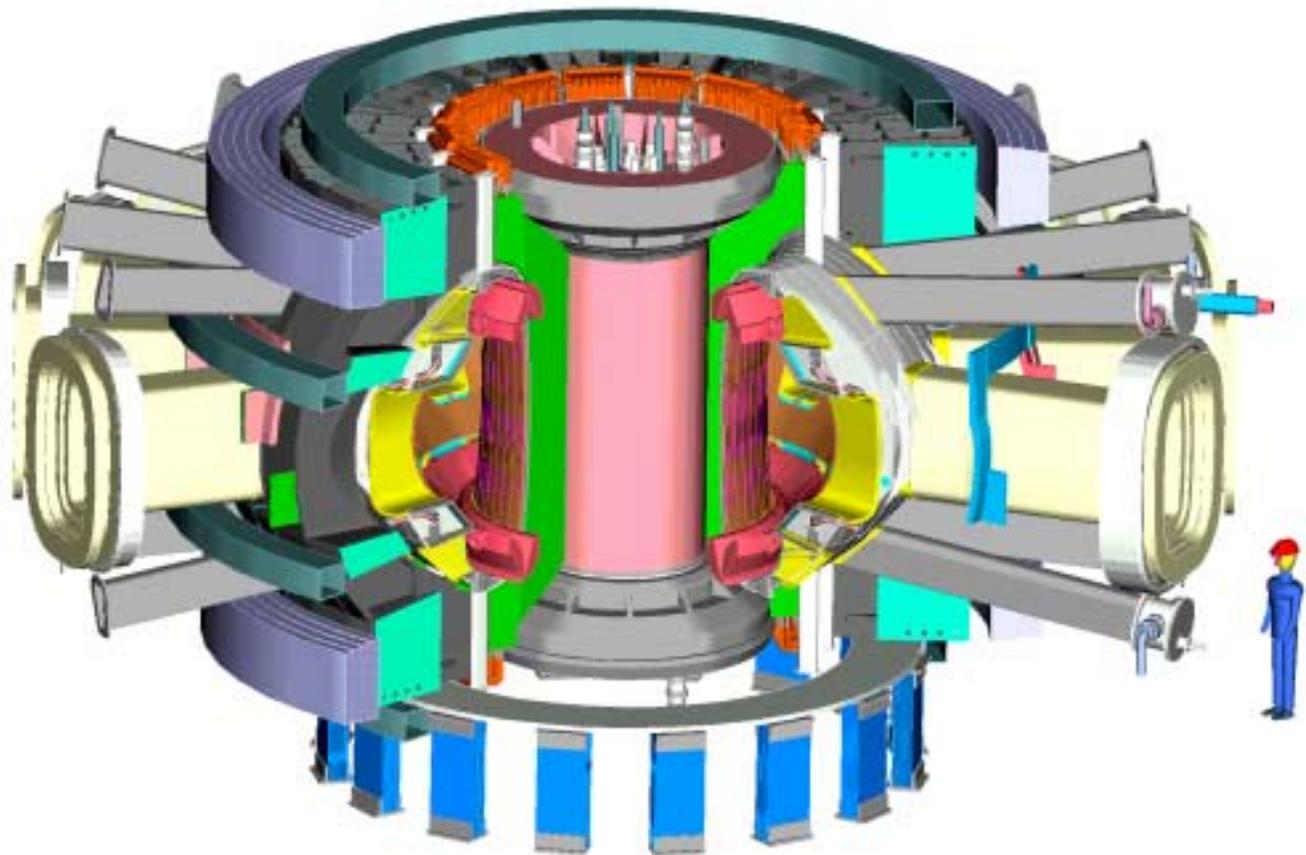
Contributors:
T. Brown, R. Ellis, H.M. Fan, P. Heitzenroeder, C. Kessel, D. Meade, J. Schmidt, R. Woolley, K. Young, I. Zatz **(PPPL)**
J. Schultz, R. Thome, P. Titus **(MIT)**
T. Burgess, B. Nelson, D. Swain, M. Gouge, G. Johnson **(ORNL)**
R. Bulmer **(LLNL);** M. Ulrickson **(SNL)**
H. Khater, M. Sawan **(UW);** D. Petti, B. Merrill , L. Cadwallader **(INEL);**
D. Dilling **(Consultant);** D. Driemeyer, F. Cole, L. Waganer **(Boeing)**
C. Baxi, J. Wesley **(GAT);** V. Christina, E. Peterson, F. Tepes A. Berger, J. Rathke **(AES)**

Foreword

A study of Next Step Options (NSO) for the US DOE Fusion Sciences Program has been organized as a national, integrated design activity, led by the Princeton Plasma Physics Laboratory for the Virtual Laboratory for Technology. The effort has focused on the Fusion Ignition Research Experiment (FIRE), a tokamak designed for burning plasma research. Engineering reports were prepared for the FY99 and FY00 activities and may be found on the website at http://fire.pppl.gov. This document is the FY00 Engineering Report.

Engineering analyses performed in FY00 demonstrated that the design proposed for FIRE has operational capabilities well beyond the basic goals adopted at the beginning of the study in FY99. Consequently, the physics requirements were refined in March,'00 to exploit these capabilities and expand the breadth and depth of the FIRE physics mission. The original goal of FIRE was to be capable of 10s pulses at 10T and I_p=6.44 MA to permit the study of burning plasmas (i.e., self heating, fast particle stability, etc.). The design has evolved such that it is capable of 18s pulses, which improves the experimental flexibility and data yield in a pulse, in addition to permitting the demonstration of "quasi steady state" plasma burns (ie, $\tau_{burn} \gg 15\ \tau_{E,}$ $2-3\ \tau_{He}$) and ~ 1.5 τ_{skin}. In addition to operating in high field, burning plasma modes, FIRE could operate in a "TPX-like mode" at 4T with pulse lengths of ~200 s and I_p=5 MA, as well as in an advanced tokamak, burning plasma mode at 8T with pulse lengths of ~46 s and I_p=5 MA.

A draft cost estimate was completed and indicated that a total project cost goal for FIRE in the range of $1B is reasonable. Work is continuing to refine the FIRE cost estimate and an update of the cost estimate will be available early in FY 2001.

The FIRE web site (http://FIRE.pppl.gov) was initiated in July, '99 and was expanded during FY '00. It has proven to be an excellent method for providing information to project participants and others interested in FIRE. It contains information on fusion program news, FIRE physics and engineering, international collaborations, FIRE reports, Snowmass and NSO-PAC meetings, as well as general fusion information. It has had more than 11,000 visitors from all areas of the world. The FIRE web site has been chosen as a selection for the Scout Report for Science and Engineering, the premier biweekly collection of useful Internet sites for researchers, educators, and students in the life sciences, physical sciences, and engineering.

FIRE has a very proactive outreach program, with one of its major goals to solicit comments and suggestions from the fusion community. Presentations have been made and comments received from:

- University of Wisconsin – Oct., 99
- SOFE – Oct., 99
- VLT-PAC – Dec., 99
- U. of Maryland – Dec., 99
- Harvey Mudd - Jan., 00
- ORNL – Feb., 00
- U. of Hawaii - Feb., 00
- U. of Georgia - March, 00
- Naval Post Grad School - March, 00
- EPS-Budapest – June, 00
- CEA, Cadarache – June, 00
- NYU – Oct., 99

- FPA – Oct., 99
- APS-DPP - Nov., 99
- DOE/OFES – Dec., 99
- Dartmouth – Jan., 00
- FESAC – Feb., 00
- Northwestern – Feb., 00
- Georgia Tech. – March, 00
- PPPL – March, 00
- U. of Wisconsin – March/April 00
- IPP/Garching – June, 00
- JET-EFDA – June, 00

FIRE Publications in FY 2000

Oral Presentations:

Meade, D.M.; "Fusion Ignition Research Experiment (FIRE): A Next Step Option for MFE." (Plenary presentation)

Thome, R. J. for the FIRE Design Team; "Engineering Overview of the Fusion Ignition Research Experiment (FIRE)."

Schultz, J.H.; "Parametric Design Studies of the FIRE/NSO."

Brown, T.; "Fusion Ignition Research Experiment System Integration."

Kessel, C.E. and Bulmer, R.H.; "Poloidal Field Design and Plasma Scenarios for FIRE."

Poster Presentations:

Heitzenroeder, P. for the FIRE Design Team; "Development of a Cost-Effective Design for the Fusion Ignition Research Experiment."

Titus, P.; "FIRE/NSO Toroidal Field Coil Structural/Thermal Analysis."

Woolley, R.; "PF and TF Power Systems for the Fusion Ignition Research Experiment (FIRE)."

Nelson, B., et al; "Fusion Ignition Research Experiment Vacuum Vessel Design and Configuration."

Fisher, P. W., et al; "Plasma Fueling, Pumping, and Tritium Handling Considerations for FIRE."

Swain, D.W., et al; "Plasma Heating and Current Drive Systems for the Fusion Ignition Research Experiment (FIRE)."

Sawan, M.E. and Khater, H.Y; "Initial Nuclear Performance Evaluation of the FIRE Ignition Device."

Khater, H.Y. and Sawan, M.E.; "Preliminary Radiological Assessment of the Fusion Ignition Research Experiment (FIRE)."

Petti, D. and Merril, B.; "Safety and Environmental Considerations in the Design of the Fusion Ignition Research Experiment."

Burgess, T., et al; "Remote Maintenance Requirements and Approach for the FIRE Project."

Dilling, D.; "Facility and Site Needs for the FIRE Project."

Other Papers Published:

Meade, D.M.; "Fusion Ignition Research Experiment"; Comments on Plasma Phys. Controlled Fusion, Comments on Modern Physics, Vol. 2(2), pp. 81-97, 2000.

Thome, R. J., et al, "Engineering Features of the Fusion Ignition Research Experiment (FIRE)," 21st Symp. on Fusion Tech., Madrid (2000)

Ulrickson, M. A., et al, "Physics Basis for the Fusion Ignition Experiment (FIRE) Plasma Facing Components", 21st Symp. on Fusion Tech., Madrid (2000)

FIRE Design Team; "Fusion Ignition Research Experiment (FIRE) Engineering Status Report for Fiscal Year 2000"; Princeton Plasma Physics Laboratory Report No. 81-001030_FIREFYRPT_FT.doc.[5]

Meade, D. M., et al, "Mission and Design of the Fusion Ignition Research Experiment (FIRE)" EX2/1, Fusion Energy 2000 (Proc. 18th Int. Conf. Sorrento, 2000), IAEA, Vienna (2000)

Meade, D.M., "Road Map for a Modular Magnetic Fusion Program", Journal of Fusion Energy, Vol. 17, No. 2, p 125 June 2000

TABLE OF CONTENTS

FIRE Fiscal Year 2000
Status Report

1.0   Introduction

The Next Step Options (NSO) study is underway to consider the logical steps that might be undertaken in a restructured U. S. Fusion Sciences Program. The findings of this study are periodically provided to the Fusion Energy Science Advisory Committee (FESAC) which advises the DOE Secretary of Energy on fusion research strategy. The NSO study has two major goals:

(1) Development of research goals and a strategy for burning plasmas in the restructured fusion sciences program.   A modular program strategy is evolving which comprises a series of experimental projects which can lead to the development of fusion energy in an environment of limited energy research funding.

(2)   Development of a minimum cost burning plasma research device.
Since the tokamak has advanced to the strongly burning plasma phase, a LN_2-cooled-copper tokamak burning plasma device will receive the major emphasis in this study. The design concept presently being evaluated is FIRE (Fusion Ignition Research Experiment)

The possibility of constructing a next step experiment in magnetic fusion will depend critically on its cost. Since the U. S. DOE has constructed ~$1B class facilities such as the Spallation Neutron Source (SNS), Advanced Photon Source (APS) and the National Ignition Facility (NIF), the construction cost target for NSO has been set at $1B.

The NSO study has been organized as an integrated physics/engineering design activity within the Virtual Laboratory for Technology. A set of preliminary goals and associated requirements were established as a first step in the development of an optimized Burning Plasma Strategy. A burning plasma experiment is one element of a "modular" strategy to accomplish many of the ITER objectives using separate lower cost facilities. These facilities would focus on physics issues such as: (1) burning plasma physics, (2) long pulse advanced toroidal physics and (3) fusion technology. This strategy reduces the technical risk and would require much smaller cost outlays compared to a single large integrated facility.

The NSO study process involves national and international communications and tasks. A workshop was held in early 1999 at PPPL to obtain fusion community feedback on the general goals and detailed requirements. The ITER and IGNITOR projects were discussed at the workshop as additional input to this process. A portion of the NSO Team participated in the May, '99 IGNITOR Workshop in Washington to discuss issues of mutual interest. An interim report was written to serve as input to the Snowmass Fusion Summer Study in July, '99, and a document was made available to FESAC as reference material for their meeting in August, '99. Work continued on the design in FY00. Several engineering meetings were held at PPPL, as well as a Physics Workshop in May, 00. A proactive outreach program was initiated to involve the fusion community and the broader scientific community in determining the mission and direction for FIRE. Over 30 presentations and discussion sessions have been held, including recent meetings at major European fusion laboratories.

The NSO study has only been underway since the beginning of FY 99 and much work is yet to be done, however, the results are very encouraging. They indicate that a compact burning plasma device can be developed which is responsive to cost issues and could be a practical and important next step in a revitalized modular fusion sciences research program.

2.0 Physics Objectives and Guidelines for a Next Step Tokamak Burning Plasma Experiment

Burning plasma physics is widely accepted as the primary objective for a major next step in magnetic fusion research. The Grunder Panel of FESAC and the Madison Forum endorsed burning plasmas as the next step. The 1999 Snowmass Summer Study endorsed burning plasmas with the Burning Plasma Working Group, the Energy Working Group B and the Magnetic Fusion evening session, all overwhelmingly supporting the burning plasma objective and that the tokamak was technically ready for a high gain burning plasma experiment. The 1999 SEAB review of fusion noted that "There is general agreement that the next large machine should, at least, be one that allows the scientific exploration of burning plasmas". If Japan and Europe do not proceed with ITER, "the U.S. should pursue a less ambitious machine that will allow the exploration of the relevant science at lower cost." "In any event the preliminary planning for such a device should proceed now so as to allow the prompt pursuit of this option."

Our present understanding of plasma transport, macroscopic stability, wave particle interactions and boundary physics while improving through experiments on existing facilities will always be incomplete until tested and understood in a "real" fusion plasma. The mission chosen for the major next step in magnetic fusion is:

to attain, explore understand and optimize alpha-dominated fusion plasmas to provide the knowledge for the design of an attractive magnetic fusion system.

Understanding the properties of high gain (alpha-dominated) fusion plasmas in an advanced toroidal configuration is a critical issue that must be addressed to provide the scientific foundation for an attractive magnetic fusion reactor. The functional fusion plasma objectives for major next physics steps in magnetic fusion research can be described as:

Fig.1 Next Physics Steps in Magnetic Fusion
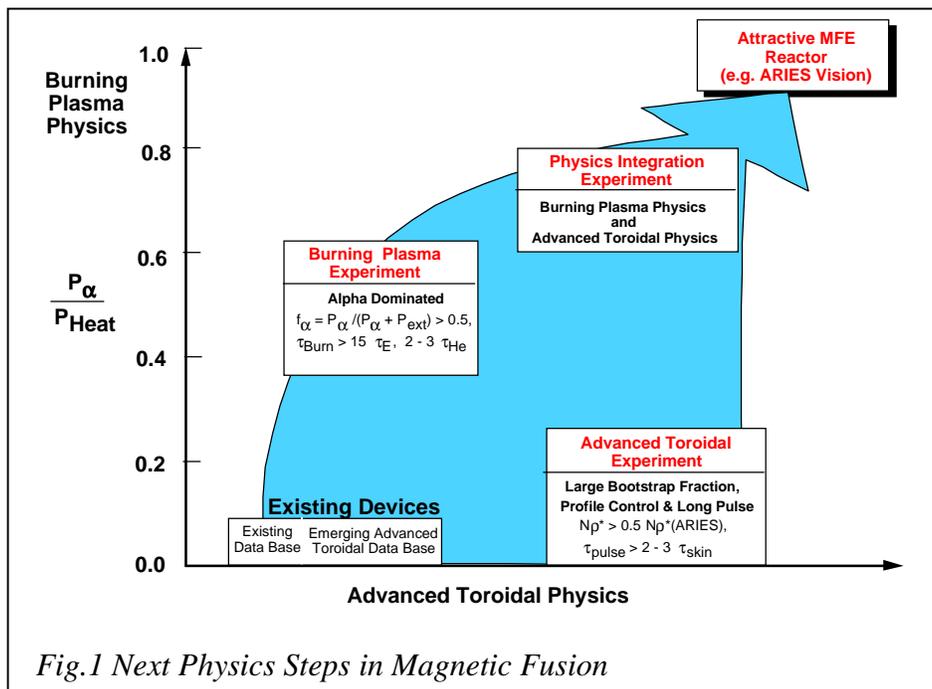
Burning Plasma Physics - The achievement and understanding of alpha-dominated plasmas that have characteristics similar to those expected in a fusion energy source, and

Advanced Toroidal Physics - The achievement and understanding of bootstrap-current-dominated plasmas with externally controlled profiles and other characteristics (e.g., confinement and β) similar to those expected in an attractive fusion system.

These requirements lead naturally to a set of fusion physics Stepping Stones as illustrated in Fig. 1. The ranges of plasma performance and duration to address these issues are shown schematically with the natural time scales for important plasma processes.

A design study of a Fusion Ignition Research Experiment (FIRE) is underway to investigate near term opportunities for advancing the scientific understanding of self-heated fusion plasmas in advanced toroidal configurations. The emphasis is on understanding the behavior of plasmas dominated by alpha heating ($Q > 5$) that are sustained sufficiently long compared to most characteristic plasma time scales ($\sim 30 \, \tau_E, \sim 6\tau_{He}, \sim \tau_{skin}$, where τ_{He} is the helium ash confinement time at $5\tau_E$, and τ_{skin} is the time for the plasma current profile to redistribute at fixed total current) to allow the evolution of alpha defined profiles. The programmatic mission of FIRE is to attain, explore, understand and optimize alpha-dominated plasmas to provide knowledge for the design of attractive magnetic fusion energy systems. The programmatic strategy is to access the alpha-dominated regimes with confidence using the present tokamak data base (e.g., Elmy-H-mode, ≤ 0.75

Greenwald density) while maintaining the flexibility for accessing and exploring advanced tokamak modes at lower magnetic fields and fusion power for longer durations in later stages of the experimental program. A major goal is to develop a design concept that would meet these physics objectives with a tokamak (load assembly) construction cost of ~$300M and a total project cost in the range of $1B.

The activities have focused on the technical evaluation of a compact, high-field, highly-shaped tokamak with the parameters shown in Table I. The

Table I. Design Goals for FIRE

R (m), a (m)	2.0, 0.525
κ_{95} , δ_{95}	$\approx 1.8, \approx 0.4$
q_{95}	> 3
$B_t(R_o)$ (T)	10(12)*
Wmag TF (GJ)	3.7
I_p (MA)	6.44(7.7)*
flattop time (s)	~20(12)*
alpha heating fraction	>0.5
τ_E, τ_{skin} (s)	~ 0.6, ~ 13
Z_{eff} (3% Be + He (5 τ_E))	1.4
Fusion Power (MW)	~ 200
ICRF Power (MW)	30
Tokamak Cost ($B)	~ 0.3
Project Cost ($B)	~1

* Upgrade capability

philosophy of FIRE is to challenge, and extend existing physics limits toward the regimes envisioned for a fusion reactor. Confinement projections are uncertain, and one of the major objectives of a next step experiment is to extend the experimental range beyond existing experiments and capability to test projections closer to reactor conditions. The plasma performance of FIRE was estimated using a zero-dimension analysis with energy confinement given
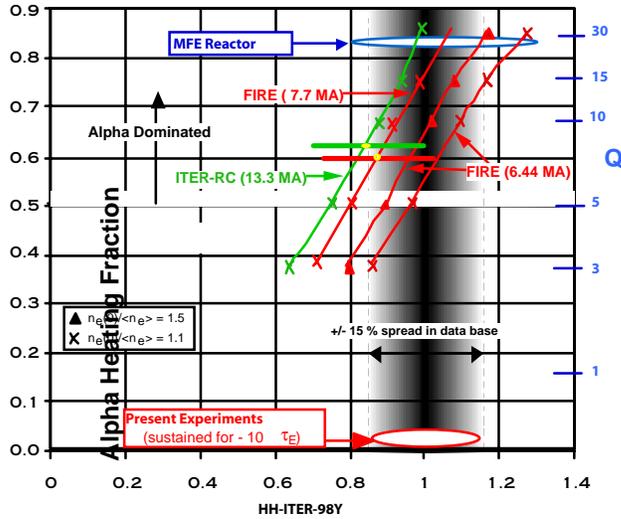
Fig.2 H-Mode Projections using ITER IPB98(y)

by ITER IPB98(y) [1]for the Elmy H-mode, $\beta_N \leq 2.5$, density ≤ 0.75 Greenwald density, $P_{threshold} \geq (0.9/A_i)n^{0.75}BR^2$, 3% Be impurities and alpha ash accumulating self consistently with $\tau_{He} = 5 \tau_E$. The results are shown in Fig. 2 for two values of density profile peaking. For the baseline FIRE parameters (6.44 MA/10T), the alpha heating fraction, f_α, rises from $\approx 40\%$ at the low end of the present database to $\approx 80\%$ at the high end. Note that the alpha heating fraction, which is important for physics studies, is more robust to confinement uncertainty and rises linearly with confinement while Q changes rapidly as ignition is approached. These parameters extend the capability to study alpha heating effects sustained for > 10 τ_E more than an order of magnitude beyond previous experiments. Additional performance (Table II.) could be obtained by adding additional power supplies and operating at 7.7 MA(12T) with a reduction in toroidal field flattop

to 12s thereby providing additional physics margin. The H-mode power threshold poses a challenge for high field tokamaks and the power transported across the separatrix in FIRE marginally exceeds the projected L-H transition threshold.

A Tokamak Simulation Code (TSC) simulation indicates that alpha-dominated plasmas can be sustained for > 30 τ_E, > 5 τ_{He} and ~ 1 τ_{skin} as shown in Fig. 3. This example shows the importance of having sufficient magnetic field flattop for plasma startup (~ 4 s), helium ash evolution (~ 4 s) prior to achieving a steady burn for experimental studies. In addition, capability must be provided for controlled plasma shutdown without
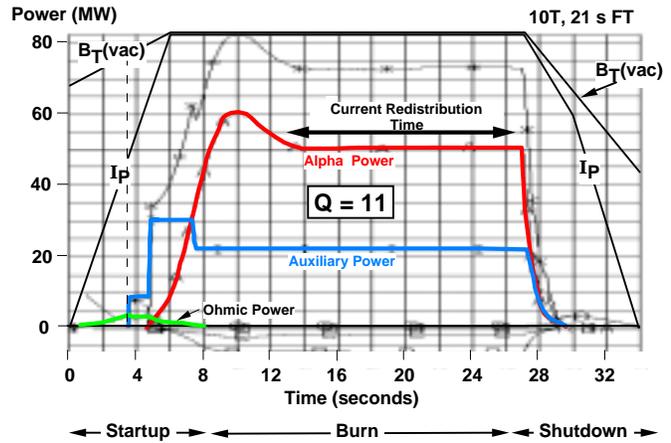

Fig. 3. Evolution of an alpha-dominated plasma.

causing a disruption on every pulse. The primary methods of burn control will be to adjust the input power and the D-T fueling rate.

A longer term goal of FIRE is to explore advanced tokamak regimes using pellet injection and current ramps to create

Table II.	$B_T(T)$	$I_p(MA)$	f_α	Q	n/n_{GW}	HH98(y)	β_N	P_{trans}/P_{thres}
Baseline	10	6.44	0.66	10	0.7	1.04	2.5	1.15
Upgrade	12	7.7	0.66	10	0.6	0.85	1.9	1.09

reversed shear plasmas (e.g., PEP modes) for durations of 1 to 3 current redistribution times. This AT capability is expected to produce modestly enhanced confinement and beta as observed in present large tokamak experiments, and provides a continuous transition from H-mode operation to advanced tokamak operation. A range of advanced tokamak modes could then be studied on FIRE. If HH98(y,1) ≈ 1.2 and $\beta_N \approx 3$ can be attained and sustained at 6.5 MA, then inductively-driven plasmas with Q >> 10 could be achieved at full field for durations of ~ 20 s(~ $1\tau_{skin}$). The cryogenically cooled coil systems on FIRE are capable of long pulses at reduced fields: 20 s at 10 T; 40 s at 8 T and 90 s at 6 T. Therefore, the magnetic field and plasma current for the modestly advanced performance case can be reduced by 20% resulting in pulses ~ 40 s (~ $3\tau_{skin}$) long that have Q > 5. Self-consistent physics scenarios and engineering solutions for power handling are not yet developed for the longer pulse (~ 40 s) scenarios.

The baseline magnetic fields and pulse lengths can be provided with BeCu /OFHC toroidal field (TF) coils and OFHC poloidal field (PF) coils that are pre-cooled to 77 °K prior to the pulse and allowed to warm up to 373 °K at the end of the pulse. The cross-section of FIRE is shown schematically in Figure 4. The key "advanced tokamak" features are: strong plasma shaping, double null poloidal divertors, low TF ripple (~ 0.34% @ outer midplane), internal control coils and space for yet to be determined wall stabilization capabilities. The 16 TF coil system is wedged with a compression ring to resist de-wedging at the top and bottom of the inner TF leg. Shielding is added

between the walls of a double wall vacuum vessel to reduce nuclear heating of the coils, limit insulation dose and allow hands-on maintenance outside the envelope of the TF coils within a few hours after a full power D-T shot. Large (1.3 m by 0.7 m) midplane ports provide access for remote manipulators and diagnostics, while 32 angled ports provide access to the divertor regions for utilities and diagnostics. FIRE is being designed mechanically to accommodate 3,000 full field, full power pulses and 30,000 pulses at 2/3 field. The repetition time at full field and full pulse length will be < 3 hr, with shorter times at reduced parameters. The fusion energy production of 5 TJ (similar to BPX) produces a lifetime neutron dose to the TF insulating material at the inboard midplane of ≈ 1.5 x 10^{10} Rads which is consistent with the polyimide insulation being considered.
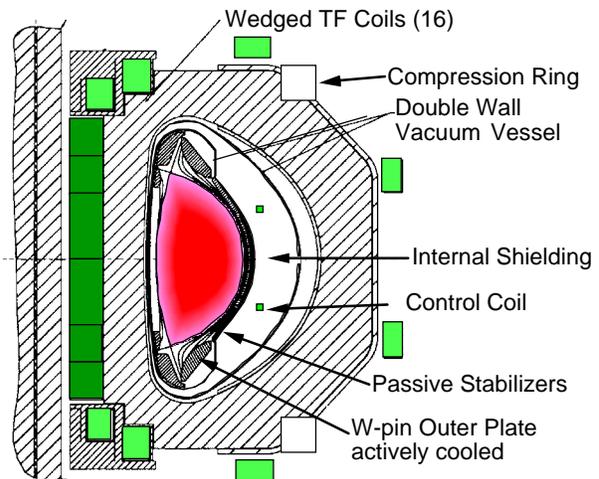

Fig. 4. Cross-section of FIRE

The power densities on the divertor plates are ~5 MWm^{-2} for detached operation and ~25 MWm^{-2} for attached operation. The divertor plasma-facing components are tungsten "brush" targets mounted on copper backing plates, similar to a concept developed by the

ITER R&D activity. The outer divertor plate is water-cooled, while the baffle and inner divertor targets are inertially cooled. The first wall is comprised of Be plasma-sprayed onto copper tiles which do not need active cooling for pulses < 15 s. The large neutron wall loading ($3MWm^{-2}$) at fusion power of 200 MW contributes significantly to the first wall and vacuum vessel heating. Either a modest reduction in fusion power due to lower H-mode threshold assumptions, or improved cooling will be required for a 20 s pulse length. The plasma facing materials were chosen to reduce the tritium inventory in the first wall. Sixteen cryopumps – closely coupled to the divertor chambers, but behind sufficient neutron shielding – provide pumping (≥ 100 Pa m^3/s) for D-T and He ash during the pulse. Pellet injection scenarios using direct injection inside the magnetic axis and guided inside launch will be incorporated, and are expected to provide a modest increase in fusion reactivity due to density profile peaking while minimizing tritium consumption. The in-device tritium inventory will be determined primarily by the cycle time of the divertor cryopumps, and can range from < 2 g for regeneration overnight to ~20 g for monthly regeneration.

The possibility of using only high conductivity (OFHC) copper in the TF coil is being investigated. This lower strength material would require the addition of TF coil bucking on the central solenoid coils near the midplane. Initial results suggest that 11.5T could be produced with a flattop of $\approx$ 40 s using about 1/2 of the electrical power that the baseline BeCu TF coil design requires. The limitation on burn time for both BeCu and OFHC designs is the

power handling capability of plasma facing components and the vacuum vessel. This option will be studied in more detail in FY01.

A number of important physics issues remaining to be addressed during the design phase, and then resolved during the experimental program. These include generic issues such as: mitigation and avoidance of disruptions and vertical displacement events, H-mode power threshold, effects of neoclassical tearing modes, detached divertor operation with good confinement, and divertor/edge plasma modeling under high power conditions.

FIRE, coupled with a non-burning steady-state superconducting advanced tokamak in an international multi-machine strategy, would address many of the objectives identified for Next Physics Steps in Magnetic Fusion (Fig. 1).

[1] ITER Physics Basis, Nucl. Fusion **39** (1999) 2208

3.0 General Design Requirements & Plan for FY00

The basic set of machine parameters and features given in Table 3.0-1 were chosen as a starting point for the FIRE engineering evaluations while the physics and trade studies proceed in parallel with pre-conceptual design of the device to assure feasibility. These parameters are expected to change and expand as the evaluations and studies proceed and as they provide feedback into the iterative design process. The table will ultimately serve as the basis of the formal General Design Requirements Document (GDRD) which will be completed prior to a Conceptual Design Review (CDR).

Table 3.0-1. Basic Parameters and Features of FIRE-I

Parameter	*Value*
R, major radius, m	2.0
a, Minor radius, m	0.525
B_t, Tesla	10 (12)*
No. TF coils	16
Fusion power, MW	200 (250)*
Max. TF ripple	0.3% (edge)
Pulse rep. Time, hr.	~3 at full power
TF and PF coil type	LN_2 cooled copper and BeCu
Plasma current	~6.5 MA (7.7 MA)*
Flat top, s	$\geq$18.5 (12)*
Triangularity, δ_{95} δ_x	~0.4 ~0.8
Elongation, κ_{95} , κ_x	~1.8 ~2.0
Neutral beam Power	None planned
ICRF Power, (MW)	30
FWCD	None in baseline-possible later option.

|	
LHCD	None in baseline-possible later option.
Vacuum level	10^{-8} torr
Bake out temp.	350 °C
Life pulses at full field	3000 (min.)
Coil initial temp.	80 °K
Coil max. temp.	373 °K
First wall materials	Beryllium
First wall replacement/maint. times	Single unit: 3wks; limiter: 6wks.; entire system 12 mos.
Total Fusion Energy	5 terajoules - DT + 0.5 terajoules - DD
Limiters	For start up
First wall life	Machine lifetime
VV pressure suppression system	No
FW heat flux	TBD
First wall cooling	Inertial
VV operating temp.	100 °C
Divertors	Double null; actively cooled outer W plate, inertially cooled elsewhere, possible upgrade to active cooling for longer pulses
In-vessel RH requirements.	Must be able to replace/repair all components
Ex-vessel RH requirements	Classification system & maintenance similar to ITER.
TF support arrangement	Wedged with compression rings

( )* values for operation at 12 T

4.0 Design Configuration/Integration

The general arrangement of the FIRE experimental device is shown in Fig. 4.0-1 (a) and (b). The main design features include:

- *High plasma triangularity (0.4 δ_{95}) is provided for improved performance.*
- *Double null gaseous divertors.* Gaseous divertors have been shown to be effective in radiating most of the power going to the divertor regions throughout the first wall rather than depositing it in a localized toroidal stripe in the divertor. They are also easier to engineer.
- *Divertor module maintenance through horizontal ports.* This enables the extraction of larger divertor components and fewer pieces.
- *A double walled vacuum vessel with integral shielding.*
- . This design approach provides improved vessel structural stiffness and makes double use of the cooling jacket as nuclear shielding. Locating shielding between the walls reduces nuclear heating in the TF coils and the dose level external to the vessel. The reduced nuclear heating permits longer flat top times and higher current densities than would otherwise be possible. This "close in" shielding arrangement reduces the dose outside the vessel and activation of nitrogen that is in the thermal shield.
- *Wedged TF coils aided by a pair of large compression rings to support torsional shear at the inner corners of the TF.*

(a) Cross-Sectional View of FIRE Through Its Insulation Enclosure
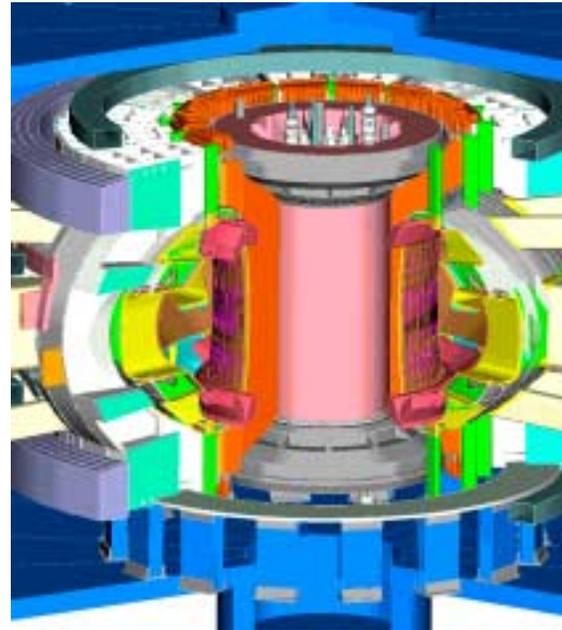
(b) Cross Section View of the FIRE Tokamak
**Fig. 4.0-1. Cross-sectional Views of FIRE**

4.1 Design Features

Figures 4.0 (a) and (b) illustrate the design features of the reference design. The major components and features are:

- 16 wedged TF coils, inertially LN_2 cooled with coil windings located in a partial coil case. High strength BeCu C17510 is used in the inner legs and OFHC copper in the remainder of the coil. Compression rings girdle the TF coils to suppress "dewedging" in the upper and lower inside corners of the coils.
- Two pairs of divertor coils (up-down symmetric). These coils are inertially LN2 cooled, strip wound OFHC copper coils.
- Two pairs of external ring coils (up-down symmetric). These are similar in construction to the divertor coils.
- A free standing segmented central solenoid (CS) that will be made of LN2 cooled, BeCu water jet cut discs.
- A double wall vacuum vessel. The inner space is filled with steel and water for nuclear shielding.
- Internal plasma facing components (shown in Fig. 4.1-1). The Be coated Cu first wall and *tungsten pin-type* inner divertor module AR inertially cooled through the vacuum vessel; the tungsten pin-type outer divertor module and baffle is actively cooled. is designed for a high triangularity, double-null plasma with a short inner null point-to-wall distance and a near vertical outer divertor flux line.
- Two outboard poloidal limiters, spaced 90 degrees apart, enclose the ICRH quadrant.
- A passive stabilization system consisting of an inboard pair of ring coils and an outboard saddle coil.
- An active control coil system consisting of a pair of coils located within the outboard vessel jacket.
- A thermal enclosure similar to the design used for C-Mod (i.e., polyimide foam insulation with fiberglass inner and outer protective/structural skins).

Fig. 4.1-1. FIRE Plasma Facing Components

Tungsten Divertor

Be coated
Cu FW
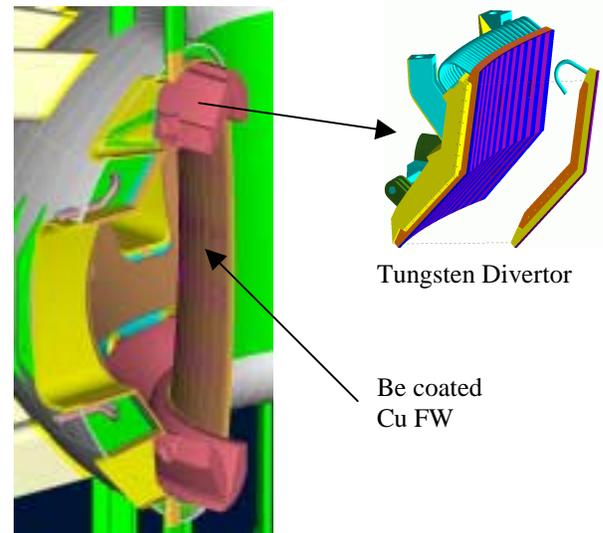
4.2 Design Choices

Sixteen TF coils were selected as the number of coils to provide reasonably large openings between coils for in-vessel access. The radial position of the coil back leg is set by a number of considerations, including access, ripple, and shield thickness requirements; FIRE's design has good balance between these considerations. The inner leg of the TF coil, where the stress is highest, is made of high strength, high conductivity variant of C17510 BeCu. This alloy was developed for BPX, and commercialized since then by its developer, Brush-Welman. The variant we propose to use has a 0.2% yield strength of 720 Mpa and an electrical conductivity of 68% IACS. The stress in the outer regions of the coil is low enough to permit less costly oxygen free

copper (C102) to be used. Large rings located outside the TF coils are used to obtain a load balance between wedging of the intercoil case structure and wedging at the upper/lower inboard corners of the TF coil winding.

The design of the baffle and outboard divertor was revised by integrating the two components into a single module. This was done to increase the baffle heat load capacity by providing coolant to the baffle, a component not actively cooled in the earlier design. The reconfigured baffle-outboard divertor module can be extracted through the horizontal ports in a maintenance scheme that provides for component rotation and a vertical lift.

4.3 Machine Assembly

The assembly sequence is illustrated in Fig. 4.3-1. FIRE is assembled from (8) 45-degree sectors consisting of two TF coils and a 45-degree vacuum vessel octant.

A vacuum vessel octant is rotated into the bore of two TF coils at assembly. Sixteen large, "straight-in" view ports are equally distributed along the vacuum vessel mid-plane. Sixteen upper and lower auxiliary ports are provided, angled in a position to allow diagnostic view of the divertor region. Small circular ports are also located at the top and bottom of the vacuum vessel, passing through the region between the TF coil winding.

The horizontal ports will provide access to the ancillary systems outside the device. Three ports are assigned to RF heating, and the remaining ports allocated between diagnostics, vacuum pumping and a pellet injection system.
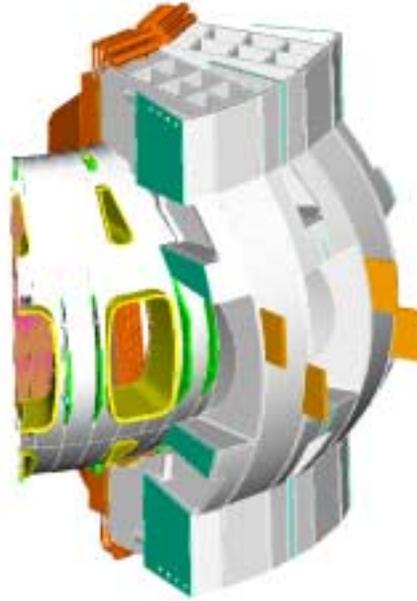

Fig. 4.3-1 45-degree Octants Assembly
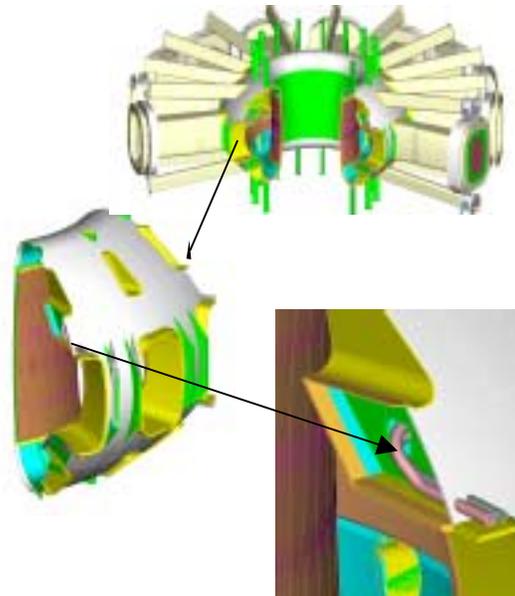
Fig. 4.3-2. The FIRE Vacuum Vessel is assembled from 45-degree Octants.

Some port space will also be used for in-vessel PFC coolant routings. The electrical feed connection to internal control coils are located above/below two horizontal ports located 180° apart. The angled auxiliary ports located in the upper and lower vessel regions accommodate cryopumps, the divertor cooling lines and diagnostics.

The radial build dimensions listed in Table 4.3-1 identifies the space allocated to the components in the confined region inboard of the plasma center.

Table 4.3-1 FIRE Radial Builds

	COMP BUILD	COMP	TOTAL
		mm	mm	mm
	Machine Center		0.0
	gap	410	410.0
CS	Insulation	10.0	
	Nom winding thk	380.0	
	CS enclosure	10.0	400.0	810.0
	gap	10	820.0
inbd TF	CS side case	0.0	
	Ground insul	12.0	
	winding pack	464.0	
	ground insul	12.0	
	plasma side case	0.0	488.0	1308.0
	Trapezoidal Effect	0.0	1308.0
	TF TPT	5.0	
	MinTF/VV gap	5.0	
	VV TPT	5.0	
	Thermal Shield	12.0	27.	1335.
inbd VV	VV shell thk	15.	
	Shield material	20.0	
	VV shell thk	15.0	50.0	1385.
	TPT	5.0	
	Alignment space	0.0	5.0	1390.
PFC	Water cooled Cu	25.0	
	gasket	2.0	
	Cu tiles	18.0	
	Be PFC	5.0	50.0	1440.0
	Plasma SO	35.0	
	Plasma minor radii	525.0	
Plasma R0			**2000.0**

5.0 Engineering Systems

Sections 5.1 to 5.15 which follow describe the engineering systems of the FIRE device. This includes the TF coils and Structure, the Central Solenoid and PF coils, the Vacuum Vessel, Plasma Facing Components, Thermal Shield which encloses the LN_2 cooled device, the Ion Cyclotron Heating System, Fueling and Pumping System, Tritium System, Neutronics and Shielding, evaluation of Activation, Decay Heat and Radiation Exposure, Remote Maintenance Systems, Magnet Power Supplies, the Cryoplant, Facilities and Siting, and Safety evaluation.

5.1 TF Coils & Global Structure

5.1.1 TF Coil Stresses and Fault Conditions

Selected characteristics of the TF coils are listed in Table 5.1.1-1.

Table 5.1.1-1 Characteristics of FIRE TF Coils

Number of TF Coils	16
Bt, Tesla	10
Flat-top, s	21 (minimum)
Life Pulses at Full Field	3000 (minimum)
Time between Pulses,hr	3
Coil Initial Temp, K	80
Coil Max Temp, K	373

The TF coil arrangement for FIRE is a wedged or vaulted design with a free-standing CS. A bucked and wedged configuration is being carried as an alternate, but the difficulties of fit-up and manufacture currently weigh on the side of the wedged design. TF wedging pressures and CS hoop tensions have determined the basic sizing of the machine, but support of torsional shear in the inner legs has had an important influence on the evolution of the FIRE structural design. To support this shear, friction between the wedged segments of the coil is all that is available. With torsional shears between 30 and 50 MPa, and friction coefficients of .3, 160 MPa wedge compression is needed on the plasma side of the TF where the torsional shear is at a maximum. Wedge pressures from a pair of large compression rings shown in Figure 5.1.1-1, provide the required load in the upper and lower inner leg corners. Centering forces supply the wedge pressure at the equatorial plane.
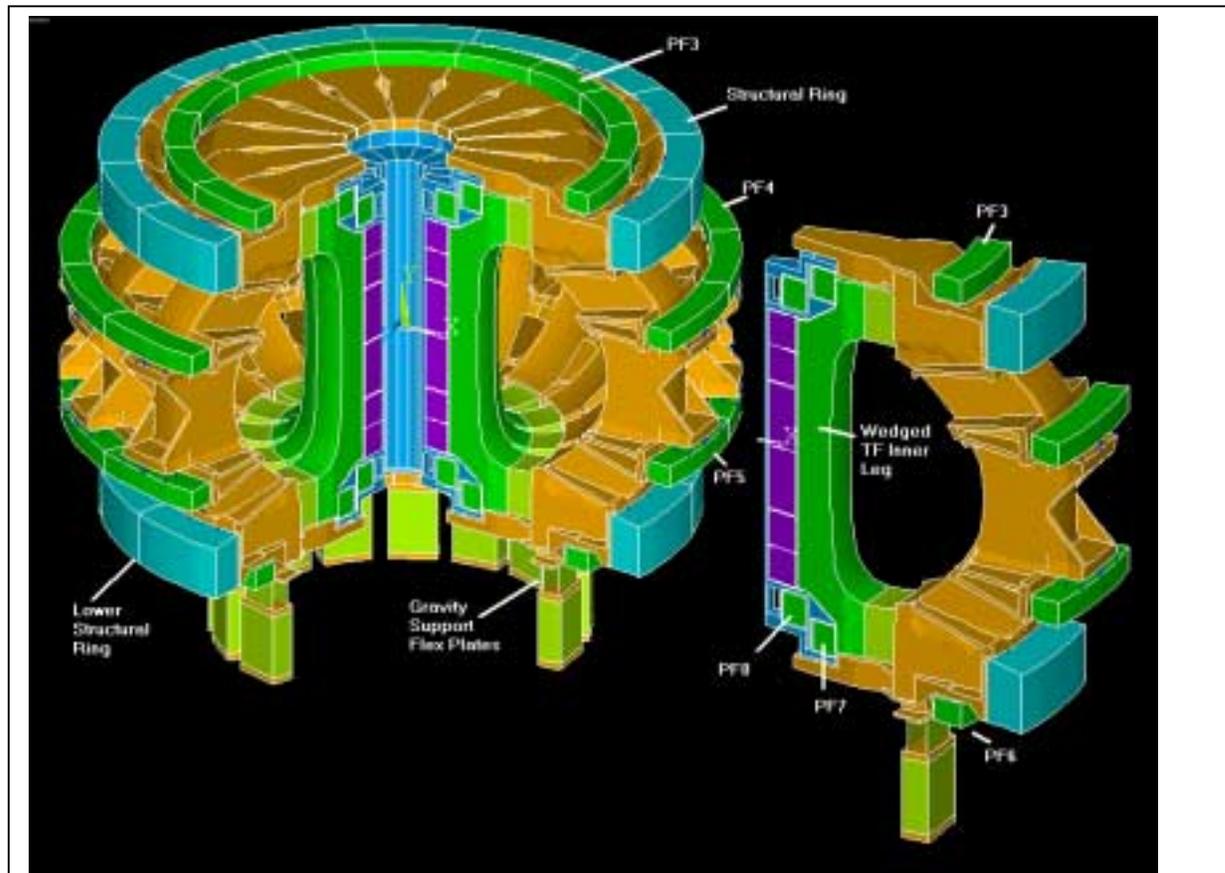

Figure 5.1.1-1

12 segment Symmetry Expansion (left) of 1/16 cyclic symmetry model (right)

Figure 5.1.1-2 shows the distribution of Von Mises stress, wedging pressure and vertical stress in the TF inboard leg for 10T operation. A variety of Beryllium Copper is the present material for the inboard legs of the TF coils, whereas the outboard sections will use OFHC (C102) copper. Peak stress in the FIRE TF is about 469 MPa at the CS side of the inner leg for 10 T operation, at precharge.

The stress criteria for conductor and structure are:

Conductor: S_m=2/3 yield and adequate ductility;
Structure: S_m=2/3 yield or ½ ultimate and adequate ductility.

Table 5.1-2 gives the properties of conductor and structural materials. Table 5.1-3 summarizes stress conditions and allowables for TF Coil and case at 10T and 12T.

Table 5.1.1-2. FIRE Conductor and Structural Materials Properties

68% IACS BeCu Cond.	60% CW OFHC Cond.	Cast 304SST	50%CW 304 SST
Sm=483 MPa at RT	Sm=200 MPa at RT	Sm=154 MPa at RT	Sm=620MPa at RT
Sm=497 MPa at 77K	Sm=233 MPa at 77K	Sm=188 MPa at 77K	Sm=834MPa at 80K

Table 5.1.1-3
Stress Summary for Operation at 10T and 12T

	Material	TF Field	Primary Stress (1)	Allowable	F.S	Membrane Plus Bending	Allowable	F.S
TF Inner Leg	BeCu	10	249(1)	480	1.9	469	724	1.5
TF Inner Leg	BeCu	12	358(1)	480	1.3	689	724	1.05
TF Outer Leg	OFHC	10	155(2)	233	1.5			
TF Outer Leg	OFHC	12	223(2)	233	1.0			
TF Case at Outer Leg			200	188				

(1)(Average Wedge Pressure, Vertical load assumed supported by the Outer TF and Case)
(2) Hand Calculations with the case contributing 200 Mpa

To demonstrate that the "adequate ductility criteria" was satisfied, the machine was analyzed with a 13T TF field with elastic-plastic TF material properties. A stress-strain curve with a 600 MPa elastic limit was used for the inner leg. This conservatively brackets the properties of the BeCu conductor which has a .2% offset yield of 724 MPa. A .6% strain resulted from the 13T loading, and the structural response remained bounded for this over-loaded condition. The .6% strain was then conservatively imposed on the insulation as though it all was in-plane in the turn to turn insulation. The resulting insulation stress was within the allowable tensile stress for the conductor. The plastic strain for a first loading to 13T is plotted in Figure 5.1.1-3 which indicates that it would be localized in the inboard leg for this extreme load condition (not a design load condition).
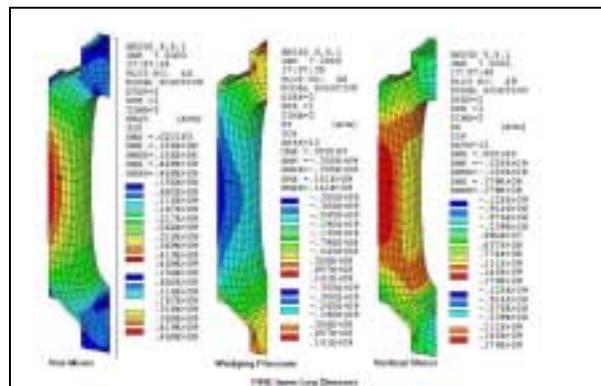
Figure 5.1.1-2

Stress Distribution for 10T Operation

During the BPX design effort, cyclic fatigue for BeCu limited the allowed tensile stress to 60 ksi (413 MPa). Fracture mechanics calculations were

Figure 5.1.1-3
Plastic Strain after 13 T loading

the basis for this with Paris Law constants measured for BeCu as a part of the CIT/BPX projects. The design number of full field pulses for FIRE is 3000 which is much less than BPX. TF stresses are predominantly compressive in FIRE and the vertical tensile component in the inner leg is about 120 MPa. This indicates margin in the fatigue behavior of BeCu for FIRE, but a test program for material properties is required for confirmation.

Survivability in off-normal or under fault loads is also a measure of design margin. A 180 degree model was built to begin investigating the sensitivity of the TF system to these unusual loads. A plot of an asymmetric condition is illustrated in Figure 5.1.1-4.
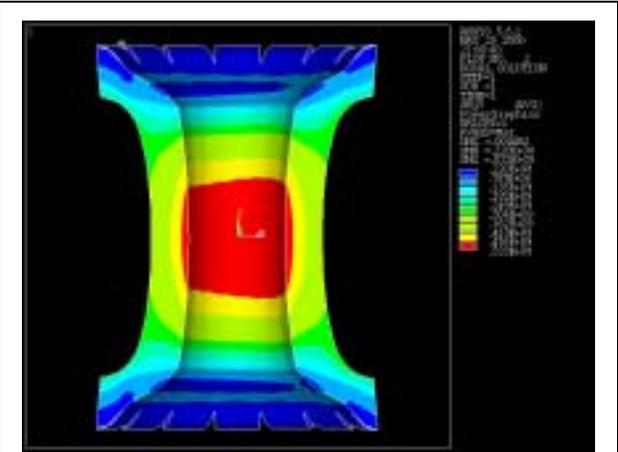
Figure 5.1.1-4
Single Coil 10% over Nominal 10T Current - 533 MPa VM

Table 5.1.1-4 compares the peak stress in the fault condition to the peak stress for the nominal 10T operating condition and shows acceptable excursions for the two fault cases considered thus far.

Table 5.1.1-4 Preliminary Fault Analysis Results	
Model and Current/Loading	Peak TF Stress Ratio
Nominal 10T Condition	1.0
Fault Model: Single Coil 10% Over Nominal	1.02
Fault Model: Single Coil 20% Over Nominal- the Rest 20% Under	0.84

5.1.2   FIRE Pulse Lengths

A zero D integration scheme was used to estimate the flat top times for various toroidal field and nuclear heat levels. This was done in parallel with a more rigorous ANSYS coupled thermal-current diffusion analysis. Results are given in Table 5.1.2-1 for several field levels, with and without nuclear heating. At 10T, the

allowable flattop time is 18.5 s, which exceeds the initial FIRE requirement of 10s. At 12 T, the allowable flattop time is 12 s. The total thermal energy to be removed for several peak temperatures following a pulse are given in Table 5.1.2-2. An example of the temperature profiles in a TF coil at 5 s and 48s during a pulse is shown in Figure 5.1.2-1

Table 5.1.2-1
TF Flat Top Times for FIRE Options 68%IACS BeCu TF
(Feb 3 Dimensions, TF Central Column OR=1.308,IR=.820),Simplified Calculations using Packing
Fraction=.9 Nonuniformity=1.0, 80° Start, 370°K Temp Limit

TF Field	4T	8T	8T	10T	10T	12T	12T
Nuc Heat MW/m^3	0.0	7.5	0.0	11	0.0	11	0.0
Time, s	214	31	46	18.5	26	12	15

Table 5.1.2-2
Thermal Energy of 16 coils after each Pulse, 80° Start. (Energy to be removed during cool-down)

Peak Temp after Pulse	292°	313°	370°
TF Coil Thermal Energy	9.96GJ	11.1 GJ	14.1GJ

Sub cooling of the coils to 65 °K was considered but does not offer substantial improvement.

5 Sec, Early in Ramp-Up   48 sec, End of Flat-Top

FIRE TF Current/Thermal Diffusion Analysis Results, 77% IACS Material
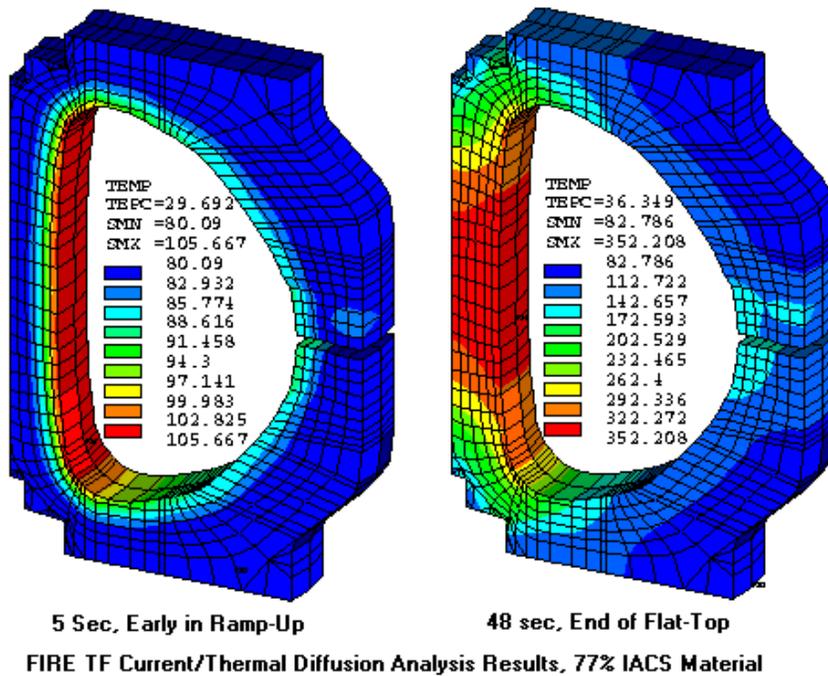
**Figure 5.1.2-1 . Temperature Distributions in the FIRE TF, 77% IACS., Packing Fraction=.9,~28 sec
Flattop**

5.1.3 Global Structural Modeling

Both linear and non-linear models have been used. The TF winding pack is connected to the external case with links that model zero sliding friction. Tensions develop in the links when gaps would have opened. This is adjusted at some locations by removing the gaps/links which open for the load cases where this is necessary.

The non-linear model used gaps at the wedge face and simulates the frictional capacity of the inner leg to resist out-of-plane torsion. Gaps also are used at the case segment to segment interface. It is intended that the case to case mechanical connections be minimized,

as these must sustain large local pressures, but be insulated. The non-linear analysis has confirmed that a compression ring size of .5m X .75 m, stressed to an average hoop stress of 500 MPa, provides adequate centering force for frictional restraint of the TF inner leg and of the case segments.

The relation between the current-thermal diffusion analysis and the structural calculation is done outside ANSYS. An algorithm is used to assign temperatures to the structural model from the current/thermal diffusion model. A typical temperature distribution for a "hot" TF coil in its case is shown in Figure 5.1.3-1 and out of plane displacements for the system are shown in Figure 5.1.3-2. There is a separate CS/PF model which is fully structurally non-linear. This has been used to investigate support structures for the CS and PF1 and 2. Since a wedged TF is used, the CS stack can be modeled independently.

Support of the TF coil out-of-plane (OOP) loads is statically indeterminate and changing structural support concepts changes the magnitude and location of the torsional shear in the inner leg of the TF. The wedged configuration has better performance with respect to the out-of-plane shear than a bucked and wedged concept. The upper and lower inner corners of the TF tend to de-wedge due to the expansion of the TF coils.

45 MPa peak torsional shear. The results are based on the linear models and some localized slippage is likely, but the non-linear model showed this to be a small effect.
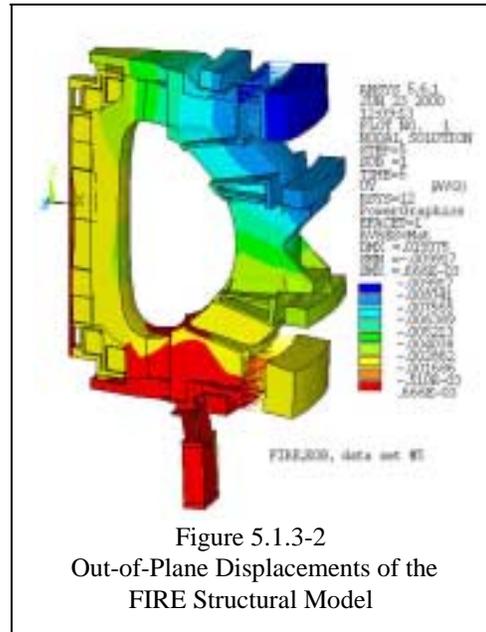
Figure 5.1.3-2
Out-of-Plane Displacements of the
FIRE Structural Model
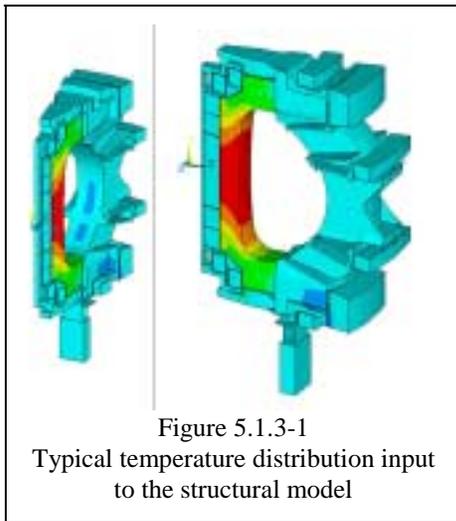
Figure 5.1.3-1
Typical temperature distribution input
to the structural model

In Figure 5.1.3-3, the TF corner stresses at assembly are shown. The wedging pressure achieved with the rings in the corner is between 60 and 90 MPa at assembly. This increased to 150 MPa compression when the coil is energized, as shown in Figure 5.1.3-4 This level is sufficient to support the
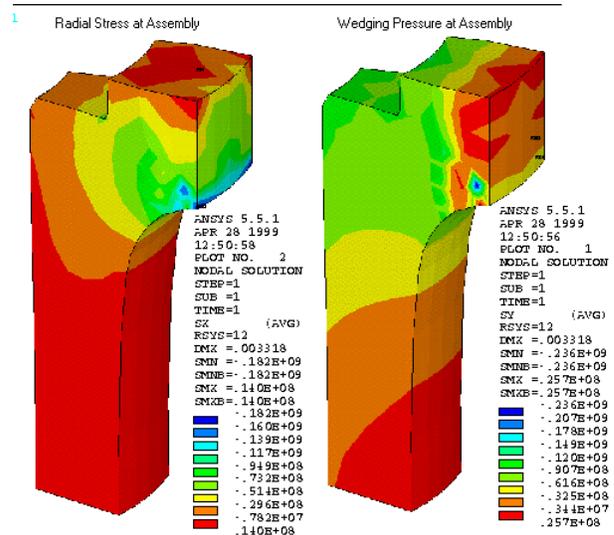
Figure 5.1.3-3 TF Inner-Upper Corner Stress Results for the "With-Ring" Model

Figure 5.1.3-4
TF Inner-Upper Corner Stress Results for the
"With-Ring" Model

uses a mechanical system which has been prototyped, and supports similar pressures as would be required for FIRE. It is illustrated in Figure 5.1.3-6.

Figure 5.1.3-6 Wedge Jack Concept
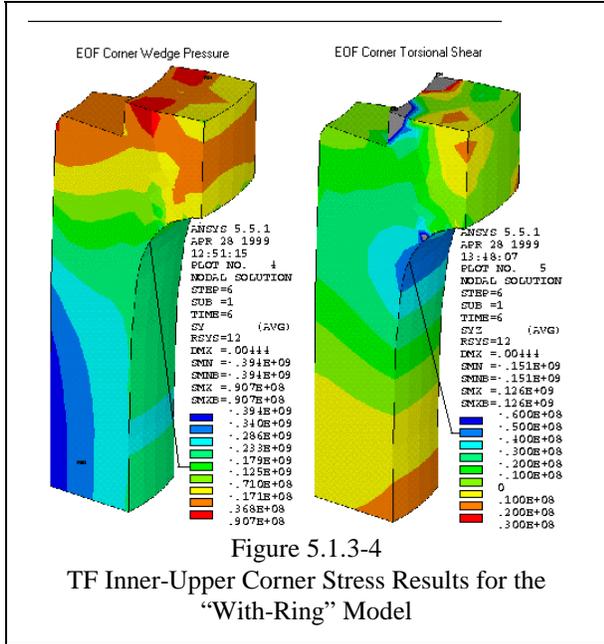
The results of shear margin calculations are shown in Figure 5.1.3-5 and indicate the improvement in the extent of the region that can frictionally support the torsional shear at the wedge faces. The region having adequate frictional support of the OOP loads is shown in red. There is a small difference in extent of this region between the cases but the added area is important because it includes the area of largest torsional shear.

Loads in the compression rings are quite large. At assembly the average ring hoop stress is about 500 Mpa. This increases by about 100 Mpa at EOF. Initial ring loading can be applied with a number of mechanisms. In the history of this concept, which is used on IGNITOR and was used on early CIT designs, hydraulic jacks and mechanical jack systems have been employed. IGNITOR currently

Case stresses are highest near the local bearing locations of the ring. Elsewhere, case stresses are below 620 Mpa. Much of the case stress at the equatorial plane relates to thermal expansion of the TF, and occurs later in the pulse. Even though the largest fraction of the stress is thermal, a high strength material is needed to eliminate the possibility of plastic strains in the case. Equatorial plane stresses are summarized in Table 5.1.3-1 and are too high for cast material (80K Yield=282 MPa,41 ksi). There is about 228 MPa from Lorentz loading and 362 MPa from thermal. Cold worked plate is suggested for the case sidewalls.

The rings are strip wound and are sized to provide wedge pressure for both the TF and Case.
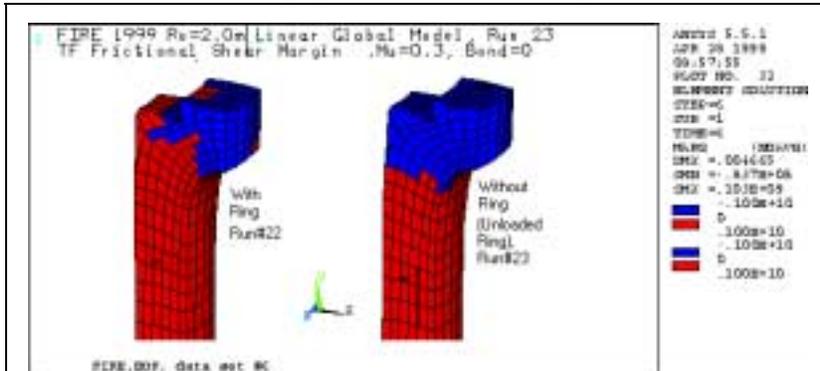
| Table 5.1.3-1 Case Equatorial Plane Stresses,12T Run#52 Results:	
Time	Peak Stress
PRE	228 MPa
SOF	448 MPa
EOB	585 MPa
EOF	617 MPa
EOP Hot	362 MP

Figure 5.1.3-5 Frictional Shear Margin is Extended into the Corner of the TF by Using the Compression Ring

5.2   Central Solenoid and PF Coils

The Central Solenoid (CS) is an OFHC copper coil. It is a free-standing coil in the baseline design. A bucked and wedged arrangement is being considered as an alternate. The CS is a pancake wound coil with turns that are water jet cut from plate. Radial coolant grooves are used between double pancake assemblies. The central solenoid is segmented into 5 coils with a large mid section coil, CS1, and two smaller coils on either end of the stack. Coil current densities vary among the coils in the CS assembly, and thus the coil segments experience different Lorentz forces, temperatures, and radial strains. Radial grooved plates at the interfaces between coil segments maintain concentricity.

The CS and PF coils are analyzed in both the global model and in a more detailed model of the free-standing CS/PF1 and PF2 coil system with their case/structure. Typical stress results at precharge and end of flattop are shown in the 1/16th model of the Central Solenoid in Figure 5.2-1. The arrangement of coils near the machine center is shown in Fig 5.2-2 and the dimensions of the PF and CS coils are given in Table 5.2-1.

Table 5.2-1 CS and PF Coil Dimensions, (m)

Coil	R	Z	DR	DZ
CS1U	.61	.398	.39	.791
CS2U	.61	1.035	.39	.44
CS3U	.61	1.475	.39	.43
PF1	0.786	1.975	0.325	0.380
PF2	1.211	2.211	0.325	0.380
PF3	3.00	2.6463	.4	.3
PF4	4.400	1.000	0.400	0.300
PF5	4.400	-1.000	0.400	0.300
PF6	3.00	-2.6463	.4	.3
PF7	1.211	-2.211	0.325	0.380
PF8	0.786	-1.975	0.325	0.380
CS3L	.61	-1.475	.39	.43
CS2L	.61	-1.035	.39	.44
CS1L	.61	-.398	.39	.791
Plasma	2.0	0.0	1.0	2.0

Figure 5.2 – 1
Typical CS Stress Results from the Global Model
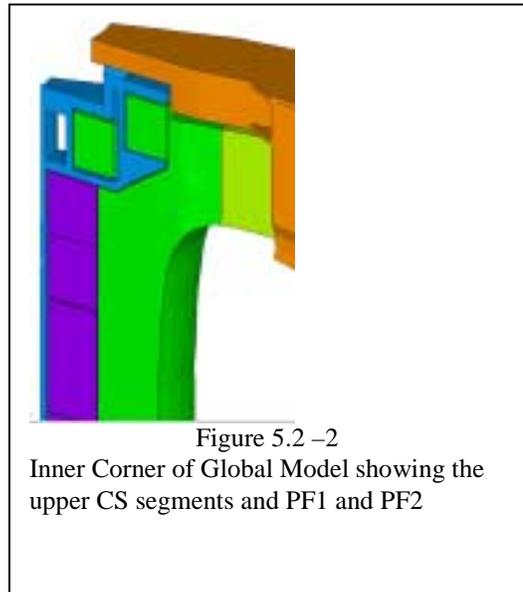
Figure 5.2 –2
Inner Corner of Global Model showing the upper CS segments and PF1 and PF2

5.2.1   CS Joints

Sizing of a reactor during the conceptual phase needs to include an allowance for the local details of the coil design. Stress analysis is initially based on "smeared" properties to which multipliers are applied to account for insulation, cooling and joint details. In the evaluation of FIRE "smeared" CS and PF stresses, the packing fraction due to insulation and cooling channels is taken as .85 and the stress multiplier for the inner joint is taken as 1.0. It is important to

achieve these factors for the size limits of FIRE to be realized.

Pancake to pancake joints may have a stress multiplier associated with them which is usually quite a bit larger than 1.0. There are two major sources of the multiplier. The geometry of the connection including the effects of the offset adds local stresses at the mechanical connection details. This usually requires the addition of material to bring the stresses within the levels experienced by the rest of the turn. The increase in metal produces a stiffer region embedded in the coil and picks up more load than a single turn would normally take, adding further stresses to the mechanical details of the joint. The increase in metal also causes the stress to increase because the larger mass of metal runs cooler in an inertially cooled coil and they don't expand with the rest of the coil. The result is additional tensile stresses in the vicinity of the joint. It is, therefore, necessary to use a special configuration to maintain the stress multiplier at unity.

The joint shape in Figure 5.2.1-1 was developed for BPX after investigating many pinned or bolted or hooked joint concepts. The scarf/transition joint is a constant cross

section design that eliminates both the stiffness and thermal anomaly. There is no void left by the joint, and no turn loss. In BPX the joint was to be soft soldered over large lapped areas. A better connection is to use electro-deposit joining at the butt ends of the scarf. Use of this detail means that the stress in the joint is the same as that computed for the larger models of the coil. This is especially advantageous at the ID of the coil. If some other joint concept is chosen, the coil stress allowable must be de-rated by the stress multiplier for the ID joint. This joint concept has similar advantages when used on the OD, but because the OD stresses in the CS are much lower than the ID, more conventional mechanical joints might be considered. For example, the double pancakes could be made an assembly with the scarf at the ID, then stacked and assembled mechanically at the OD. Since the coil segments are small enough the scarf could be used at the OD as well. This would require electro-deposit forming at the coil assembly, but C-Mod has shown that this is feasible.
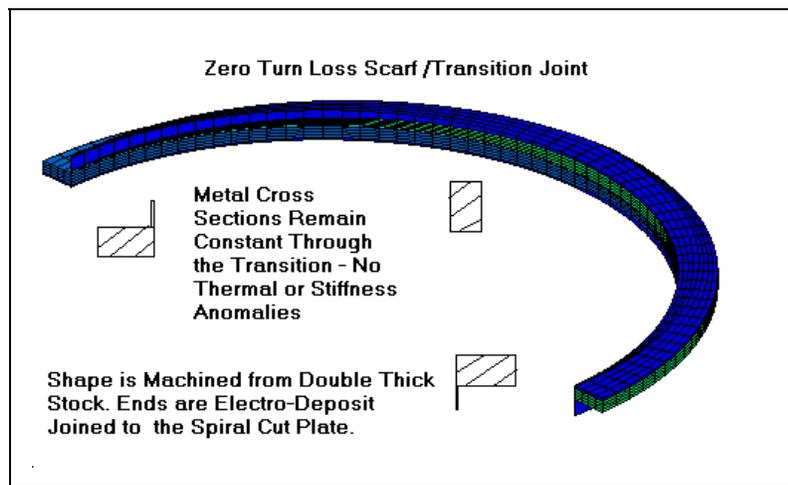

Figure 5.2.1-1

Figure 5.2.3-1
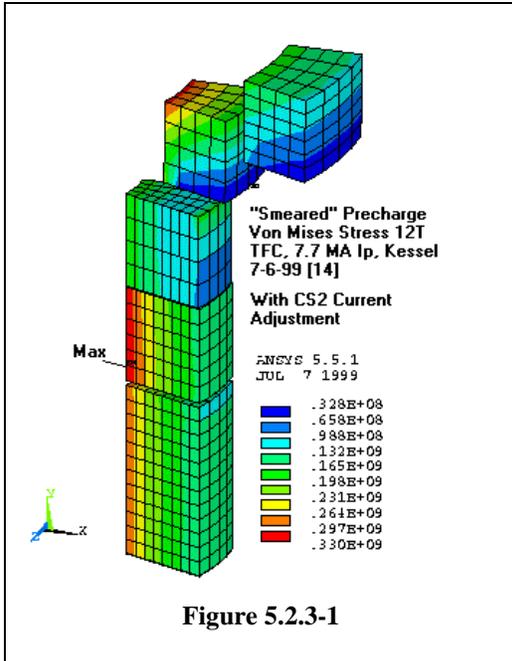
5.2.2 CS/PF Stress Analysis Summary

Three analysis models have been used, the global model, an axisymmetric model and a 3D model derived from the global structural model. There are significant stresses in the PF 1 coil. This stress however has a large component relating to "roll-over" of its cross-section resulting from the structural over-hang of PFs 1 and 2. A stiffer structure would improve this. Other significant stresses typically occur in CS1 and CS2. These are enhanced by self loads appearing as hoop stresses. The worst stresses should be biased to occur earlier in the pulse when the temperatures would be low and the physical properties of the candidate materials are better. The CS and PF coils are wound conductors and if 1.5 Sm is allowed for these, the ID turns will be operating close to yield. For 3000 full power pulses, fatigue is not expected to be a problem but this will need confirmation through material testing. Stress states in the coils are acceptable for all the PF Scenarios proposed for FIRE, but with a slight negative margin for the high performance 12T 7.7 MA scenario. Further adjustments to the high performance scenario will be considered.

### 5.2.3 12T TF, 7.7 MA, 15 second PF Scenario

The scenarios available for this case produce stresses that are either too large early in the pulse or too large later in the pulse, but at different locations. Estimates based on an intermediate flux state also produce stresses slightly above the allowable, but further adjustments are under consideration. Typically in these scenarios, either CS2 is highly stressed at precharge or CS1 is highly stressed at EOB. Temperature effects on the allowable favor higher Precharge currents.

To evaluate the potential for a workable scenario, the effects of the flux shift was estimated by weighting the stress states of the two 12T 7.7 MA scenarios. A rigorous stress evaluation needs to consider a packing fraction (taken as 85% to allow for cooling channels) and temperature effects on the stress allowable. The FIRE criteria set the primary membrane allowable at 2/3 yield for conductor. If the conductor is also primary structure, the calculation of Sm should be the lesser of 1/3 ult or 2/3 yield. For 60%CW OFHC the ultimate stress criteria governs and the Sm values are 235 at 80K and 167 at RT. The peak stress of the FEM analyses has been compared with 1.5 Sm, as being similar to a bending stress. This assumes that the distribution of stress in the coil is linear from ID to OD. In actuality it is peaked at the ID, and the linearized "bending" stress that should be compared with 1.5 Sm, will be somewhat lower than the peak stress from the FEM analysis. However, this effect is only about 10 MPa. The thermal effect on the reduction of the allowable stress is: 1.5Sm=350-100*(T-80)/212.

Figures 5.2.3-1 and 5.2.3-2 show results at Precharge and EOB for one of the scenarios. Table 5.2.3-1 shows results estimated by weighting the scenarios to estimate the effect of an adjusted flux state. Since the resulting margins are slightly negative relative to the criteria, further adjustment of the scenario will be considered.

Table 5.2.3-1

Results of Weighted Scenarios 12 T 7.7 MA scenarios, Packing fraction=.85

Weight New - shifted, flux, state, everywhere, back by,5,V with CS2 Precharge adjustment	Weight Old 12 T 7.7 MA scenario	PRE	EOB
3/4	1/4	CS2 PRE VM=354 Temp=85 1.5Sm=347 F.S.=.98	CS1 EOB VM=332 Temp=176 1.5Sm=305 F.S.=.92

Figure 5.2.3-2
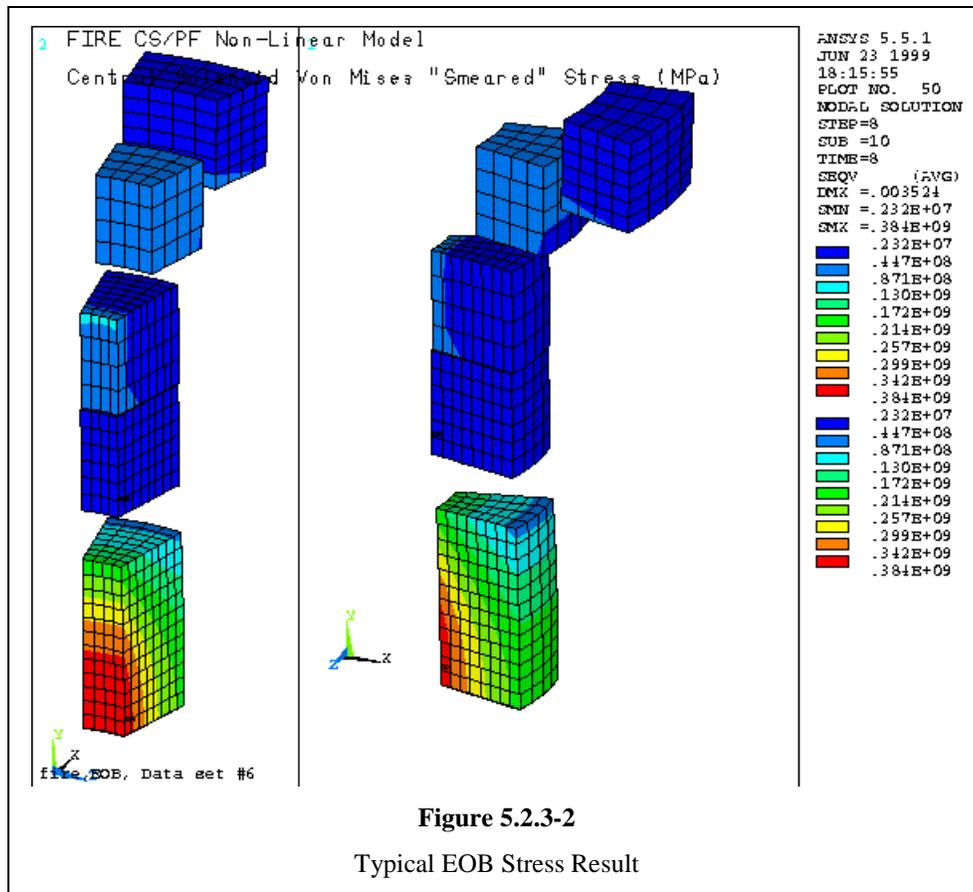
Typical EOB Stress Result

5.2.4 10T TF, 6.4 MA, 21 Second PF Scenario

Stresses are acceptable for the long pulse for the baseline requirement using OFHC. The peak stress for all coils and all times is 294 Mpa which is less than the 1.5 Sm allowable of 350 Mpa for work hardened OFHC Copper. The highest peak temperature is 182°K in PF2 (for a packing fraction of .8). Results are given in Table 5.2.4-1

Table 5.2.4-1
CS/PF Peak Von Mises, MPa, (Kessel with 21 second PF Scenario, kcs4,pic Scenario, Upper Number is "Smeared", Lower Number is for Packing Fraction=.85 ,No Preload)

	PRE	SOD	SOF	SOB	EOB	EOC	EOD
CS1	209	164	164	127	164	109	5.6
	246	192	182	149	214	128	6.6
CS2	265	208	208	28.7	164	50.9	6.6
	311	244	244	33.7	193	60	7.7
CS3	133	107	105	101	56	131	3.3
	156	126	120	119	66	154	3.9
PF1	180	131	144	169	132	86	4.4
	212	154	170	199	155	101	5.2
PF2	135	107	127	90	71	45	3.9
	159	126	149	106	84	53	4.6
PF3	1.07	.84	.8	36	39	20	~0
	1.26	.98	.94	42	46	24	
PF4	.5	.4	.4	120	120	54	~0
	.65	.47	.47	141	141	64	

5.2.5 CS and PF Coil Temperatures
Coil temperatures throughout a pulse for three different scenarios are given in Tables 5.2.5-1 to 5.2.5-3

Table 5.2.5-1
CS and PF coil Temperatures, 15 second 12T TF, 7.7 MA PF Flux Shifted 5V
Copper IACS=100%, Packing Fraction=.85 (pfk7.inp)

Time (sec)	CS1	CS2	CS3	PF1	PF2	PF3	PF4
0	80	80	80	80	80		
4.64	84.8	87.7	82.1	82.4	86.3	80.1	80.0
5.00.	85.7	89.0	82.5	82.8	87.4	80.1	80.0
12.00	93.3	99.9	87.3	103	115	85.4	84.1
14.5	102	102	89.0	113	126	87.6	90.1
24	142	108	95.6	145	163	89.6	120
27	155	111	98.0	157	178	90.9	127
31	161	112	98.9	162	182	91.7	129
35	161	112	99.0	162	183	91.7	129

Table 5.2.5-2
CS and PF coil Temperatures, 250 second 4 TF, 2MA PF Scenario [7]
Copper IACS=100% Packing fraction = .85 (pfk5.inp)

| Time(sec)	CS1	CS2	CS3	PF1	PF2	PF3	PF4
0	80	80	80	80	80	80	80
4.6	80.9	81.4	80.4	80.4	81.2	80.0	80.0
5	81.0	81.6	80.4	80.5	81.4	80.0	80.0
7	81.2	82.2	80.7	80.8	81.9	80.0	80.2
10	81.7	82.6	80.9	81.6	82.6	80.0	80.9
255	144	86.8	87.9	119	125	80.2	170
257	145	86.8	87.9	119	125	80.2	170
260	145	86.8	87.9	119	125	80.2	170

Table 5.2.5-3
Coil Temperatures, °K, Kessel June 8 1999 21 second PF Scenario, 6.44 MA, 10T, kcs3,kpf4 Copper
IACS=100%, Packing Fraction=.85

Time(sec)	CS1	CS2	CS3	PF1	PF2	PF3	PF4
0	80	80	80	80	80	80	80
4.64	83.5	85.5	81.5	81.7	84.5	80.1	80.0
10	88.0	92.0	84.0	92.4	98.8	82.8	82.1
12.5	93.6	92.8	84.7	99.6	106	84.8	86.3
31	141	96.8	88.6	151	162	90.2	129
34	150	98.1	90.0	159	170	90.9	135
38	153	99.4	91.1	162	174	91.0	136
42	153	99.4	91.1	162	174	91.0	136

5.2.6   PF Supports

The PF coils are self-supporting with respect to their radial Lorentz Loads. The coils must be allowed to grow thermally and elastically in the radial direction, but must be constrained to move concentrically with respect to the machine centerline. Vertical loads must be supported against the case. In FIRE, PF1 and PF2 are included in the CS stack. PF 3-6 require out of plane supports. Radially grooved plates, as illustrated in Figures 5.2.6-1 and 5.2.6-2 are being considered.
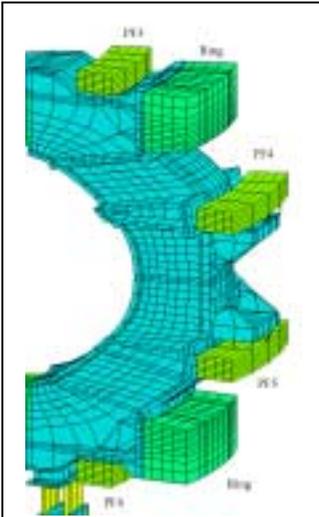
Figure 5.2.6-1

Structural Model PF
Supports

GRP Male
Groove Pad
with
Fibreslip
Bonded to it,
Pad Bonded
to G-10
Ground
Wrap/Case

Lateral
Bearing
Height

Steel Female
Groove Pad,
Polished
Surface Finish

RADIAL GROOVE
FIRE PF SUPPORT CONCEPT
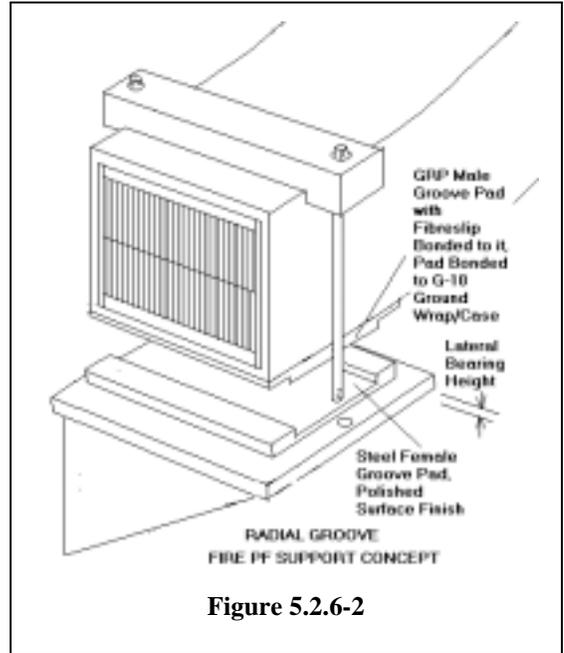
Figure 5.2.6-2

5.3   Vacuum Vessel

5.3.1   Introduction

The vacuum vessel, shown in Fig. 5.3.1-1, provides the vacuum environment for the plasma as well as the first confinement barrier for radioactive materials. The vessel also serves as the support structure for all in-vessel components, provides the first level of nuclear shielding, and helps provide for the passive stabilization of the plasma. The vessel system includes the torus, the ports and port extensions, the gravity supports, the supports for internal components, the passive stability plates, the internal control coils, and the integrated coolant/bake-out lines.

5.3.2   Vessel Concept

The vessel torus is a double wall sandwich structure consisting of 15 mm thick inner and outer facesheets attached to poloidal ribs. The space between the facesheets, which varies from 20 mm on the inboard side to 540 mm on the outboard side, is filled with radiation shielding material and coolant. Water at 20-50 C and 1 MPa is used to remove nuclear heating during normal operation. The water temperature is raised to 150C for heating the vessel and internals during bake-out. The shielding material can be single sized stainless steel balls with a packing fraction of about 60% or stacked plates with a similar packing
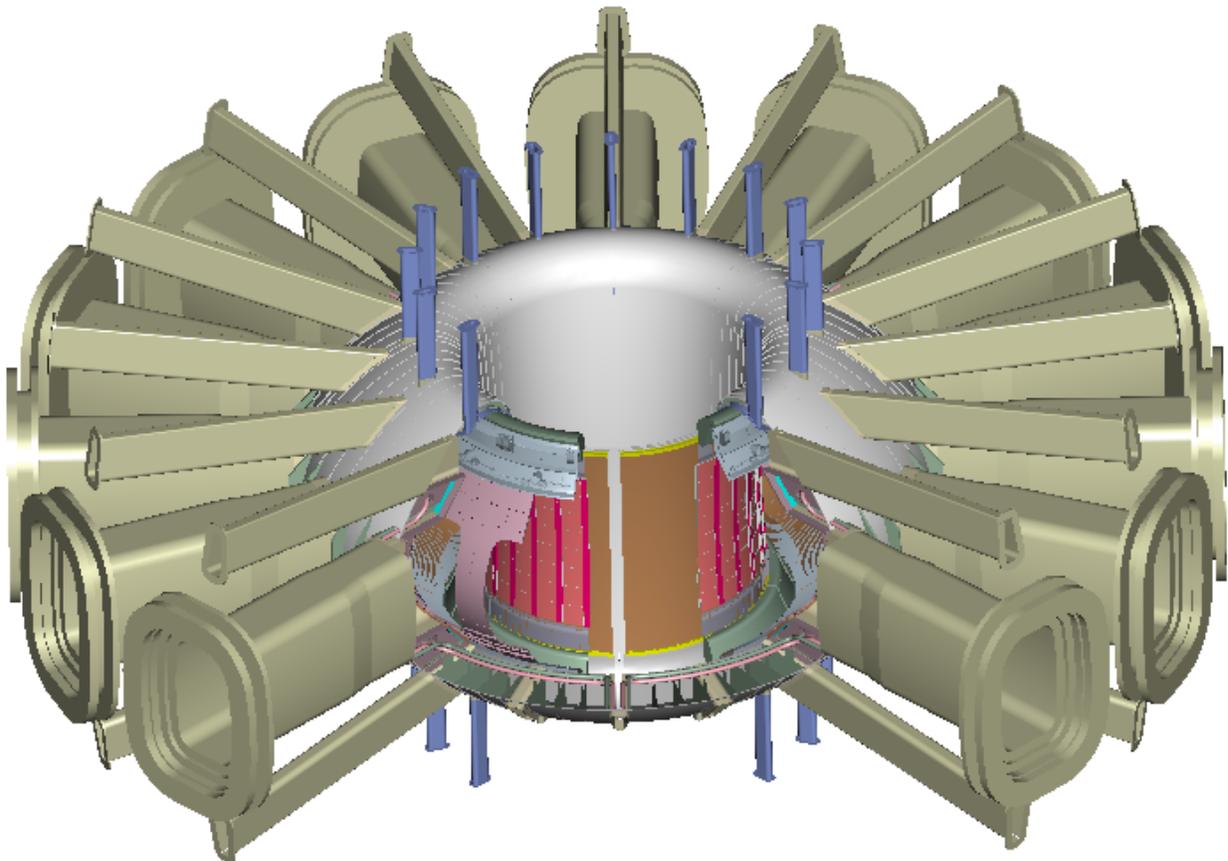

Figure 5.3.1-1 Vacuum vessel with port extensions and internal components

fraction. The vessel parameters are summarized in Table 5.3.2-1.

The primary advantages of the double wall structure include higher bending stiffness (for a given total material thickness) and better integration of cooling and shielding. Most vacuum vessel designs in use (JET, JT60, DIII-D) and most designs on the drawing board (ITER, KSTAR) use full or partial double wall vacuum vessels. Figure 5.3.2-2 shows a cutaway of the vessel and pertinent dimensions.

There are 16 sets of access ports around the torus, which are used for RF heating, remote maintenance, diagnostics, and internal cooling. There are large, 1.3 x 0.7 m midplane ports, upper and lower trapezoidal ports approximately 0.15 x 0.5 m, and upper and lower oblong vertical ports approximately .08 x 0.15

Table 5.3.2-1 Vacuum Vessel Parameters

Dimensions and Weights

Vol. of torus interior	35 m^3
Surf. area of torus interior	89 m^2
Facesheet thickness	15 mm
Rib thickness	15 to 30 mm
Wt. of structure , incl ports	50 tonnes
Wt. of torus shielding	80 tonnes

Power

Direct neutron heating:	~200 MW
Indirect first wall load	< 40 MW

Cooling

Coolant	Water
Pressure	~ 1 Mpa
Normal oper. temp.	< 100C
Bake-out temp.	~150C

Materials

|	
Torus, ports and structure	316L ss
Shielding	304L ss
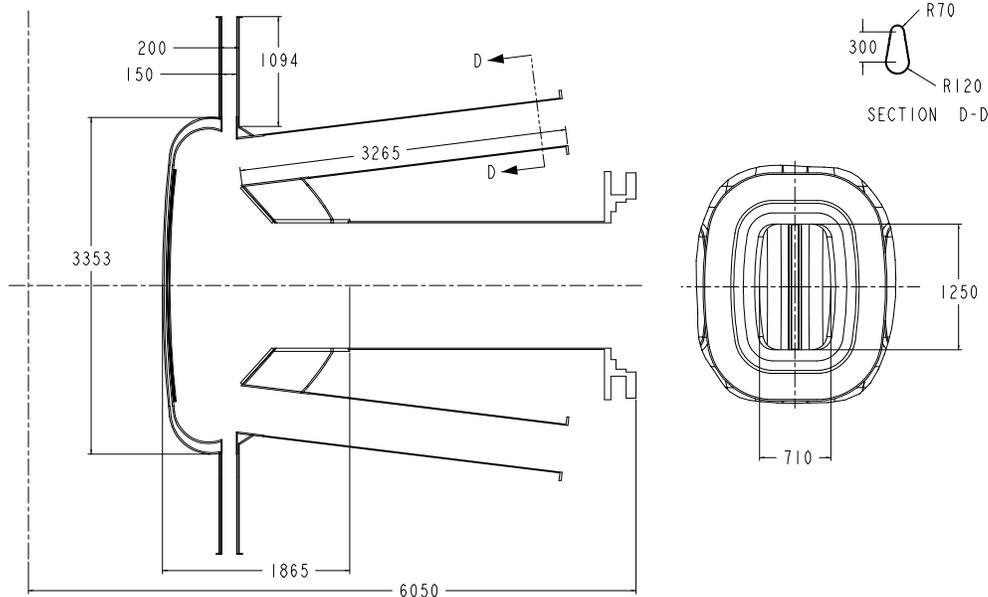
Figure 5.3.2-2 Vessel and port dimensions

m in size. The sets of port openings are identical at each toroidal location to provide structural and design symmetry, but the port extensions may be varied to match their specific purpose. The port extensions are required to extend the vacuum boundary past the TF coil legs and through the cryostat region.

5.3.3   Vessel loading and analysis

The vessel is subjected to large gravity, seismic and electromagnetic loads, as summarized in Table 5.3.3-1. The total vertical load is estimated to be about 20 MN, while the net lateral load is about 7 MN. To react these loads, the vessel is

supported near the midplane on the outboard side via vertical and lateral links to the TF coil structure. The vertical links are attached to the radial ribs to spread the applied loads vertically into the vessel. This minimizes the local bending stresses in the vessel and provides a means for adjusting the vessel location globally relative to the TF coils. Lateral supports are located near the vertical links, and are tied to the top of the midplane ports.

The vessel must support all internal components, including the divertor assemblies, the passive stability structure, the poloidal limiters and the first wall tiles. The outboard divertor

Table 5.3.3-1 Vacuum Vessel Loading Conditions

Load	Value	Unit	Comment
Gravity load	~ 3.5	MN	Vacuum vessel = ~130 tons FW tiles and divertor= ~tbd ton Port mounted equip = ~100 - 150 tons
VDE load 　　　Vertical 　　　Lateral, net	 16-32 6-11	 MN MN	[ref. J. Wesley, "Disruption, VDE, and runaway electron conversion: physics basis and issues for FIRE", May 1, 2000]
Seismic load 　　　Vertical acceleration. 　　　Lateral acceleration	 0.2 (tbd) 0.2 (tbd)	 g g	
Max total vertical load	~ 42	MN	Gravity + VDE*1.2 dyn. factor
Max total lateral load	~ 13	MN	VDE*1.2 dyn factor + seismic
Max local EM load 　　Local pressure on vv 　　From internal components	 ~ 8	 MPa	Local pressure on inboard wall due to halo currents, peaking factor of 2
EM load from TF field ramp	~ 0.3	MPa	Assumes 20 s ramp to or from full field Max load at inboard midplane
Coolant pressure 　　　Normal operation 　　　Bake-out	 < 10 < 10	 atm atm	Water assumed as coolant and for bake-out

modules are actively cooled via pipes at each of the upper and lower auxiliary ports. The two poloidal limiters are also actively cooled via piping located in the midplane ports. The first wall, inboard divertor, and passive stability structures are cooled by conduction to the vacuum vessel. All components must have robust supports to react the electromagnetic loads from a plasma disruption.

Preliminary structural analysis of the vessel indicates that the present dimensions are acceptable to support the various loads. A finite element model was developed for an earlier version of the vessel geometry, and the stresses and deflections obtained are summarized in Table 5.3.3-2. As seen in the table, there are some peak stresses around the port openings and at the top of the vessel that must be mitigated with additional structure. These reinforcements have

already been incorporated in the vessel design, but the analysis has not been repeated. Details of the stress and deflection analysis are contained in Appendix D of this report.

5.3.4 Passive plates and internal coils

As indicated in Section 2, Physics, a system of highly conducting and actively cooled passive plates and a set of internal control coils must be incorporated into the vacuum vessel. The passive plates consist of 25 to 30 mm thick copper sheets that are bonded directly to the surface of the vacuum vessel. The sheets are actively cooled via internal water passages connected through manifolds into the vessel cooling system. A bonded connection is thought to be the most straightforward approach, since cooling can be provided directly by the copper plates to both the

Load condition	Preliminary Von Mises stress estimates for vacuum vessel			
	Torus		Ports (unreinforced values)	
	General stress (Allow. stress= = 195 Mpa)	Peak local stress (Allow. stress= 390 Mpa) [note 1]	General stress (Allowable stress = 195 Mpa)	Peak local stress (Allow. Stress = 260 Mpa) [note 1]
Vacuum load	< 60	~ 170	< 100	~ 170
Coolant pressure (1 Mpa) [note 2]	< 150	~500	< 250	~ 500
VDE [note 3]	< 400	~ 480	< 50	~ 400
Thermal stress from nuclear htg [note 4}	< 150	~ 340	< 150	~ 340
TF ramp-up [note 5]	< 30	TBD	TBD	TBD

Notes: 1. Estimated demarcation between general and peak local stress, peak primary + secondary = 3 x Sm
2. Stress values reduced from App. D calculations by ratio of applied pressure (1.0 / 2.7)
3. VDE loads applied in simplified manner as described in Appendix D, supports on outside
   Latest design has 50% thicker section at top / bottom, stress reduction should be factor of >2
4. Temperature gradient of ~ 60 C based on 10 second full power pulse, preliminary geometry
   Allowable secondary stress = 390 MPa
5. Stress estimate based on hand calculation of hoop stress in inboard facesheets

Table 5.3.3-2 Von Mises Stress Analysis Summary for the FIRE Vacuum Vessel
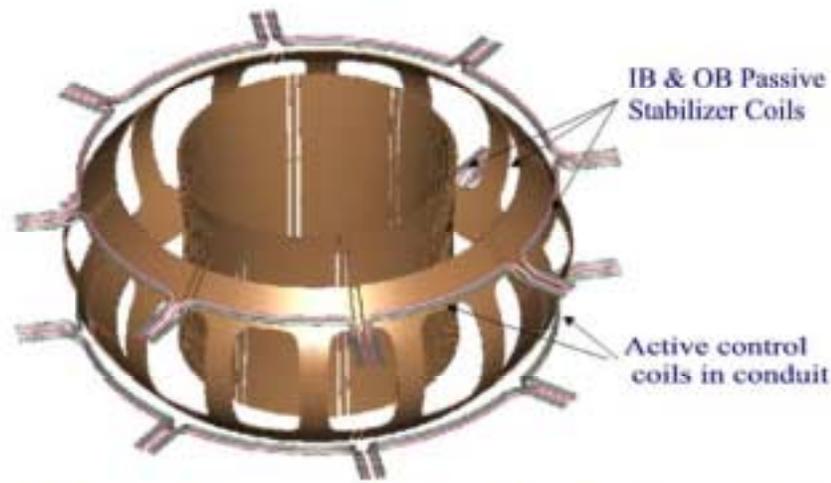
Fig. 5.3.4-1. FIRE Passive Stabilizer and Active Control Coils

first wall tiles and the vessel, and continuous structural support can be provided to the passive plates by the vessel. The method of bonding has not been decided, but hot isostatic pressing (hipping) is one possibility. The geometry of the passive plate system is shown in Figure 5.3.4-1.

In addition to the passive plates there are a pair of control coils located between the outboard walls of the vessel above and below the midplane ports. Multiple turns of conductors are run in permanent pairs of conduits that are routed directly through the outboard wall. The conductor will receive a moderately high radiation dose ($>10^9$ Rad) and will be insulated with either MgO or a polyimide insulation system. Redundant turns are being considered to mitigate one of the failure modes. Each coil is designed to carry up to 75 kA.

5.3.5 Fabrication and assembly

The vessel is fabricated in octants, as shown in Figure 5.3.5-1 Each octant consists of the torus, associated gravity and internal supports, short reinforcing stubs around the major port openings and the active and passive stabilizer systems. At assembly, each vessel octant is rotated into the bore of a preassembled TF coil pair and connected via the support links. The TF/VV subassemblies are then positioned relative to each other with the mating joints located at radial planes between TF coils, through the center of the ports.

When all the octants are in place and positioned, they are welded together from the plasma side of the torus. The field joint for the double wall structure uses splice plates on the plasma side to provide a means for accessing the coil-side facesheet from the plasma side of

the torus. This type of joint has undergone significant, full scale testing using remote welding equipment as part of the ITER R&D program. After the vessel is welded, the gaps in the passive stabilizers are filled with plasma sprayed copper to complete the upper and lower stabilizing circuits. After the torus is welded, the port extensions are fitted and welded to the port stubs. This completes the vessel assembly.
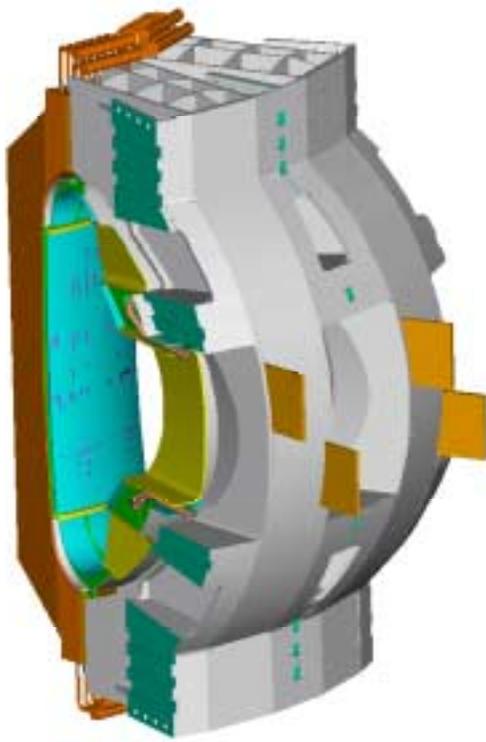
TF / VV octant assembly
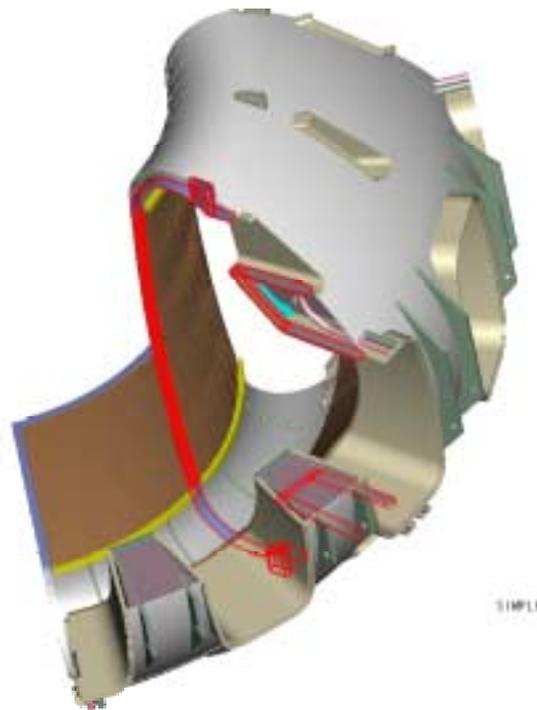
VV field assembly joint connecting
two octants with splice plates
(TF coils not shown)

Figure 5.3.5-1 Vacuum Vessel Assembly Via TF/VV Octants

5.4 Plasma Facing Components Design Description

5.4.1 Divertor Design Requirements

The FIRE device is designed for high power density and advanced physics operating modes. The divertor must accommodate the high elongation and high triangularity plasma needed for advanced physics modes. The range of triangularity, internal inductance and plasma beta are TBD. This section describes the initial divertor design based on a single plasma shape. Some design issues still remain to be resolved. The divertor geometry is forced to be quite open due to the short distances from the x-point to the plate and the spreading of the field lines. The connection lengths are short and the scrape-off layer (SOL) thickness is small. It may be hard to achieve a radiative divertor with such an open divertor. Without a radiative divertor the heat loads are high (~25 MW/m^2). While there are designs for actively cooled divertors having the capability of removing such a heat load, those designs are not yet fully qualified.

The divertor plate geometry is shown in Figure 5.4.1-1. The outer divertor plate is at an angle of 30° with respect to the flux lines. This is driven by the flux surface spreading close to the X-point. The inner divertor plate is nearly normal to the field lines. The divertor is relatively open and may not be suitable for radiative operation. The slot between the outer divertor plate and the baffle provides for pumping plasma exhaust particles.
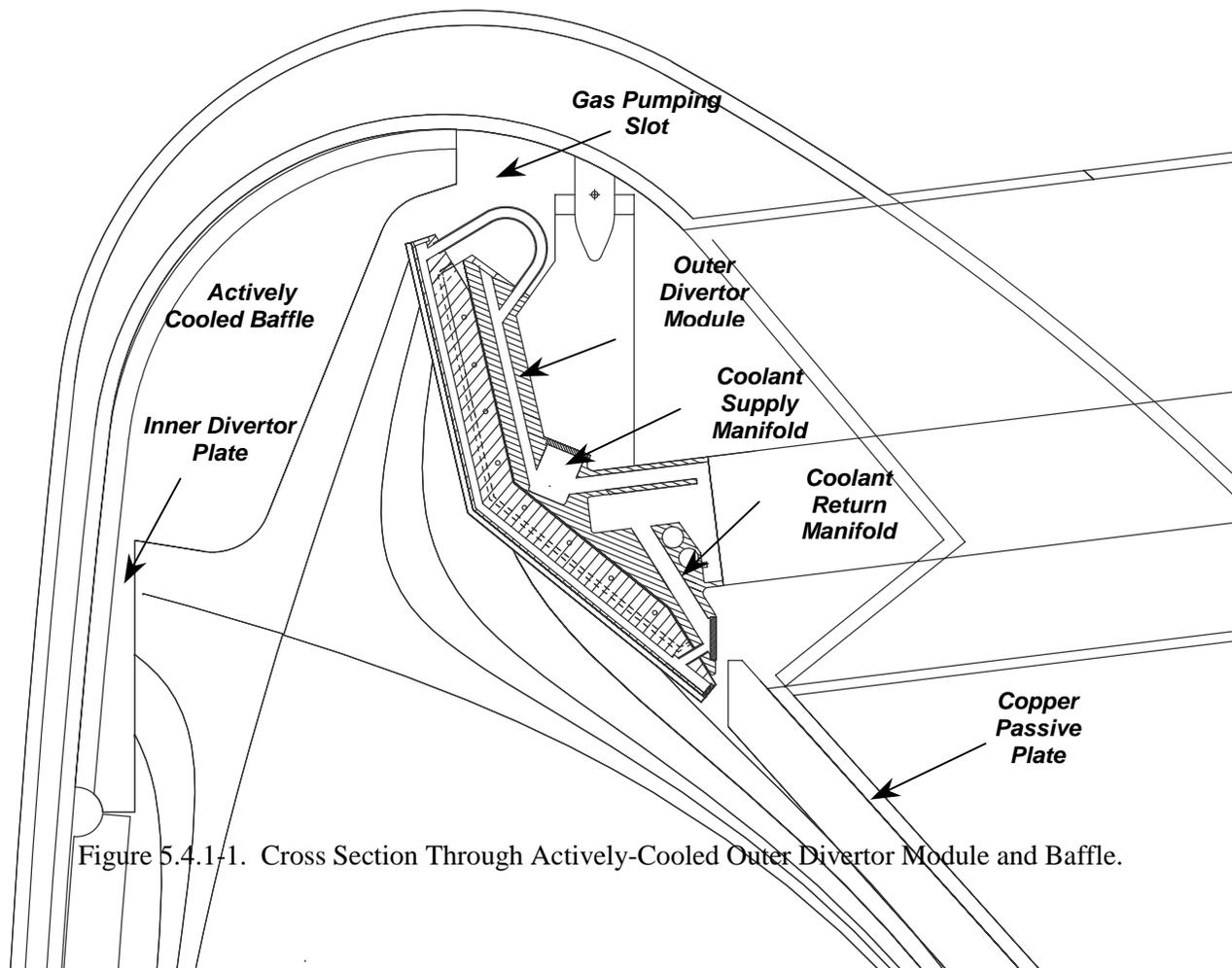
Figure 5.4.1-1. Cross Section Through Actively-Cooled Outer Divertor Module and Baffle.

The FIRE device is a very compact machine with high current and high magnetic field. The connection length along the field lines from the outer mid-plane to the divertor plate determines how much time is available for plasma energy to diffuse across the field while being transported to the divertor. The shorter the connection length, the narrower the scrape-off length. Using the magnetic field data from the equilibrium code, the connection length is 13.1 m for FIRE. Of that length, 7.4 is from the mid-plane to the divertor throat and 5.7 m in the divertor. These distances are to be compared to 125 m total length in ITER. We thus expect a narrower SOL in FIRE.

5.4.1.1 Power Flows and General Thermal-hydraulic Design

Divertor component power flows are summarized in Table 5.4.1.1- for three cases: (1) the baseline D-T operating mode (10 T, 6.6 MA, 10 s) with a plasma exhaust power of 67 MW; (2) an advanced physics D-D operating mode (4 T, 2 MA, 200 s) with a plasma exhaust power of 21 MW; and (3) a long-burn D-T mode (8 T, 5.5 MA, 50 s) with a plasma exhaust of 52 MW. The following assumptions are made concerning the distribution of these total exhaust powers: 20% is radiated from the main plasma, 20% is radiated from the scrape off layer with all being deposited on the baffle, 20% is deposited on the inner divertor plate, and the remainder goes to the outer divertor

plate. These assumptions lead to the total power distribution given in the first row of Table 5.4.1.1-1 for the three operating modes.

There are 32 modules of each type (16 upper and 16 lower). For a uniform power distribution over these modules, each must handle the average power loads given in row two of the table. Assumptions used to arrive at the peak module power loads summarized in row three of the table include: (1) 1.2 for roof-tile shadowing of the module leading edges, (2) 1.2 / 1.5 for toroidal asymmetries in exhaust power on the inner plate and baffle / outer plate, and (3) 1.2 for up-down asymmetries in exhaust power distribution. Based on proposed pulse lengths, the total energy that must be dissipated in each component is calculated in row 5 of the table. This shows that the most challenging of the three cases for the passively-cooled inner plate and baffle is the long pulse D-D mode. Passively-cooled component temperatures at the end of the pulse are estimated in the last two rows of the table, based on proposed module sizes and weights. This highlights that it is advantageous to combine the inner plate and baffle into a single component, assuming that both are copper which provides a good thermal conduction path. The large mass of the baffle helps dissipate the inner plate power deposition and keeps final temperatures at a more manageable level.

Table 5.4.1.1-1 Divertor Module Power Flow Summary.

Divertor Module Parameter	10 T Baseline (52 MW, 18 sec)			12 T Mode (66 MW, 12 sec)		
	Inner	Baffle	Outer	Inner	Baffle	Outer
Total Power Distribution (MW)	8.3	10.4	33.3	10.6	13.2	42.2
Avg Power to Module (MW)	0.26	0.33	1.04	0.33	0.41	1.32
Peak Power to Module (MW)	0.45	0.56	2.25	0.57	0.71	2.85
Pulse Length (sec)	18	18	18	12	12	12
Max Total Energy Input (MJ)	8.1	10.1	40.4	6.8	8.6	34.2
Module Volume (m³)	0.0076	0.0476	0.0437	0.0076	0.0476	0.0437
Module Mass (kg)	67.7	339.2	388.5	67.7	339.2	388.5
Initial Temperature (°C)	30	30	30	30	30	30
Average Final Temp (°C)	122	105	–	101	93	–
Front (W) Surface Temp (°C)	220	250	–	193	193	–
Rear Surface Temp (°C)	92	–	–	75	–	–
Divertor Module Parameter	Long Pulse (17 MW, 215 sec)			Long Burn (44 MW, 31 sec)		
	Inner	Baffle	Outer	Inner	Baffle	Outer
Total Power Distribution (MW)	2.7	3.4	11.0	7.0	8.8	28.2
Avg Power to Module (MW)	0.09	0.11	0.34	0.22	0.28	0.88
Peak Power to Module (MW)	0.15	0.18	0.74	0.38	0.48	1.90
Pulse Length (sec)	215	215	215	31	31	31
Max Total Energy Input (MJ)	31.8	39.8	159.1	11.8	14.7	58.9
Module Volume (m³)	0.0076	0.0476	0.0437	0.0076	0.0476	0.0437
Module Mass (kg)	67.7	339.2	388.5	67.7	339.2	388.5
Initial Temperature (°C)	30	30	30	30	30	30
Average Final Temp (°C)	100	325	–	146	139	–
Front (W) Surface Temp (°C)	153	>700	–	251	350	–
Rear Surface Temp (°C)	80	–	–	112	–	–

Using the same power loading conditions, module cooling channel design parameters and flow rates have been estimated. The results of this are summarized in Table 5.4.1.1-2. Based on the ITER vertical target design and manufacturing development, the FIRE divertor modules are divided into 24 copper "finger" plates across the front surface. This modular design configuration is described in the next section. It provides a simple part for initial fabrication and tungsten-armor joining / acceptance testing, and reduces electromagnetic loads by breaking up eddy current loops in the front, copper structure. The Critical Heat Flux (CHF) margin is provided by 10-m/s flow in the 8-mm-diameter cooling channels with swirl-tape inserts. Each copper finger includes 2 cooling channels for a total of 48 across the heated surface. All channels are supplied in parallel giving an 18 liter/s inlet flow rate for each module and an estimated 0.4 MPa pressure drop in the module. The recommended inlet water conditions of 30°C and 1.5 MPa pressure give a minimum exit subcooling of 124°C for the peak heat loading condition. Remote cutting and welding operations for module removal are simplified by using a coaxial supply pipe layout. The inner coaxial pipe diameter of 80-mm accommodates insertion of remote cutting / welding equipment down the supply pipe, and also gives a supply pipe flow velocity of 3.6 m/s, which keeps pressure drops manageable in this portion of the cooling system.

Table 5.4.1.1-2   Outer Divertor Module Thermal-Hydraulic Design Summary.

Divertor Module Parameter	Value
Avg Power to Module (MW)	1.07
Peak Power to Module (MW)	2.32
Number Cooling Channels	48
Cooling Channel Dia (mm)	8.0
Flow Area, 25% SWT (mm²)	37.7
Water Flow Velocity (m/s)	10.0
Module Flow Rate (liter/s)	18.1
Water Inlet Temperature (°C)	30
Inlet Pressure (MPa)	1.5
Pressure Drop (MPa)	0.4
Exit Pressure (MPa)	1.1
Exit Saturation Temp (°C)	184.3
Nominal Temp Rise (°C)	14.2
Nominal Exit Temp (°C)	44.2
Nominal Exit Subcooling (°C)	140.1
Maximum Temp Rise (°C)	30.7
Maximum Exit Temp (°C)	60.7
Min Exit Subcooling (°C)	123.6
Inlet pipe flow velocity (m/s)	3.6
Inlet pipe ID (mm)	80.0
Coaxial pipe OD (mm)	122.7

5.4.1.2   Disruption Heat Loads

Using the disruption conditions specified in the Physics Design Document, the energy deposition on the divertor plates and first wall can be estimated. Two phases have been identified for disruptions; the thermal quench phase when the plasma stored energy is lost to the divertor and the current quench phase when the plasma current decays and the magnetic stored energy is lost to the first wall. We have assumed a plasma-stored energy of 33 MJ. There is a wide range of possible parameters describing disruption energy deposition, so the energy deposition is specified as a range of possible values. The wide range arises because of incomplete understanding of disruption deposition on existing devices, variation in the deposition observed, and uncertainties in the extrapolation to FIRE conditions. The values specified for the disruption analysis are shown in Table 5.4.1.2-1.

During the current quench phase of a disruption, the plasma is very cold and highly radiative. The magnetic stored energy is radiated to the first wall during the current decay. The stored magnetic energy in the FIRE reference plasma is 35 MJ. The expected minimum current decay time is 2-6 ms. The average energy deposition on the

Table 5.4.1.2-1 Disruption energy deposition on the divertor plates

	Low End	Most Likely	Reference	High End
Inner Divertor	8 MJ/m^2	31 MJ/m^2	13.4 MJ/m^2	96 MJ/m^2
Outer Divertor	4MJ/m^2	16 MJ/m^2	6.8 MJ/m^2	48 MJ/m^2

first wall is 0.5 MJ/m^2. If we assume a toroidal peaking factor of 2:1, the peak energy deposition is 0.67 MJ/m^2. This is enough energy to melt 0.12 mm of Be if all the energy goes into melting. Thermal conduction and radiation will reduce the amount of melting. This should give an adequate lifetime for the first wall but further modeling is required.

5.4.1.3 Halo Current Loads

The halo current specifications from the Physics Design Document were used to estimate the halo currents flowing through the divertor and first wall components. Since the product of the maximum halo current fraction and the toroidal peaking factor is a constant for the worst case halo currents, the halo current in the worst location is constant. The maximum current flowing through a divertor module is 200 kA. The longest current path through the outer divertor is 0.4 m and the longest path through the inner divertor is 0.14 m. The calculated force on the outer divertor is 0.77 MN while that on the inner divertor is 0.3 MN. These forces are one of the requirements for sizing the supports for the divertor and the thickness of the support plates.

5.4.1.4   Disruption Eddy Current Loads

The duration of the current disruption specified in the Physics Design Document was used to estimate the eddy currents induced in the divertor structures for the case of a stationary plasma disruption. The maximum current decay rate is 3 MA/ms. This implies that a 6.5 MA plasma will decay in 2.2 ms. The only disruption case available is for a plasma that disrupts without moving. Both a radial inward

motion case and a vertical displacement event need to be calculated before the disruption analysis is complete. The divertor plates have been modeled assuming they are independent of the rest of the machine structure (i.e., assuming no vacuum vessel or protective plates. The outer divertor plate is 0.73m by 0.63m and is 0.06m thick. The L/R time for the outer divertor plate is 30 ms. Similar values are obtained for the inner divertor plate. Since the L/R time is much longer than the disruption time, the purely inductive solutions for the eddy currents are taken. The induced currents are 300kA for the outer divertor and 750 kA for the inner divertor. The force on the divertor modules is then 1.9 MN (outer divertor) and 2.8 MN (inner divertor). These loads will determine the size of the divertor supports and backplate.

5.4.2   Outer Divertor Module Design

5.4.2.1   Design Description and Tungsten Armor Concept

The actively-cooled, outer divertor module design is shown in Figure 5.4.2.1-1 which can be used in conjunction with the Figure 5.4.1-1 cross-section to describe the module design features. The design concept builds on fabrication technologies developed for the ITER divertor and consists of 24, modular, copper-alloy "finger" plates that are mechanically attached to a stainless-steel support structure that spans the toroidal width of the module. The support structure includes machined distribution and collection manifolds that route coolant to the individual finger plates and features for remotely attaching the modules to the vacuum vessel.

Alternating colors denote copper-alloy finger plates. Left-most plate is separated from backing plate for clarity.
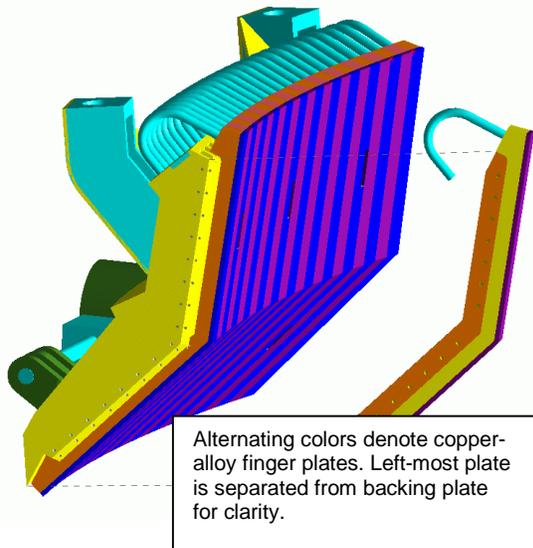
Figure 5.4.2.1-1. Outer Divertor Module Design

The Figure 5.4.1-1 cross-section depicts the coolant flow path in the module. Coolant enters through the outer annulus of the coaxial supply pipe. It is distributed across the module toroidal width in the upper supply manifold and then flows upward through gun-drilled holes in the steel backing plate to curved, welded pipes that feed the front copper finger plates. Flow then passes down each finger plate in two parallel 8-mm-diameter channels, and exits at the bottom into the lower return manifold. A machined slot at the toroidal center of the return manifold routes coolant back to the inner return pipe. The 8-mm front-plate channels include swirl-tape inserts over the upper straight section for heat transfer enhancement.

5.4.2.2   Module Fabrication and Assembly

Figure 5.4.2.2-1 illustrates further design features of the module using a toroidal section view. The copper alloy finger plates have a T-shaped back surface that fits into machined slots in the stainless structure as indicated. Press-fit pins are then inserted into angled holes to attach the copper front plates to the support structure. Over the upper section of the plate, where surface heat fluxes are highest, machined slots are used in place of the angled holes to allow the pins to slide axially relieving some of the stress build-up from thermal expansion in the highly-heated copper front plate. The upper looped-pipes provide a flexible cooling attachment to the backing structure to accommodate this motion. These features are not needed at the lower end of the target where surface heat fluxes are much lower. Finger plates are identical except at three locations in each module where one of the two axial holes is eliminated. This provides poloidal slots, as indicated in Figure 5.4.2.2-1, for insertion of remote handling grippers near the module outer edges and diagnostic access at the module centerline.
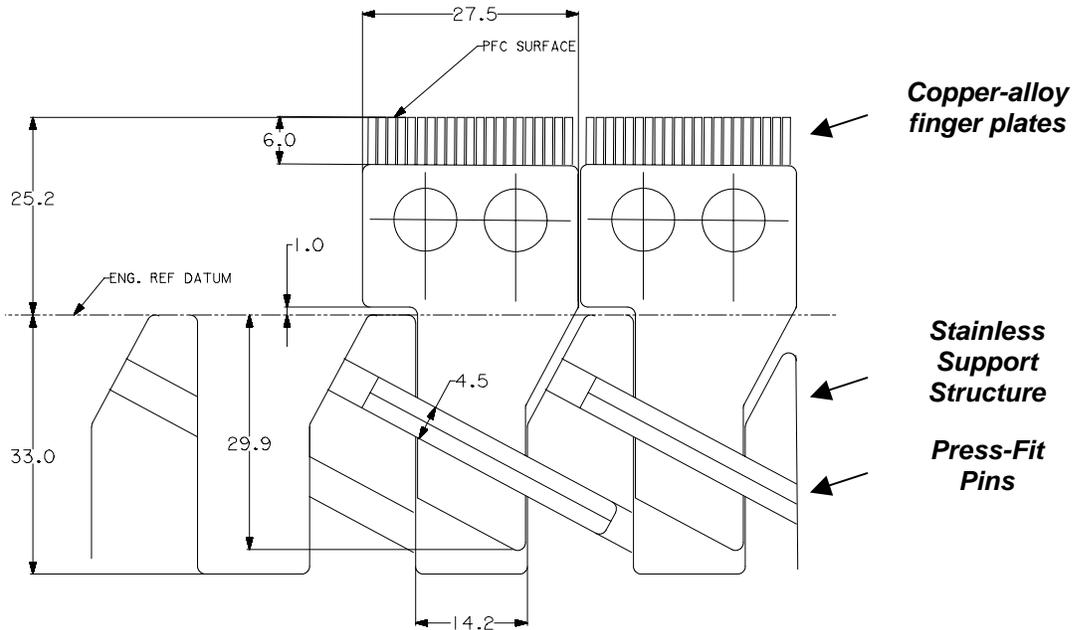
Figure 5.4.2.2-1. Angled Press-Fit Pins Attach Finger Plates to Stainless-Steel Backing Structure.

The copper fingerplates include tungsten-brush armor similar to the mock-ups depicted in Figure 5.4.2.2-2. This armor geometry has been shown to survive incident heat fluxes of 25 MW/m² for 1,000 cycles in testing at Sandia Labs [Ref.] using several different joining procedures. All of the brush armors use small-diameter tungsten (W) weld electrodes (3-mm preferred based on testing) that are fixtured in thin welded metal honeycomb for joining to the heat sink. The rod assembly can be direct-bonded (vacuum hot press or Hot Isostatic Press – HIP) to the heat sink or embedded in a layer of plasma sprayed copper and then HIP-bonded or e-beam welded. Work is currently planned to down-select two of the W-brush-armor joining approaches for the fabrication of armored copper finger plates that are comparable in size to those proposed for the FIRE divertor. These mock-ups will include a heat-transfer enhancement mechanism in the cooling channel (swirl tape or helical wire insert) and be HHF tested under similar exit CHF conditions. This will complete a full-scale demonstration of critical heat sink fabrication and armor joining procedures for advanced, actively-cooled divertor concepts like FIRE.

1/16-inch dia W-rods with plasma-sprayed copper layer HIP-bonded to Cu-alloy heat sink

1/8-inch dia W-rods vacuum hot pressed to Cu-alloy heat sink with explosion-bonded copper
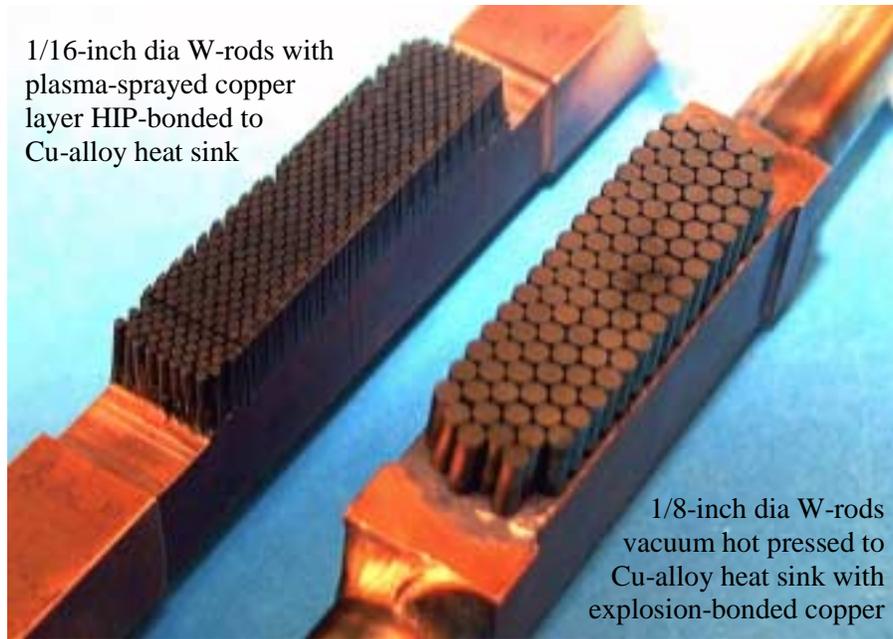
Figure 5.4.2.2-2. Two of the Tungsten Brush Armor Configurations Tested at 25 MW/m².

5.4.2.3   Vessel Attachment and Remote Handling

The divertor modules are mounted to the vessel using the lug and shear-pin arrangement indicated in Figure 5.4.2.3-1. To accommodate remote insertion and removal operations, the primary module-positioning feature involves two 42-mm-diameter vertical pins that are attached to the vessel as shown in Figure 5.4.2.3-2. The large mounting brackets shown in Figure 5.4.2.3-1 engage these conical-ended pins as the modules are raised or lowered into position by the in-vessel handling system. Final mounting holes in the modules are individually machined based on an in-vessel survey of the pin locations so the plasma-facing surface is correctly positioned in the magnetic field geometry. The upper section of these large pins are cylindrical allowing the module vertical position to be adjusted until the lower, locking pins can be inserted. The two locking pins are activated by radial drive shafts that extend out the vacuum port adjacent to the cooling pipe as indicated. These pins are offset so each can retract into the solid lower portion of the inlet piping interface connection.

The module mounting hardware shown in Figure 5.4.2.3-1 was sized based on preliminary guidelines for halo current loading conditions. These guidelines assumed 240 kA for the maximum current. For the reference toroidal field strength of 10 T, and module poloidal length of 0.63 m, this implies a peak module halo current loading of 1.5 MN that must be reacted in the support structure. Assuming this load is distributed among the four module attach points with a peaking factor of 1.5, the design load on any one attachment is 0.56 MN. Using Inconel 718 pins, which have a structural allowable of 393 MPa at 200°C, the pin diameter must be 42 mm for a single shear-interface attachment. The lower locking pins use multiple shear interfaces to reduce the pin diameter to 20-mm. These halo currents are slightly larger than the

physics specification (see Sections 1.1.3 and 1.1.4), but the range of disruption eddy

current loads, yet to be analyzed will likely require a larger pin.
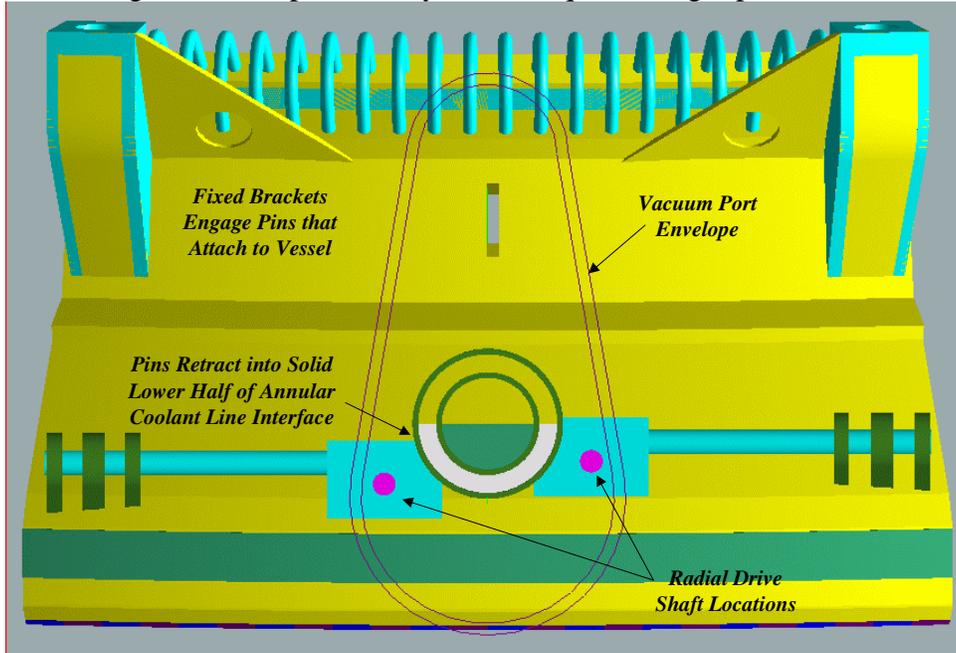
Figure 5.4.2.3-1 Outer Module Vessel Attachment and Remote Handling Features.
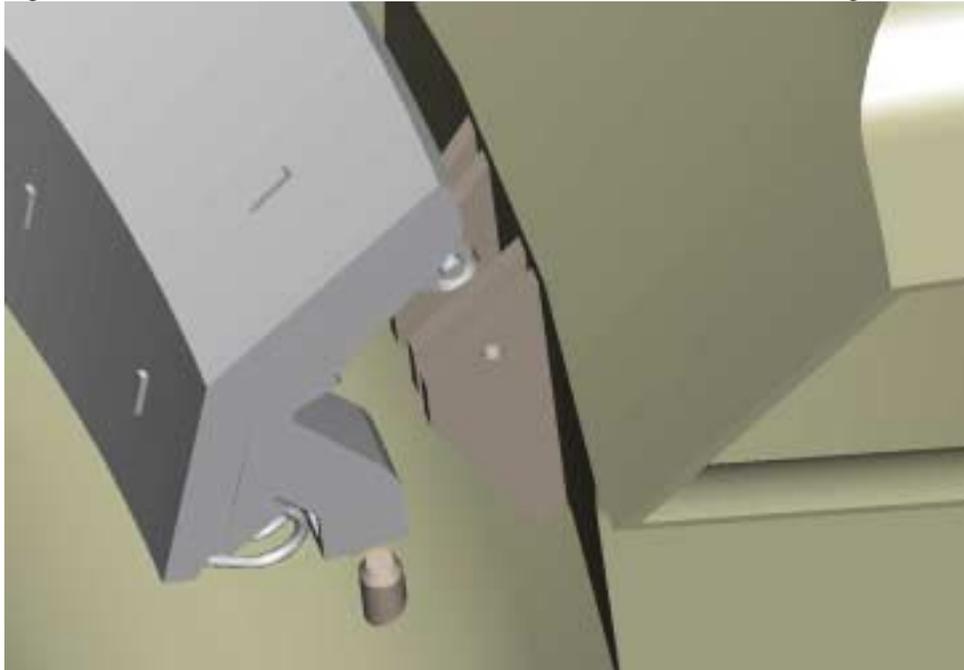
Figure 5.4.2.3-2. Divertor Module In-Position to Engage Vessel Attachment Hardware.

Additional divertor module design and handling constraints are illustrated in the Figure 5.4.1-1 cross section view. Copper passive plates are required near the X-point

for plasma stability, as indicated in the figure. These plates are mounted to the vacuum vessel for cooling and form a low-resistance toroidal loop. The outer divertor

modules must clear the upper end of these passive plates during vertical installation and removal operations.   This severely limits the space envelope for attachment and cooling interface structure at the lower end of the module. The cooling interface must remain at its present elevation in the vacuum port envelope because the upper section of the ports is reserved for cryo-pumps and diagnostic access. Finally, the attachment structure must not interfere with the finger plate cooling supply tubes and manifold channel cover plates, yet be stiff enough to react disruption electromagnetic loads. Detailed loading conditions have not yet been calculated for the FIRE modules, but it appears that the general attachment layout shown in Fig. 5.4.2.3-1 can be adapted to meet these design constraints.

5.4.3   Inner Module, Baffle and First Wall Design

5.4.3.1   *Inner Plate and Baffle Design and Armor Concept*

The inner divertor plate and baffle are expected to require minimal cooling for the reference FIRE power loads and pulse lengths. The baffle structures are passively cooled elements that fill the flux space between the inner and outer divertor channels. The baffle configuration is shown in Figure 5.4.3.1-1 for reference.
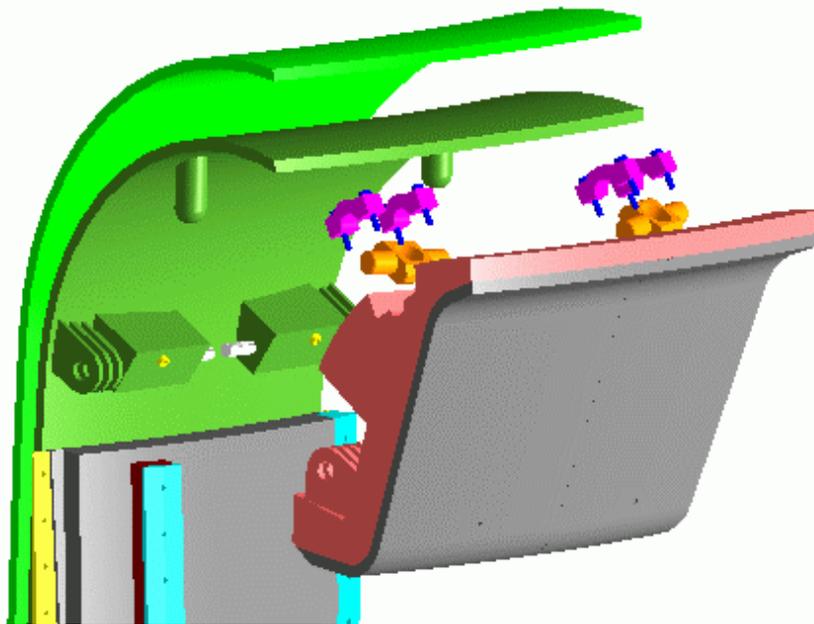
Figure 5.4.3.1-1 Baffle configuration and attachment concept.

The first wall consists of passively-cooled, mechanically attached tiles that line the inner and outer vessel surface between mid-plane ports. They are made from 40-mm thick formed/machined CuCrZr plate covered with 5-mm of plasma-sprayed Be armor. The plates fit between wedge-shaped vertical rails that are bolted to the vacuum
.

vessel as indicated in Fig. 5.4.3.1-2.   The rails are segmented to facilitate local tile removal. The gaps allow for easy insertion and differential tile thermal growth during operation. Armored copper cover plates secured by washer-loaded quarter-turn fasteners hold the tiles against the vessel during normal operation
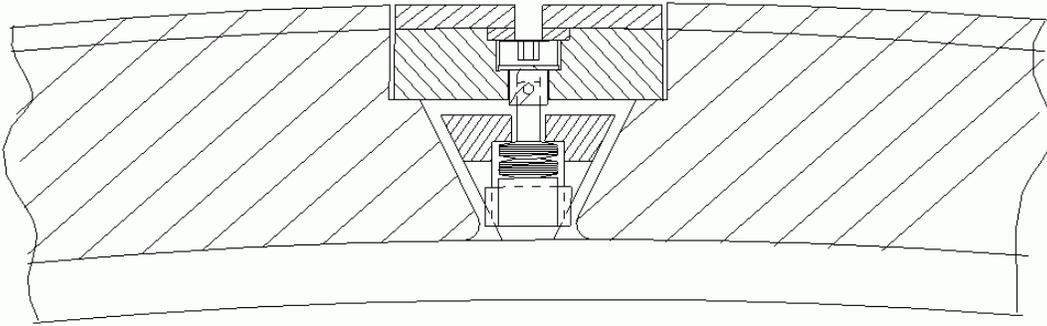
Figure 5.4.3.1-2 First-wall tile attachment concept.

Passive inner plate and baffle temperature excursions for the proposed FIRE operating conditions are summarized in Table 5.4.1.1-1. This table shows that the low field, long pulse operating mode is the most challenging one for passive cooling. As is summarized in Table 5.4.1.1-1, these plates appear to have sufficient energy storage to survive anticipated heat loads without excessive temperature excursions. They are then slowly cooled between pulses by conduction to the vacuum vessel. When more definitive power flow distributions and design concepts are available, 2-D thermal models will be developed to determine temperature distributions in these components and verify that temperature excursions are acceptable for all operating modes.

The design requirements call for a 10 sec pulse length. Since the heat soaks into the plasma-facing component during the pulse, the back surface temperature where the material is attached to the heat sink will likely be the most limiting factor (not the surface temperature). Figure 5.4.3.1-3 shows the allowed pulse duration for various heat fluxes assuming the temperature at the connection does not exceed 700°C. Heat loads on the first wall are low compared to the divertor. Beryllium on the first wall can be used up to about 3 MW/m^2 for 10 sec.
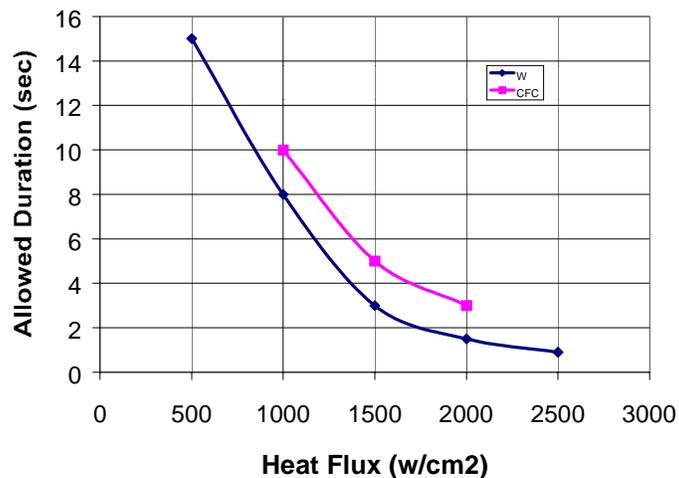

Figure 5.4.3.1-3. Allowed pulse duration to not exceed 700°C on the back face of a 3 cm thick tile.

5.4.3.2 First Wall Design Considerations

Figure 5.4.3.2-1 shows the temperature increase a 5-mm tungsten / 30-mm copper first wall structure experiences, under 30 W/cm^2 incident heat flux, for different thermal cooling assumptions at the rear surface. The upper curves assume no rear surface cooling. The middle curves assume a 0.14 W/cm^2-K interface conductance at the rear surface, which is representative of limited-area mechanical attachments. The lower curves assume a 1.4 W/cm^2-K interface conductance at the rear surface, which is representative of active cooling over ~10% of the rear surface area. The 30 W/cm^2 incident flux is derived for the

long pulse D-D operating mode assuming that all 21 MW of exhaust power is radiated uniformly to the first wall. Figure 5.4.3.2-1 shows that active cooling is likely to be required for the long pulse operating modes. Mechanical attachments could possibly accommodate a 2-min pulse, but the vessel must provide a 30°C heat sink at the mechanical attach points. This would require special cooling of these attachments to assure that large temperature gradients are not induced in the 15-mm thick, stainless-steel vessel shell.
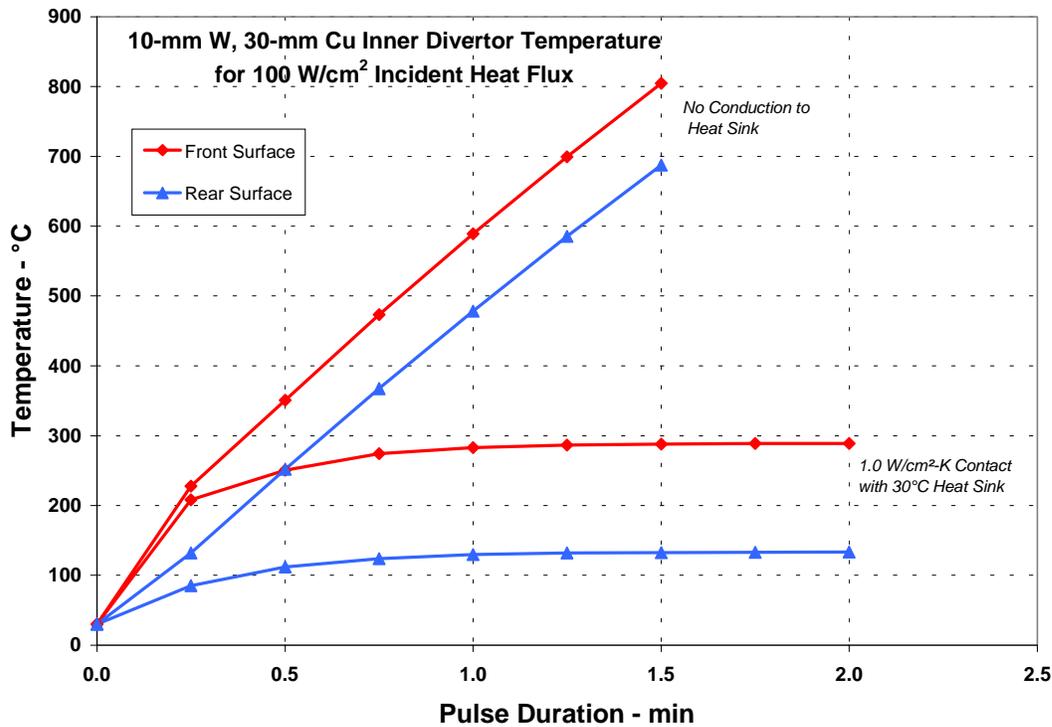

Figure 2. First Wall Temperature Increase at 1.0 MW/m^2 Incident Heat Flux for 1 W/cm^2 °C heat transfer at the Rear Surface.

It therefore appears that active cooling of the first wall should be considered to provide more robust long-pulse operation. This could be accommodated by incorporating a cooling header between the two vessel shells at the top and bottom of the machine that feeds water to the baffle. The water would then flow through the first wall modules in a limited number of cooling channels to keep the copper temperatures under control and exhaust into the vessel at the mid-plane. Non-uniform radiative loading effects must also be evaluated to determine appropriate local peaking factors for the 30 W/cm^2 incident flux.

5.4.4 Performance Assessments

5.4.4.1 Edge Plasma Modeling For Attached Divertor Conditions

The UEDGE code was used to calculate the expected edge conditions in FIRE. For all cases considered the power into the scrape-off layer was 28 MW and the separatrix density was 1.5 x 1020 /m^3 with a wall recycling coefficient of 1.0. Three different values of the particle and heat diffusivity were considered. The parameters in Case C duplicate edge plasma data from existing machines the best and were the conditions used for the ITER design. The divertor plate was kept perpendicular to the field lines for most cases. Case D is the same as Case C with the divertor plate tilted as in the baseline design and with 10^{21} particles/sec pumping. The conditions for the various cases are shown in Table 5.4.4.1-1.

Table 5.4.4.1-1 Plasma transport parameters used for modeling the FIRE edge plasma.

Case	Description	Thermal diffusivity (m^2/s)	Particle diffusivity (m^2/s)
A	High Conductivity	1.5	1.0
B	ITER Conductivity	0.5	1.0
C	Bohm like diffusivity	0.5	Dbohm + 0.1
D	Tilted plates and pumping	0.5	Dbohm + 0.1

Note: Dbohm = Te/16 eB

The results are shown in Table 5.4.4.1-2. The peak heat flux is less than 25 MW/m^2 for all cases. The outer divertor is not detached under any of the conditions considered. Additional gas will have to be added to the model to get the outer divertor to detach. Table 5.4.4.1-3 shows the ratio of the power to the divertor plates to the power in the scrape-off layer. The power radiated to the first wall (Pwall) and the power radiated by hydrogen are also shown. It can be seen that the inner divertor is detached for all cases considered.

Table 5.4.4.1-2 Results of UEDGE modeling of the FIRE edge plasma

Case	Te$_m$ (eV)	λ_m (cm)	Te$_p$ (eV)	ne$_p$ (10^{21}/m^3)	Q$_p$ (MW/m^2)	λ_p (cm)
A	106	0.8	1.5	61	5.7	6.5
B	152	0.6	15	44	25	1.8
C	138	0.7	14	43	23	2.3
D	138	0.7	13	52	19	2.5

Table 5.4.4.1-3 The ratio of power to the divertor plates and the wall to the power in the scrape-off layer for the various cases.

Case	P_{in}/P_{sol}	P_{out}/P_{sol}	P_{wall}/P_{sol}	P_{hrad}/P_{sol}
A	0.003	0.24	0.34	0.42
B	0.002	0.53	0.12	0.35
C	0.005	0.58	0.11	0.31
D	0.09	0.57	0.10	0.24

5.4.4.2   Edge Plasma Modeling for Detached Divertor Conditions

The UEDGE Code has been used to study the effect of adding Beryllium and Neon to the edge plasma to stimulate detachment of the plasma in the outer divertor channel. The divertor plates were placed at the proper angle relative to the field lines for these calculations. The particle diffusivity and thermal conductivity had to be reduced on the small radius side of the plasma to achieve a single solution. One expects that the transport will be reduced on the small radius side of the plasma because of the good curvature in that region (this is consistent with the observations of less power transport to the inner divertor in a double null configuration).

The inner divertor is easily detached from the plate. With no impurity addition to the inner divertor the heat flux to the plate is about 1 MW/m^2 from particle transport and 1.8 MW/m^2 from hydrogen radiation. We used 3 MW/m^2 for the heat flux on the inner divertor.

The results for the outer divertor with the angled plates are very similar to the results for the plate normal to the field lines (26 MW/m^2). When Be is added to the divertor region, the peak heat flux is reduced to 20 MW/m^2 with about 5 MW/m^2 of radiated power located at a different location from the peak particle heat flux. There was no detachment with the addition of Be alone. With Neon injection, the plasma could be detached from the divertor plate. For 4.1 Pa m^3/s (31 Torr l/s) Ne injection there was no detachment but the peak heat flux was reduced to 15 MW/m^2. With 4.7 Pa m^3/s (35 Torr l/s) Ne injection, the plasma did detach from the divertor plate but the solution evolved toward an x-point MARFE (see Figure 5.4.4.2-1. Note that the radiated power is 80 MW/m^3 in the MARFE region. It is clear that the amount of Ne injected into the divertor needs to be controlled, but the range of injection that is needed is TBD. A scheme for feedback control of the Ne injection will have to be developed.
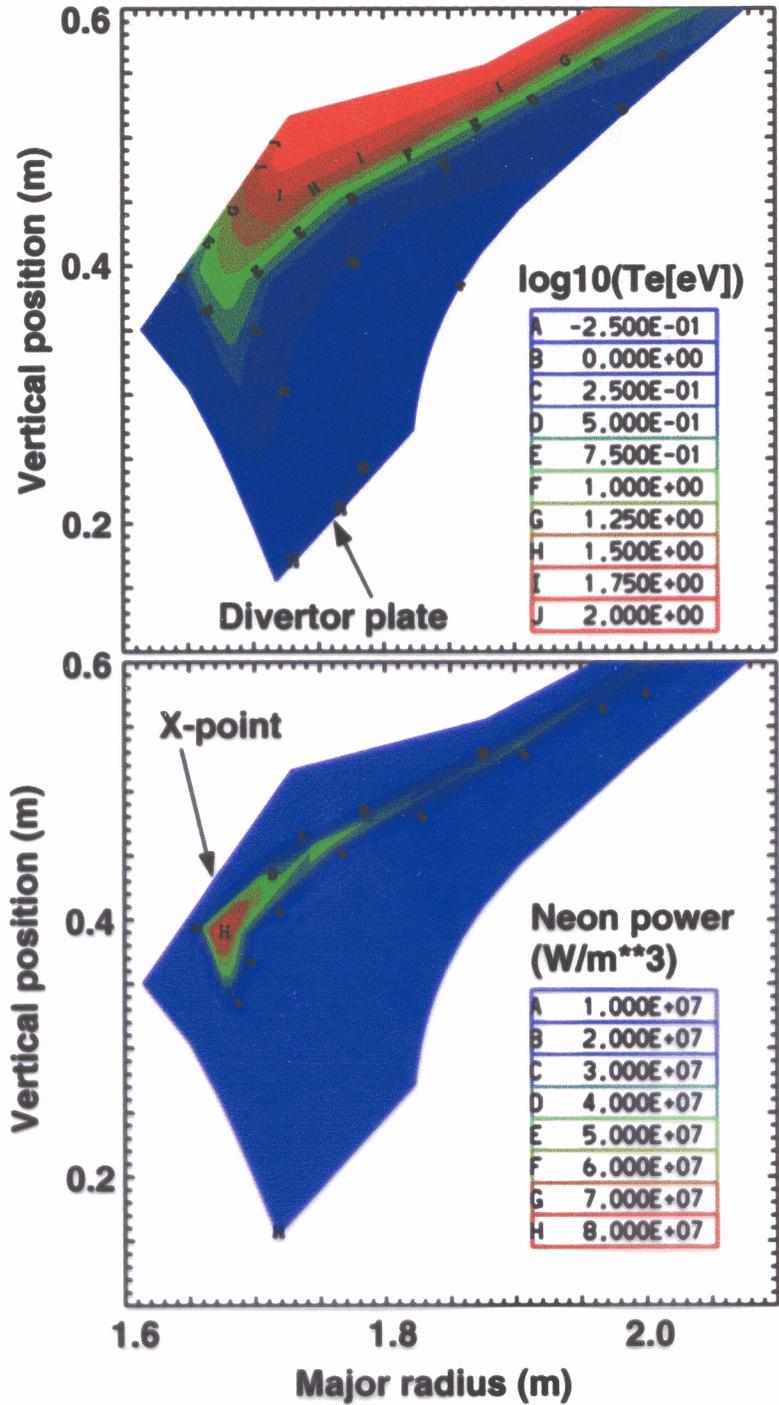
Figure 5.4.4.2-1 Detached outer divertor solution calculated by the UEDGE code

5.4.4.3   Particle Pumping Requirements

The loss of particles from the plasma can be estimated by considering the total number of particles in the plasma and the particle confinement time. The total number of particles in the plasma (NV) is 1 x 10^{22}. The

energy confinement time is 0.5-0.8 s (we will use 0.65 s). Typically we take the particle confinement time to be 2-10 τ_E. This yields a required fueling rate of 3.1 x 10^{21}/s (1.25-10 x 10^{21}/s). If we assume the fueling efficiency is 50%, the required fueling rate is 6.2 x 10^{21}/s (23 Pa m^3/s; range 10-75 Pa m^3/s). We recommend 75 Pa m^3/s as the maximum fueling rate (net with equal D and T).

We have also estimated the particle pumping rate required for He removal. The fusion burn rate (helium generation rate) is 1 x 10^{20}/s (200 MW). If we assume the He fraction in the divertor is 0.02 and the wall recycling coefficient 0.5, the required divertor pumping is 1.4-2.7 x 10^{22}/s (50-100 Pa m^3/s). This result is very similar to the previous estimate of fueling required. In order to have some excess capacity in the pumping system, we recommend providing pumping for up to 100 Pa m^3/s.

5.4.4.4   CHF Assessment

As described in Section 5.4.2, each outer divertor module consists of 24 segments, 28 mm in width and 550 mm in length. There are two coolant channels of 8 mm ID per segment. The flow direction is poloidal so that power input to each channel is equal. The maximum power flow to a divertor module is 2.32 MW. Since the peak heat flux is estimated to be 20 to 25 MW/m2, a heat transfer enhancement method will be used to achieve the necessary critical heat flux (CHF) with moderate velocities and flows. A review of enhancement methods shows that a swirl tape insert is an attractive option due to available performance data and extensive fabrication experience for this geometry.

Figure 5.4.4.4-1 shows CHF at the coolant channel wall (WCHF) calculated for the divertor module at three different inlet

pressures and a range of inlet flow velocities for an inlet temperature of 30 C. This plot includes the effect of coolant temperature rise and pressure drop and calculates the CHF at the worst location, i.e. the exit where the pressure is lowest and coolant temperature is highest.

Figure 5.4.4.4-1. Predicted Wall CHF for the Proposed FIRE Divertor Module Cooling Channel Design Concept and Exit Coolant Conditions
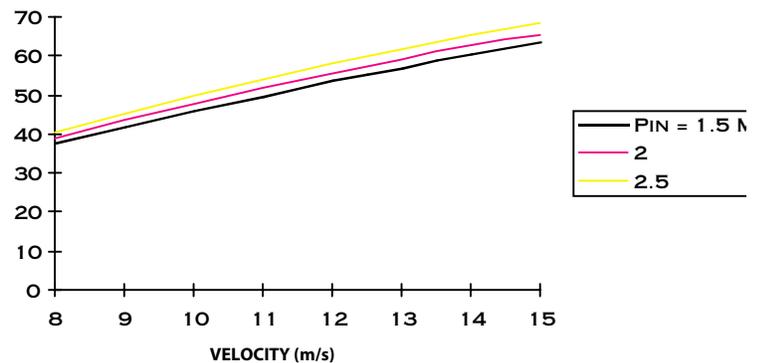
For the conditions described above, an inlet pressure of 1.5 MPa and a flow velocity of 10 m/s should be adequate for the divertor cooling. The ratio of the incident heat flux to wall heat flux for a 28 mm wide Cu-Cr-Zr module with two 8 mm channels is estimated to be 1.33, based on previous analysis done for ITER. Thus, the cooling will permit an incident critical heat flux of 34.6 MW/m^2, allowing a sufficient safety margin. The estimated pressure drop in the module is 0.45 MPa, including the effect of the swirl-tape insert.

A 3-D finite element analysis with axial heat flux profile will be undertaken in the future.

5.4.4.5 Erosion Due to Normal Plasma Operation

The erosion of the W and Be plasma facing materials due to normal plasma operation has been assessed using a combination of the DEGAS2, REDEP/WBC and BPHI codes. The plasma conditions calculated by UEDGE, were used as input to the DEGAS2 code to determine the charged and neutral particle fluxes to the divertor plates. An example of the results of the DEGAS2 modeling for the attached outer divertor case is shown in Figure 5.4.4.5-1. The plasma temperature and density profiles from UEDGE were then used to calculate thedetailed characteristics of sputtered tungstentransport using the WBC code. The code includes the sputtered atom velocity distribution, electron impact ionization, Lorentz force motion, magnetic and Debye dual structure sheath, impurity-plasma charge changing and velocity changing collisions.

The WBC redeposition parameters were used as input to the REDEP code that computes self-consistent gross and net erosion rates over the entire outer divertor region. The results predict zero net erosion of the divertor plate and no plasma contamination (see Figure 5.4.4.5-2). This is mostly due to the short mean-free path for ionization for W (2.4×10^{-5} m). The gross sputtering is mostly due to impurity sputtering (due to 0.1% O impurity) and self-sputtering. The effect of Be and Ne impurities in the edge plasma need to be added to the calculation. The detached plasma solution will also have to be analyzed.

Fig. 5.4.4.5-1. Particle flux on the outer divertor plate from DEGAS2
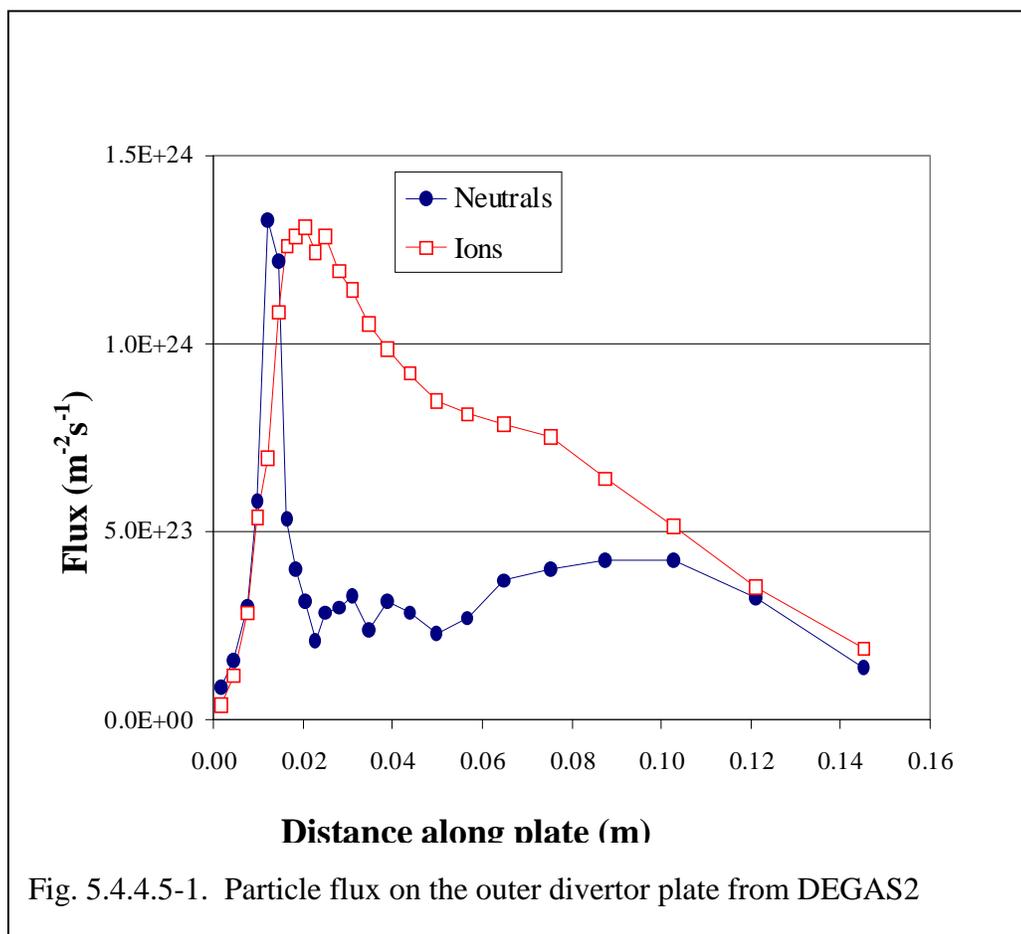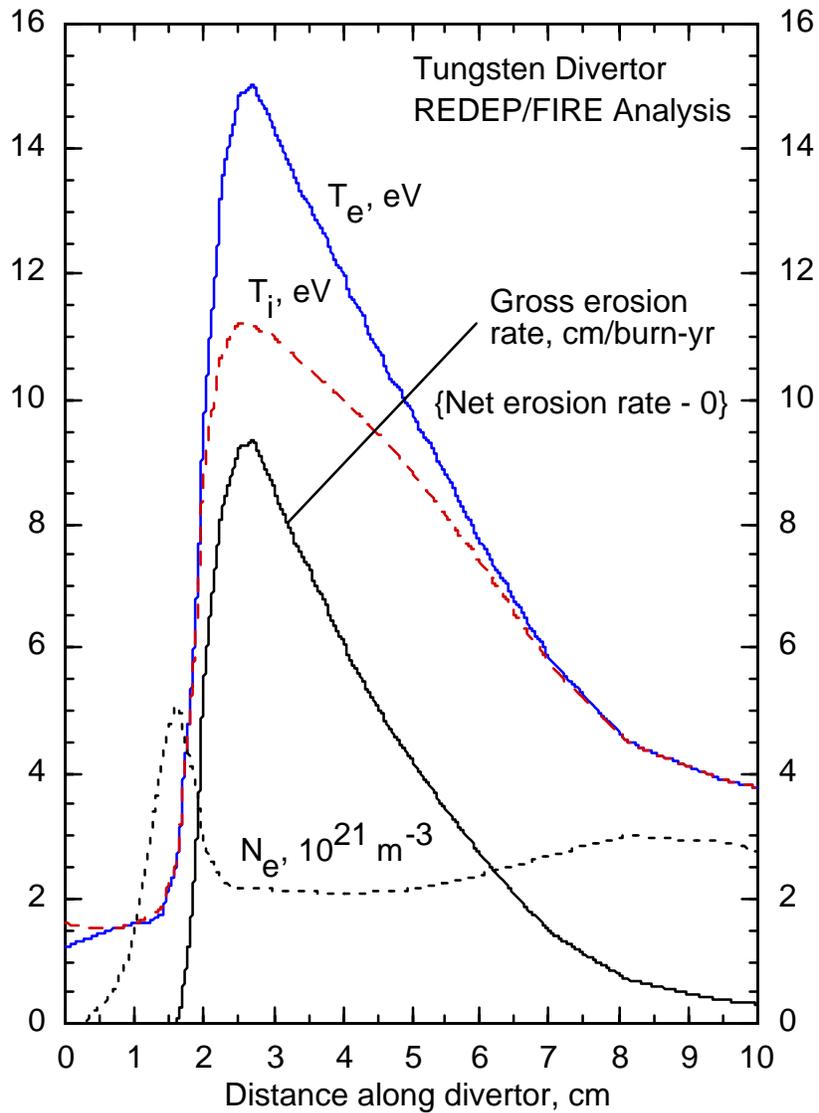
Figure 5.4.4.5-2. Results of the REDEP/WBC analysis of gross and net erosion on the outer divertor

5.4.4.6   Assessment of Disruption Damage to the Divertor Plasma Facing Surfaces

The HEIGHTS computer code package was used to model the damage of plasma facing components due to disruption energy deposition. The code package includes the effect of plasma-target interactions, plasma-debris interactions, photon radiation and transport, and plasma-melt layer interaction. A typical result for 10MJ/m^2 deposition in 1 ms is shown in Figure 5.4.4.6-1. It can be seen that melting starts about 10 μs after the disruption thermal quench starts. Vaporization starts about 20 μs later. Once vaporization starts there is a strong reduction in the heat flux because of interaction between the plasma and the atoms in the vapor (vapor shielding). Because of vapor shielding, the amount of melted and eroded

material is only weakly dependent on the energy deposited. A comparison of 100 MJ/m^2 and 10 MJ/m^2 is shown in Figure 5.4.4.6-2. It can be seen that the amount of vaporized material increases by about a factor of two due to the ten-fold increase in energy deposition. This insensitivity of the amount of melted or vaporized material to the energy deposition eliminates much of the variation due to the uncertainty in the disruption energy deposition. The analysis of divertor lifetime is therefore easier to estimate. The melt layer is predicted to be 150 to 200 μm thick and 2-4 μm is predicted to evaporate due to a disruption.
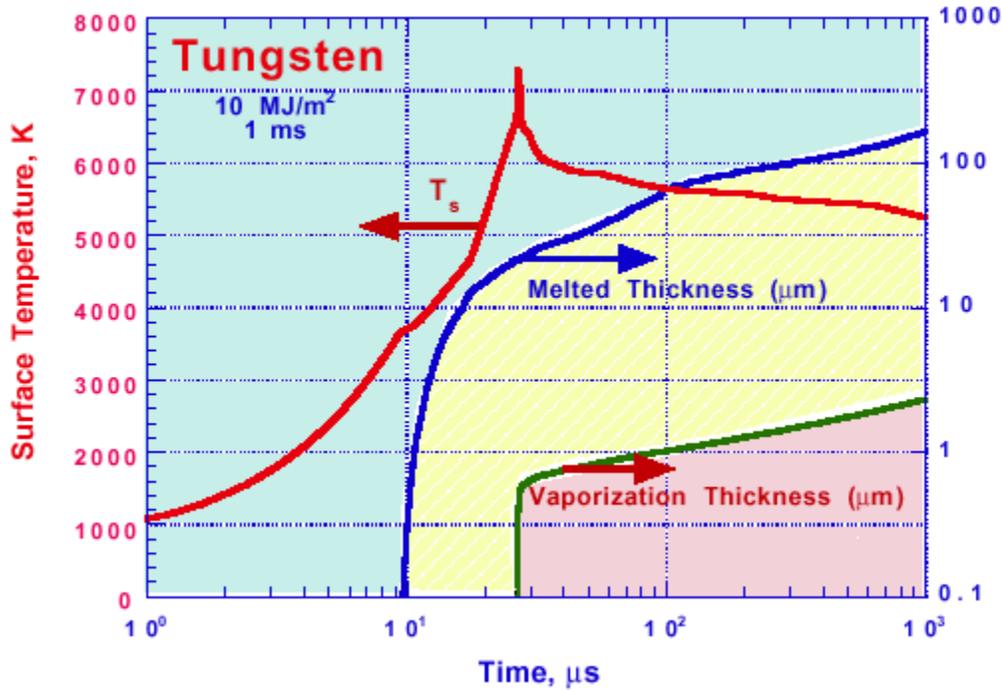

Figure 5.4.4.6-1. Calculation of the effects of disruption energy deposition on the divertor.
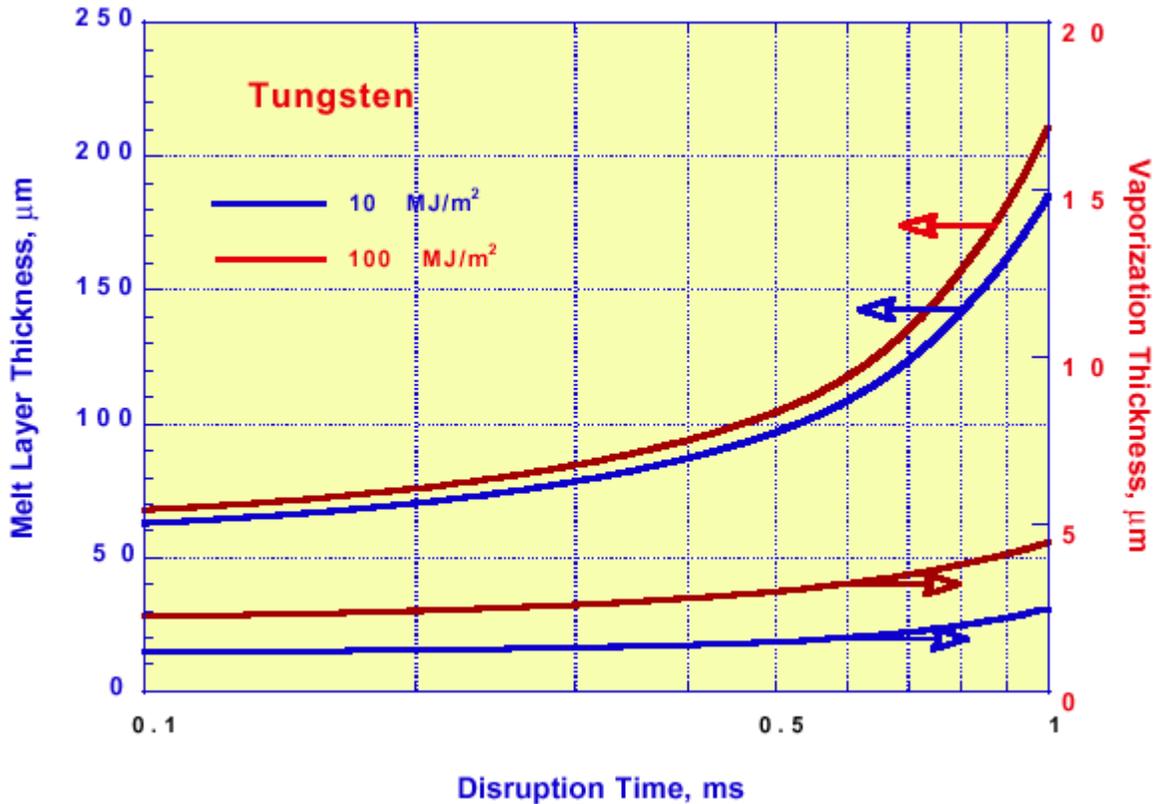
Figure 5.4.4.6-2. The effect of the size of the energy deposition on the amounts of material melted and vaporized in a disruption.

Sudden melting of a tungsten surface can cause splashing of the melted layer. Analysis of the amount of splashing has started. The droplets of splashed material will also interact with the incoming plasma (droplet shielding). The lifetime of the divertor depends strongly on the fraction of the melt layer that is lost on each disruption. If no melted material is lost, the lifetime of

5.4.4.7   Thermal Analysis of Divertor Components

Temperature distributions for the divertor components have been calculated with a thermal analysis code for normal operation. The analysis assumed a CuCrZr heat sink

the divertor tungsten is a few thousand disruptions (or nearly the life of the machine since only 3000 full power pulses are planned). Loss of the melt layer (or even as little as a quarter of the layer) will result in a lifetime of only a few hundred disruptions. Replacement of the divertor a few times during the life of the machine is expected if part of the melt layer is lost. with 5 mm W rods on the surface. The water inlet temperature was 30°C at a pressure of 1.5 MPa. Both the outer divertor plate and the baffle plate were analyzed. The peak heat flux was 20 MW/m^2 on the outer divertor (attached plasma case) and 6 MW/m^2 on the baffle plate (detached plasma case). The effect of 13-16 W/cm^3 nuclear heating was included. The outer divertor

heat sink was assumed to have a swirl tape in the coolant channel to enhance the heat removal while the baffle plate was assumed to have smooth tubes. The flow velocity in the outer divertor was 10 m/s while the baffle was 3 m/s. The coolant exit temperatures were 95 and 73°C, respectively. The temperature profiles are shown in Figure 5.4.4.7-1 and Figure 5.4.4.7-2.
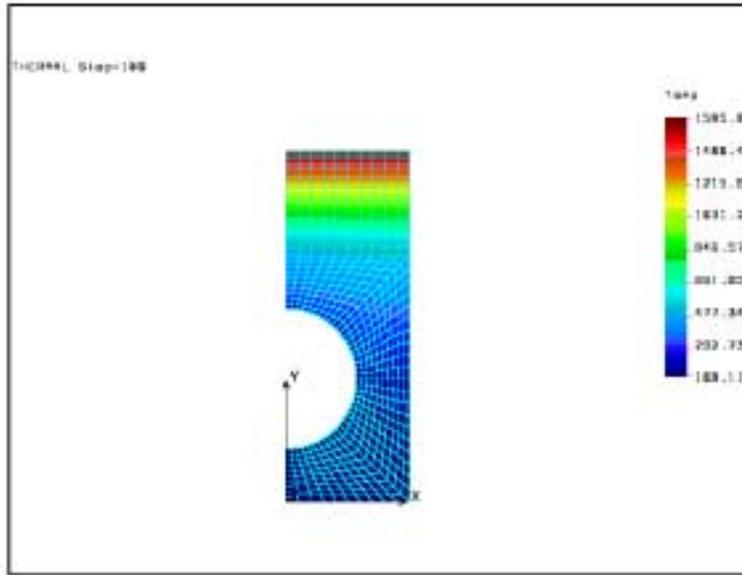

Figure 5.4.4.7-1. Temperature distribution in the actively cooled outer divertor plate with 20 MW/m^2 heat flux.
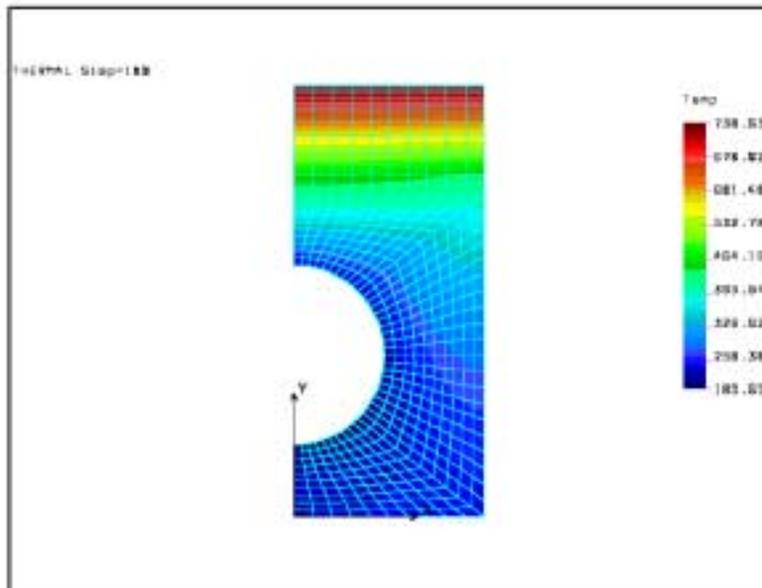

Figure 5.4.4.7-2 Temperature Distribution in the actively cooled baffle plate with 6 MW/m^2 heat flux.

5.4.5 Materials Selection

We recommend the following selection of materials for the plasma facing components:

<u>Divertor high heat flux areas</u>: tungsten rods 3 mm in diameter attached to actively cooled copper alloy heat sinks.

<u>Divertor heat-sink structure</u>: CuCrZr alloy, Elbrodur-G for copper-alloy heat sinks based on ITER fabrication experience.

<u>First wall:</u> plasma sprayed beryllium 10 mm thick attached to copper heat sinks that are passively cooled.

Tritium retention in redeposited carbon material has been identified as a major R&D issue to be investigated in the extension of the ITER project. This is due to the experimental data from both JET and TFTR that showed the retention to be approximately 50% of all the tritium injected into the machine. There is no satisfactory method for removing this trapped tritium from the machine. This issue argues strongly for avoiding carbon-based materials in a burning plasma device.

5.4.6 On-going Design and Fabrication Issues

Active cooling of the first-wall, inner divertor plate and baffle components will be needed for the longer pulse lengths proposed. More detailed designs and 2-D analyses are needed to verify design concepts and establish pulse limits for these parts.

Finite element analyses of the proposed PFC designs are needed under projected disruption and thermal loading conditions to assure that the structures and attachments are sufficient. Proposed sliding pin concepts

for relieving thermal stress must also be evaluated.

Mitigation of the eddy current loads on the divertor plates may require that a toroidally conductive path be provided between the outer divertor modules. This would significantly complicate the module design and associated remote installation and removal operations.

In general, reliable, yet easily detachable electrical contact must be provided between the plasma facing components and the vacuum vessel. Grounding straps and Multilam® contacts were proposed for this in ITER, since each of these can accommodate thermal cycling and relative motion. Similar design concepts must be developed and tested for FIRE.

When design analyses are completed, armored, medium-scale hardware needs to be fabricated and tested to verify the module manufacturing / assembly operations and performance models.

5.5   Thermal Shield

5.5.1   Introduction

The main function of the thermal shield system is to provide the required thermal environment around the coils, which operate at cryogenic temperatures. To maintain this environment, the nitrogen gas inside the shield must be contained (not allowed to leak out) and the air on the outside of the shield must not be allowed to leak into the shield. The main reason to exclude air from the inside of the enclosure is to prevent the accumulation of ice on the cold surfaces. In addition to maintaining the required thermal environment on the inside of the shield, it is also important to maintain the exterior surfaces of the shield at a high enough temperature to prevent water condensation, which can result in corrosion and operational and safety problems.

The basic design concept for the thermal shield is to have a stainless steel structure (channel beams) on the inside of the shield that can support panels made of insulating materials (Figure 5.5.1-1). The SS structure will be covered with a thin SS shell, which will form part of the sealed boundary for the shield. Insulation will be sprayed directly onto this shell. Penetrations will be sealed with rubber or fabric bellows that accommodate the relative motion between the VV and thermal shield.

5.5.2   Requirements

The most important requirements for the thermal shield relate to maintaining the 80 K thermal environment inside the shield. To do this efficiently, the maximum heat loss through the shield has been set at 15 kW. To prevent

condensation on the exterior of the shield, the surface temperature must be maintained above the dew point for air with a relative humidity of 50%. In addition, the constraint has been imposed to maintain the shield exterior within 10 °C of the test cell ambient temperature.
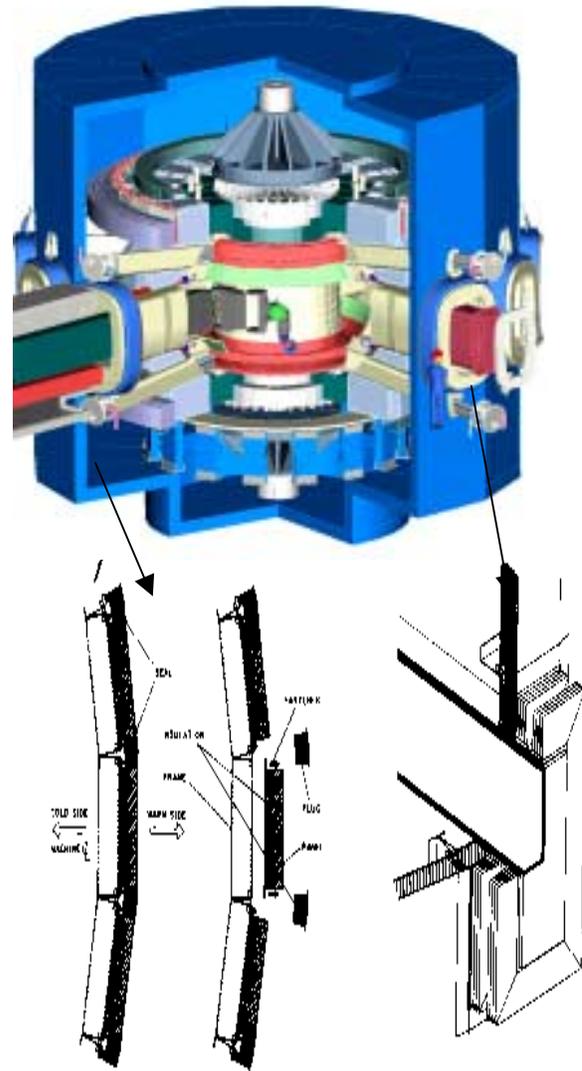

Figure 5.5.1-1   Thermal Shield Design Concept

Another important requirement pertains to pressure loads on the shield. If we have an open LN_2 system, interior

pressure will be due to N_2 gas flow through the system and out the vent. The maximum Δp across shield wall (maximum pressure on inside) has been set at 0.8 kPa (0.12 psi or 3 inches of H_2O). A higher pressure on the outside of the system could occur during cool down of the system if N_2 flow is not maintained. In this case, the maximum Δp across the shield wall (maximum pressure on outside) has been set at 0.1 kPa.

Requirements related to the flexible joints that accommodate the relative motion between the VV and thermal shield include a maximum integrated leak rate for all seals of 1 l/s (at 1 atm exterior pressure) with a Δp across the joint of 0.8 kPa. The joints must accommodate relative motions between the components up to $\pm$ 25 mm.

The requirements for the thermal shield are summarized in Table 5.5.2-1.

5.5.3 Description

The thermal shield has three basic parts, (1) the SS structure and shell which support the insulation and form part of the sealed boundary for the shield, (2) the insulation itself, and (3) the flexible joints that accommodate the relative motion between the VV and thermal shield. The shield is semi-cylindrical in shape (formed by 16 flat facets) with a flat top and bottom. Its OD and height are 11.2 and 11.5 m, respectively. The total wall thickness of the structure and insulation is 0.65 m.

Table 5.5.2-1 Thermal Shield Design Requirements – Summary

Design Parameter	Value
Thermal	
1. Condensation on surfaces of the shield.	None
2. Max. temp. difference between shield exterior and test cell temp.	10 °C
3. Max. heat flow through the shield assembly	15 kW
4. Minimum gas temp. contained by the shield	80 K
5. Max. gas temp. contained by the shield (during VV baking)	150 °C
6. Max. temp. around feedthroughts	200 °C
Structural	
1. Max. Δp across shield wall (max. pressure on inside)	0.8 kPa (0.12 psi)
2. Max. Δp across shield wall (max. pressure on outside)	0.1 kPa
Mechanical	
1. Max. integrated leak rate of all seals (between penetrations and thermal shield wall panels)	1 l/s at 1 atm (Δp- 0.8 kPa)
2. Seals must accommodate relative motion between penetrations and thermal shield panels (Initial Design Values)	Vertical - $\pm$ 25 mm Toroidal - $\pm$ 10 mm Radial - $\pm$ 18 mm

Sixteen (16) flat panels that are centered on each row of ports form the vertical sides of the thermal shield. Bolting the panels together forms the complete cylinder (each panel spans 22.5 degrees). Each panel consists of a perimeter frame, which is made with 10-inch channels. A thin SS skin is welded to the frame to form part of the barrier for the shield. Insulation is sprayed directly onto this skin. Holes are provided through the skin and insulation where the vacuum vessel ports, buswork, cooling and other services pass through. Clearance is provided between the ports and the hole in the thermal shield to allow for the relative motions of the VV and the shield. The maximum relative motion ($\pm$ 25 mm) results from the condition when the VV and thermal shield are at normal operational temperatures and simultaneously are under seismic conditions.

The seal around the ports is provided by a flexible joint (similar to a bellows) that is attached to the VV port and the SS sheet part of the structure. The joint is a

single layer of silicone rubber on a fabric base that is ~ 12 inches long (in the direction of the port axis). It can flex and buckle to accommodate the relative motion.

The insulation is the most important part of the shield. Several types were considered and compared before making a selection. The candidates are shown in Table 5.5.3-1. As can be seen, the thermal conductivity and cost of the cryo-lite and the polyurethane foam are similar. The solimide polyimide foam has a higher thermal conductivity and cost. Due to the ease of application of the polyurethane foam, (which is sprayed on) this insulation has been selected for the thermal shield. This material can be sprayed directly onto stainless steel to any desired thickness. A rubber vapor barrier can then be sprayed onto the exposed surface, which also enhances its abrasion resistance.

Table 5.5.3-1 Insulation Comparison

Mtl Name	k (W/m-K)	Cost ($/m³)
Polyurethane Foam (Manufactured by Foam Enterprises) (Spray foam for tank insulation.)	0.033	~400
Cryo-Lite (Manufactured by Johns Manville) (Used to insulate LN₂ over-the-road tanks.	0.033	~320
Solimide Polyimide Foam (TA-301) (Manufactured by Laporte plc)	0.042	~1150

The top and bottom of the TS are the same basic construction as the vertical sides. The structural frame consists of 10 inch channels positioned side by side and spaced ~ 0.5 m apart. The thin SS skin will be welded to the frame and

insulation will be sprayed on as described above.

Several important thermal characteristics of the shield have been estimated. These include the total heat loss through the shield and the inner and outer surface temperatures. The nitrogen gas temperature in the shield was assumed to be 90 K and the air temperature in the room was assumed to be 300 K (27 °C). Given these temperatures, the natural convection heat transfer coefficients were estimated for both the inside and outside of the shield. The insulation thickness was adjusted so that the outside surface temperature would be high enough to avoid condensation during operation. The resulting inner and outer surface temperatures are 100 K and 290 K (17 °C) respectively, for an insulation thickness of 0.4 m. The outer surface temperature is comfortably above the dew point of 283 K (10 °C) (for air at 21 °C with a relative humidity of 50 %), so condensation is not expected. The total heat flow through the insulation is ~11 kW which is below the requirement limit of 15 kW.

The basic parameters for the thermal shield are shown in Table 5.5.3-2.

Table 5.5.3-2 Thermal Shield Design Parameters

Parameter	Value
Size	
Outside Diameter	11.2 m
Outside Height	11.5 m
Total Wall Thickness	

Structure	0.25 m
Insulation	0.4 m
Inside Surface Area	375 m^2
Weight	
Insulation (0.4 m thick)	2400 kg
SS Structural Frame (10 inch channels)	24000 kg
SS Shell Around Insulation (0.5 mm thick)	7100 kg
Thermal Characteristics	
Nitrogen Gas Temp. Inside Thermal Shield (assumed)	90 K
Shield Inside Surface Temp. (with natural conv.)	~100 K
Shield Outside Surface Temp. (with natural conv.)	~290 K
Air Temp. in Room Outside of Thermal Shield (assumed)	300 K
Dew Point for Air at 21 C (75 F) and 50 % humidity	283 K
Condensation Expected	None
Total Heat Flow Through Shield	~11 kW

5.6 Ion Cyclotron Heating

5.6.1 Introduction

Ion cyclotron waves will be used to heat the plasma. Based on calculations of plasma transport, 30 MW of heating power will be required.

A design that can deliver this power consists of four two-strap antennas mounted in main horizontal ports, as shown in Fig. 5.6.1-1.

The amount of power that can be delivered to the plasma depends on several items that are not yet well-quantified, such as:

• Distance between the first wall and the plasma separatrix at the outer midplane – a smaller distance allows higher power per antenna.

• Maximum voltages that can be sustained in the antenna and transmission line – 30 kV is a relatively conservative number; 40 kV has been used on some experiments and would provide considerably higher power per antenna ($P \sim V_{max}^2$).
• The density and density profiles (both inside the separatrix and in the scrape-off region) of the plasma.

We have concentrated on the antenna configuration and the coupling of the antenna to the plasma, as these are the most critical parameters for initial system design. Power sources, along with tuning and matching equipment and
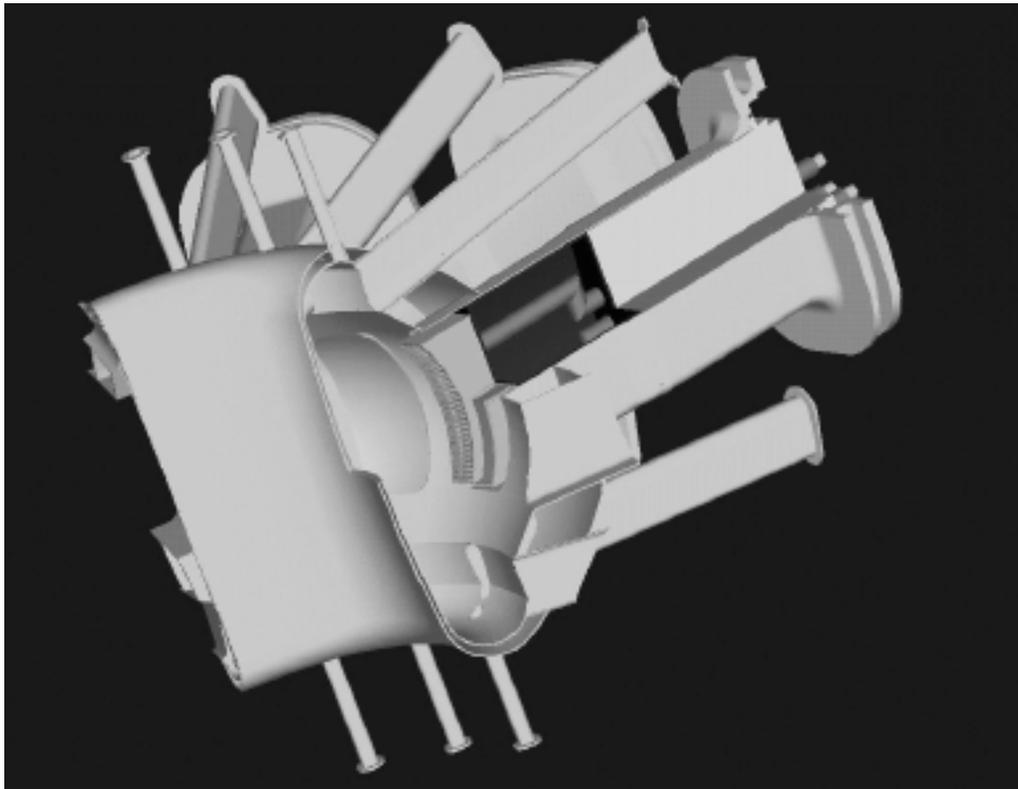

Fig. 5.6.1-1 – Cutaway view of one two-strap antenna in main horizontal port.

concepts, should follow reasonably conventional (although state-of-the-art) designs. While optimizing the parts of the system external to the vacuum vessel is necessary, we do not regard it as critical.

5.6.2 Heating scenarios

We assume that the machine will operate at the nominal field of 10 T and have a 50:50 mix of D and T, with the possible addition of minority species such as H or He^3, if needed. Figure 5.6.2-1 shows a plot of resonant frequencies of various ion species as a function of major radius. Based on this plot, we see that two reasonable scenarios for heating ions are:

- H minority or second harmonic D at 150 MHz
- He3 minority or second harmonic T at 100 MHz

5.6.3 Antenna geometry

Figure 5.6.3-1 shows a proposed antenna configuration that fits into a main horizontal port and can operate at the frequencies chosen above.

The antenna consists of two current straps, each strap about 15 cm wide and 117 cm tall. Each strap is grounded to the case at both ends. The straps are grounded at the center point also for increased mechanical strength. This results in a very strong strap arrangement that can resist the disruption-induced forces. For
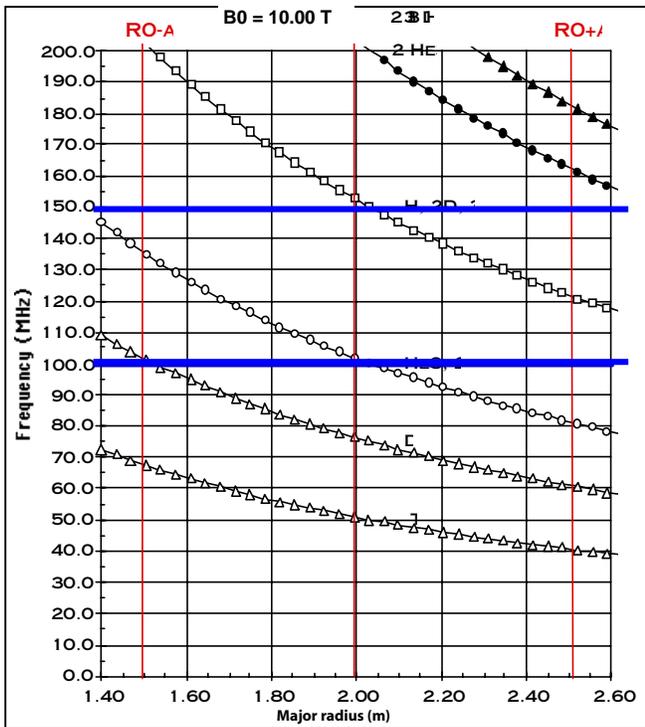
Fig. 5.6.2-1 Resonant frequencies vs. major radius, for B$_0$ = 10 T.
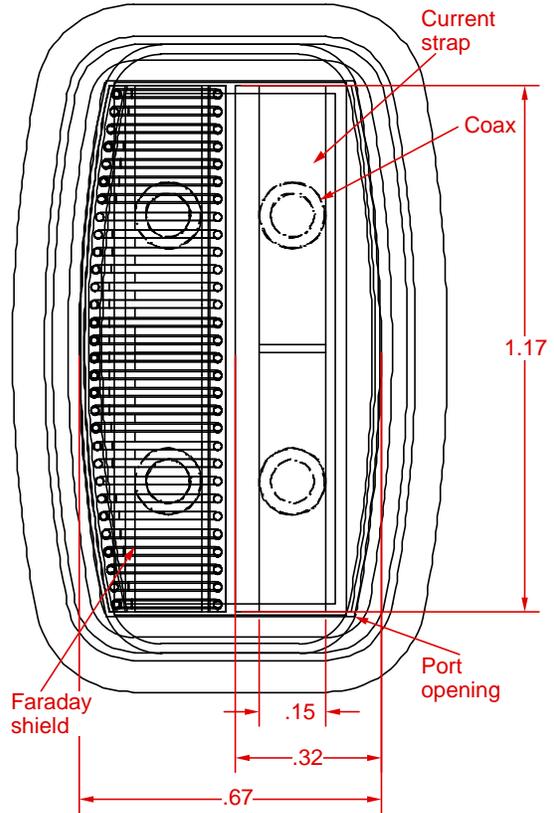
Fig. 5.6.3-1 View of antenna from the plasma. One Faraday shield removed. Dimensions in m.

reasonable assumptions about the strap electrical properties, the electrical length of the straps is near one wavelength in the 100 – 150 MHz frequency range, making this configuration feasible.

Each strap is driven by two coax feeds at the locations shown in Fig. 5.6.3-2 by the dashed circles. The two feeds on each strap are driven out of phase. We assume that there is π phasing between adjacent straps, since there is no current-drive requirement on the IC system.

A Faraday shield consisting of a number of metal tubes covers the antenna. Based on predicted thermal heat loads and pulse lengths of 10 s or greater, it is likely that active water cooling will be required during a pulse to prevent the Faraday shield tubes from getting too hot.

5.6.4   Power to the plasma

Figure 5.6.4-1 shows the maximum voltage in the RF system vs. gap, with the constraint that the IC system must deliver 30 MW of power to the plasma
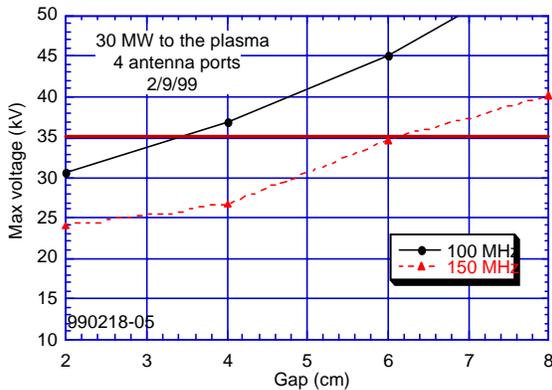
Fig. 5.6.4-1 Maximum voltage in the IC system needed to deliver 30 MW to the plasma vs. gap, for antennas in four ports.

using four antennas. The line at 35 kV indicates a nominal value of limiting voltage. A *conservative* design choice

would set this value at 30 kV, while a more aggressive design would increase it to 40 kV. These curves were calculated for the nominal density profiles (parabolic-to-a-power) with $<n> = 4.5 \times 10^{20}$ m^{-3} and $= 0.5$. Details are given in the Appendix on this subject.

Based on these results, a four-port system can deliver 30 MW to the plasma at 150 MHz for up to a 6-cm gap, provided it can operate at 35 kV. At 100 MHz, full power would require a gap $\leq$ 3.5 cm. The present design value for this gap is in the 3 to 4 cm range.

5.7 Plasma Fueling and Pumping

5.7.1 Introduction

Tritium pellet injection will be utilized on FIRE for efficient tritium fueling and to optimize the density profile for high fusion power. Conventional pellet injectors coupled with a guide tube system to launch pellets into the plasma from the high field side, low field side, and vertically will be provided for fueling along with gas puffing for plasma edge density control. Recent experiments on ASDEX Upgrade and DIII-D indicate that these pellets will penetrate a sufficient distance into FIRE plasmas to provide peaked profiles. About 1 -2 x 10^{21} tritons/s are required to sustain the plasma density in FIRE which is a modest extrapolation of existing pellet injection technology. About 0.1 g of tritium must be injected during each 10 s pulse. The tritium and deuterium will be exhausted into the divertor. The double null divertor will have 16 cryogenic pumps located near the divertor chamber to provide the required high pumping speed of 375 torr-l/s The tritium from the regenerated cryopumps will be directed to gas holding tanks and fed into a cryogenic distillation system that will separate hydrogen isotopes and purify the tritium for return to the fueling system.

The plasma fueling system design for FIRE is based on previous designs for CIT, BPX and ITER as well as more recent developments and plasma physics results in the area of pellet launch from multiple locations relative to the magnetic axis. The goal is to produce a flexible fueling system that would require minimum change in the progression from FIRE to ITER or a fusion demonstration (DEMO) plant. In the past, tokamaks have generally used gas puffing for establishing and maintaining the plasma density. With this method, the sources of plasma particles are located at the plasma surface. There is general consensus, however, that gas puffing alone will not be sufficient to fuel the next generation of large, long-pulse fusion devices with thick, dense, scrape-off layers, and that core fueling, where the particle sources are located

well inside the plasma edge, will be necessary.

A pellet fueling system (PFS) is provided for core fueling and a gas fueling system (GFS) for edge fueling. The FIRE fueling system provides plasma fueling from all sources (D, T, impurity gases) at a rate of 200 torr-liter/s for 20 s to support all fueling functions. The fuel rate to replace the D-T ions consumed by the fusion reaction is quite modest, about 2 torr-liter/s for a fusion power of 200 MW; the resulting burn fraction is thus only 1% of the steady-state fueling rate. Such low burn fractions result in large vacuum pumping and fuel processing systems with associated tritium inventories and were not anticipated in early (1,2) and even more recent (3) fusion power plant assessments, which had burn fractions in the 10-40 % range. The low burn fraction is only partially due to the finite fueling efficiency (see next section). The fueling system (4,5) must also maintain the required plasma density (near the empirical Greenwald density limit), establish a density gradient for plasma particle (especially helium ash) flow to the edge, and also supply hydrogenic edge fueling for increased scrape-off layer flow for optimum divertor operation. Still another function is to inject impurity gases at lower flow rates (25 torr-l/s or less) for divertor plasma radiative cooling and wall conditioning. Finally, the plasma fueling system provides for plasma discharge termination on demand via massive gas puffing or injection of cryogenic mass via pellets or liquid jets. A concept called isotopic fueling (6) can be used to improve the tritium burn fraction above the nominal 1% level described above by frugal use of tritium fuel to those functions only related to the fusion burn and using deuterium for edge fueling. This can reduce in-vessel tritium inventories and the required tritium-breeding ratio for fusion reactors.

The tritium inventory inside the FIRE vacuum vessel is a major consideration. Due to the large retention of tritium observed in carbon plasma facing components and in co-deposited carbon layers on TFTR and JET, carbon PFCs will not be allowed in FIRE. The divertor plates will be tungsten and the first wall protection will use Be tiles.

5.7.2   Fueling Efficiency

The fueling efficiency of tokamaks has been studied since the early 1980's. For gas fueling, the determination of fueling efficiency of short pulse tokamaks has been difficult to quantify because of an outgassing source of hydrogenic fuel from the plasma facing components that can be of the same magnitude as the external gas fueling. Pellet fueling is easier to quantify in terms of fueling efficiency due to the rapid deposition of the fuel (100's of μs) and its deposition beyond the last closed flux surface, which avoids most atomic physics complications in fuel transport to the plasma. In contemporary tokamaks, fueling provides the required density level for a particular plasma experiment. There is incentive to maximize the tritium plasma fueling efficiency due to the cost and safety implications of a large tritium throughput and the complexity of reprocessing large torus exhaust gas loads (6). Fueling efficiency of gas and pellet injection are summarized in Table 5.7.1 and Figure 5.7.1

Device	Gas Fueling Efficiency (%)	Pellet Fueling Efficiency (%)	Remarks
ASDEX	20	30-100	high density
PDX	10-15		high density
Tore Supra	1	30-100	ergodic divertor for gas fuelling
JET	2-10	20-90	active divertor
TFTR	15		low density DT
ASDEX-U		8-50	
DIII-D	10	40-100	active divertor

Table 5.7.1. Tokamak fueling efficiency.

(7,8). Generally, in diverted discharges of the larger tokamaks, gas fueling efficiency is in the range 1-10 % and pellet fueling efficiency is an order of magnitude larger. Recent results from ASDEX-Upgrade (9) are also shown in Figure 5.7.1 which compares the penetration and fueling
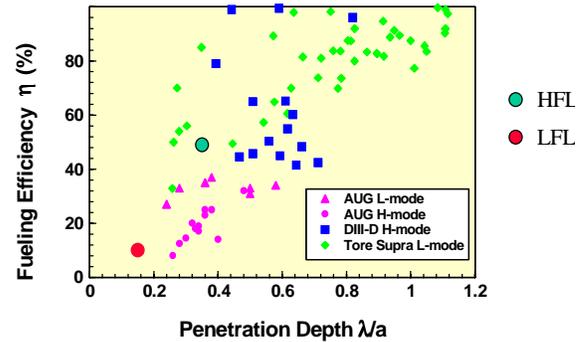
Figure 5.7.1.   Pellet fueling efficiency for several experiments. *(Also shown are recent results from high field launch (HFL) and low field launch (LFL) on ASDEX Upgrade.)*

efficiency of pellets launched into the same plasma conditions from the high magnetic field side and low magnetic field side; improvements in pellet penetration and fueling efficiency for high field launch are substantial.

Deuterium pellet injection from four different poloidal locations has been used in experiments on the DIII-D tokamak (10, 11, 12) to investigate several aspects of plasma confinement and density control (see Figure 5.7.2). Pellets can be injected in four locations: outside midplane, vertically inside the major radius, inside launch at ~ 45 degree angle and inside midplane. Pellets injected from the outer horizontal midplane (low field side) show a large discrepancy in the measured fueling efficiency and mass deposition profiles from pellet ablation theory, while the penetration depth compares favorably with theory. An apparent outward displacement of the deposited pellet mass is observed and hypothesized to occur from ∇B and curvature induced drift effects. Injection of pellets inside the magnetic axis from a vertical port and inner wall ports using curved guide tubes has been employed on DIII-D to investigate these effects.

The resulting density profiles show pellet mass deposition well inside the expected penetration
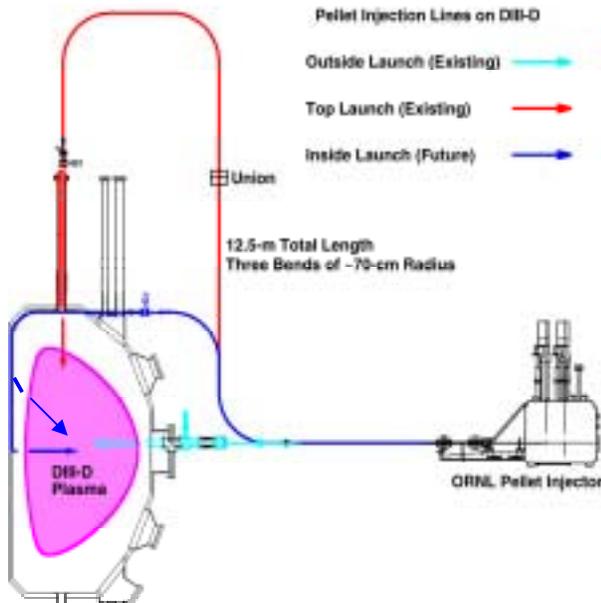
Figure 5.7.2. Pellet launch locations on DIII-D.

radius, suggesting that a drift of the pellet ablatant is occurring toward the low field side (LFS) edge of the plasma (Figure 5.7.3). The formation of highly peaked density profiles with pellets injected from the high field side is possible at higher heating power than is possible from pellets injected from the low field side.

On FIRE, pellet injection will be possible from the outside midplane, vertically and from the inside lower quadrant aimed towards the plasma center. This will be accomplished by three sets of guidetubes.

Recently, there has been interest in repetitive impurity pellets or impurity gas puffing to foster enhanced radiation in the outer plasma and divertor regions and large ("killer") pellets for a controlled, preemptive plasma shutdown in anticipation of a major disruption or vertical displacement event (VDE). These systems typically operate at room temperature or higher cryogenic temperatures, but require similar technology for pellet feed and acceleration as are used on H/D/T pellet fueling systems. Major issues for impurity pellet injection include

development of pellet production and feed hardware optimized for the pellet material (i.e.

Figure 5.7.**3**. Plasma density increase from a pellet launched from the inner wall (high field side) launch compared with launch from the outer wall (low field side).
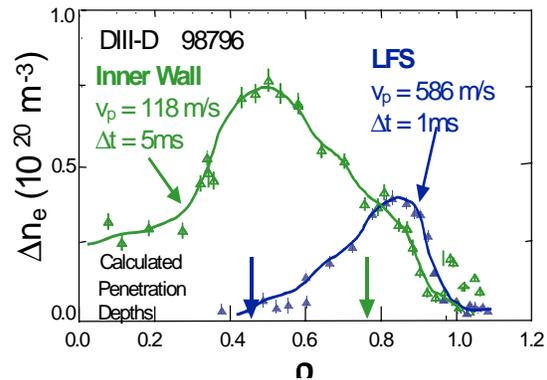
lithium, carbon, nitrogen, argon) and, for killer pellet injectors, high reliability for a single large pellet or liquid jet on demand. Impurity pellet injection systems (typically small lithium or carbon pellets) have been developed for wall conditioning and plasma diagnostics.

5.7.3   FIRE Fueling System Overview

The FIRE fueling system will use a combination of gas puffing and pellet injection to achieve and maintain burning plasmas. This combination will provide a flexible fueling source with D-T pellets penetrating beyond the separatrix to sustain the burning fusion plasma and deuterium-rich gas fueling the edge region to meet divertor requirements in a process called isotopic fueling (6). The isotopic fueling concept was developed to allow independent control of the plasma deuterium and tritium density profiles which can lead to reduced (by factors of 2-4) tritium inventory in plasma facing components. The higher tritium burn fraction allows a significant reduction in tritium gas flows into and out of the vacuum vessel and, for fusion reactors, implies lower required tritium breeding ratios. The fueling system includes; a conventional gas puffing system, using all-metal electromagnetic dosing valves, (four toroidal stations at two poloidal locations at each divertor level), and a

pellet injection system.

The FIRE pellet fueling system (PFS) design includes a long pulse pneumatic pellet injector capable of injecting D-T or tritium. It will be a repeating pneumatic injector using an extruder-based hydrogenic feed system. It will be configured to inject pellets using propellant gas for pellet acceleration (up to 1.5 km/s pellets) or a mechanical punch accelerator (up to 100 m/s for pellet injection into curved guidetubes for vertical or high field side launch) or a combination of these two drivers. The mechanical punch operating alone or with a small amount of propellant gas would reduce considerably the need for differential pumping of the pellet injection line and the reprocessing requirements for propellant gas. The PFS comprises a pneumatic pellet injector with three separate pellet extruders/guns, installed in a containment area in the basement below the torus. The PFS and GFS manifolds are also located in a basement area below the FIRE torus. Pellet injection will be possible via curved guidetubes from the outside midplane, vertically and from the inside lower quadrant aimed towards the plasma center. This will be accomplished by three sets of guidetubes. The pellets will be injected to the high magnetic field side of the machine through a curved flight tube routed through the lower divertor region. The hydrogenic feed for the injector is provided by a conventional linear piston hydrogen extruder (sized for a 20 s supply of pellets) or by a continuously rotating screw extruder. Deuterium and tritium pellets up to 10 mm in size have been extruded at rates up to 0.26 grams/sec (for short pulses only); this pellet size and feed rate is sufficient for fueling fusion reactors at the gigawatt power level. Table 5.7.2 below shows preliminary parameters for the FIRE hydrogenic fueling system.

Parameter	Gas Fueling System	Pellet Fueling System	Remarks
Design fueling rate	200 torr-l/s for 20 s	200 torr-l/s for 20 s	Torus pumping capacity is 375 torr-l/s
Operational fuel rate	100-175 torr-l/s	100-25 torr-l/s	Isotopic fueling
Normal fuel isotope	D (95-99%) T,H (5-1%)	T (40-99 %) D(60-1%)	D-rich in edge, T-rich in core
Impurity fuel rate	25 torr-l/s	TBD (prefer gas for impurity injection)	25 torr-l/s reduces DT fuel rate due to fixed pumping capacity
Impurity species	Ne, Ar, N_2, other?	TBD	TBD
Rapid shutdown system	Massive gas puff	"killer" pellet or liquid D jet	For disruption/VDE mitigation
Pellet sizes (cyl. diameter)	N/A	3, 4, 4 mm	3 mm for density rampup, 4 mm for flat-top

Table 5.7.2. Preliminary FIRE fueling system parameters.

5.7.4   FIRE Fueling System R&D

The screw extruder concept has been demonstrated by a Russian Federation prototype system which ran for 1-hour pulses using hydrogen feed gas producing ~2 mm extrudant.

This needs to be extrapolated to deuterium and tritium feed and larger pellet sizes using this technology or variants such as gear or double-screw extruders. ITER-scale (10-mm) pure tritium and D-T pellets have been extruded with a piston-type linear extruder and accelerated to about 1 km/s (see Figure 5.7.4) in the Tritium-Proof-of-Principle Phase II (TPOP-II) experiment at the Tritium Systems Test Assembly (13)

The technology to deliver intact pellets at the highest possible speeds around curved surfaces (guide tubes) is under development (11, 12). This is a complex issue and depends on the pellet speed and temperature (strength) as well as the guide-tube radius of curvature, its diameter relative to the pellet size, and its cross-sectional shape. The speed dependence of penetration for high field side or vertical launched pellets is not known.

5.7.5   FIRE Pumping System

The current baseline design is a set of refrigerated duct D-T cryoconden-sation/diffusion pumps backed by turbo/drag pumps. This system is designed to pump in both the free-molecular and viscous flow regimes. Water is pumped on the inside diameter of the 160 mm diameter by 1 meter long 30 K entrance duct which connects the divertor to the cryocondensation pump. Other impurity gases and hydrogen are pumped by cryocondensation on a 1/2" O.D. x 0.035 wall stainless steel tubing coil refrigerated by liquid helium. The 2 torr-l/s helium gas produced by the D-T fusion reaction is compressed by viscous drag in the entrance duct by a factor of up to 100. The compressed helium gas is carried from the cryopump to a turbo/drag pump located outside the biological shield through the divertor duct. The design D-T throughput is 200 torr-liter/s for the 20 s pulse length. The partial pressures prior to a discharge are 10^{-7} torr for fuel gases (H, D, T) and 10^{-9} torr for impurities. There will be a total of 16 cryopumps with 8 each top and bottom (at alternate divertor ports) located 1 meter into the pump duct from the double-null divertor. The duct behind the cryopump will be constructed with transverse optically opaque shielding baffles which will allow 200 l/s helium gas conductance per port to the turbo/drag pumps located outside the biological shield. There are no moving parts inside the torus.

A layout of the cryopumps is shown in Figure 5.7.5. The cryopumps are designed to have a low mass and active helium gas cooling. Between shots the helium flow will be stopped to allow the pumps to regenerate into the compound turbo/drag pumps. This will limit the tritium
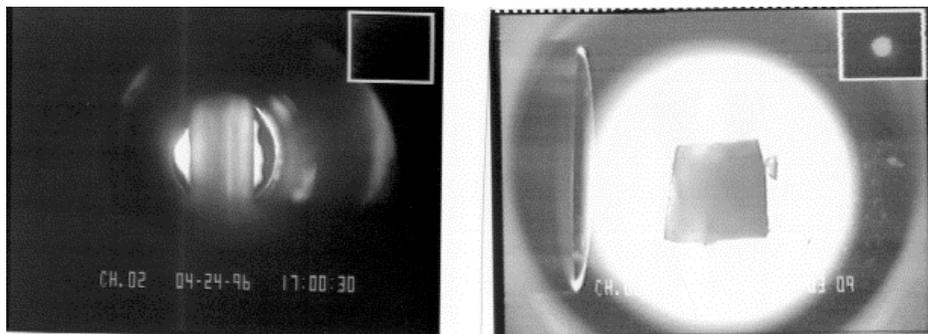

Figure 5.7.4. Pure tritium extrusion and pellet.

contained on the cryopumps to less than 1 gram for a 20 sec. discharge. Gas will be returned to the tritium system where it will be processed through an impurity removal step and a cryogenic distillation system that will separate the hydrogen isotopes and purify the deuterium and tritium for return to the fueling system.

The cryogenic cooling requirement for the 16 pumps for the design pumping rate of 375 torr-l/s and the nuclear heating loading which is estimated at 0.03 watt/cm^3 at the proposed cryopump location 1 meter from the divertor is 3 watts per pump. The liquid helium cooling rate required during a shot is 64 l/h for the 16 pumps.

The maximum divertor pressure during the pulse is ~0.02 torr. At this pressure and the design duct size the Knudsen number is 0.01 so the gas transport is in the viscous flow regime dominated by gas-gas interaction. In this case the minority gas species such as helium and impurities will be carried by viscous drag to the cryopump. This effect can be used to achieve a helium compression of 100 in the inlet duct so that the required helium pumping speed can be reduced and still maintain a high effective helium pumping speed at the divertor.

During the tokamak discharge the effective pumping speed for 375 torr-l/s flow is 2,000 l/s per duct (32,000 l/s total) at the divertor for D-T, He, and impurities. After the shot the pumps will be warmed and regenerated. The 4,000 torr-l of D-T pumped during the shot will raise the 18 m^3 torus chamber to 0.2 torr. The pumping time constant for the 16 turbo-drag pumps with 3,200 l/s combined speed will be 6 seconds. Between discharges, with the cryopumps warmed to 100K, the turbo/drag pump set will have a speed of 3,200 l/s for all gases. Prior to the discharge, with the pumps cold, in the free molecular flow regime, the pump set will have an effective speed of 16,000 l/s for D$_2$, 6,400 l/s for air, 46,000 l/s for water vapor, and 3,200 l/s for helium.

The sixteen evacuation locations will be grouped in four sets of four. Each set will have its own cryogenic control system. Liquid helium will flow in series through the four cryocondensation pumps and will go through a heat exchanger to completely flash it before it is sent in parallel through the four cooled ducts. The four turbo/drag pumps in the group will be backed by a single 3.3 l/s scroll pump that is backed with a metal diaphragm pump.
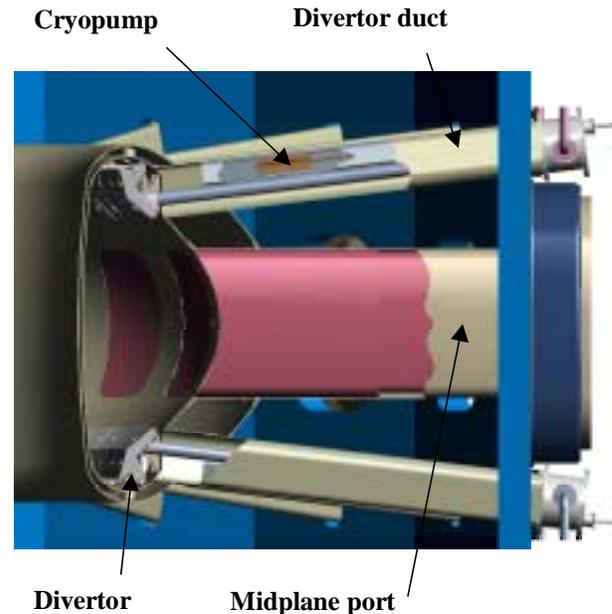
Figure 5.7.5. Elevation view of FIRE torus showing divertor duct and cryopump.

REFERENCES

1. C. C. Baker, M. A. Abdou, *et al.*, "STARFIRE-A Commercial Fusion Power Plant Study," Argonne National Laboratory Report ANL/FPP-80-1 (1980).
2. M. A. Abdou, *et al.*, "A Demonstration Tokamak Power Plant Study (DEMO)," Argonne National Laboratory Report ANL/FPP-82-1 (1982).
3. The ARIES Team., "The ARIES-1 Tokamak Reactor Study, University of California at Los Angeles report UCLA-PPG-1323 (1991).
4. Gouge, M. J., *et al.*, "The CIT Pellet Injection System: Description and Supporting R&D," *Proceedings of the 13th Symposium on Fusion Engineering*, Vol. II, p.1240, IEEE 1990.

5. M. J. Gouge, "Fuelling of ITER-Scale Fusion Plasmas," *Fusion Technology,* **34**, 435 (1998).

6. Gouge, M. J., *et al.*, "Fuel Source Isotopic Tailoring and Its Impact on ITER Design, Operation and Safety," Fus. Tech. **28**, 1644 (1995).

7. L. R. Baylor, et al., "Deposition of Pellets into Tokamak Plasmas," *Fusion Technology,* **34**, 425 (1998).

8. L. R. Baylor, et al., "Pellet Injection into H-mode Plasmas on DIII-D," *to be published in 26th Europ. Conf. on Contr. Fusion and Plasma Physics* (1999).

9. P. T. Lang, et al, "High-efficiency Plasma Refueling by Pellet Injection from the High-Field Side Asdex Upgrade," *Phys. Rev. Lett.* **79**, 1478 (1997).

10. S. K. Combs, et al., "Experimental Study of Curved Guide Tubes for Pellet Injection," *Proc. 1997 IEEE/NPSS 17th Symp. Fusion Eng., San Diago,* 1102 (1998).

11. S. K. Combs, et al., "High-Field-Side Pellet Injection Technology," *Fusion Technology,* **34**, 419 (1998).

12. S. K. Combs, et al., "New Pellet Injection Schemes on DIII-D," *to be published in the proceedings of this conference*.

13. P. W. Fisher and M. J. Gouge, "TPOP-II: Tritium Fueling at a Reactor Scale," *Fusion Technology,* **34**, 515 (1998).

5.8 Tritium System Requirements

5.8.1 Introduction

The tritium system is a key system for FIRE operations, as well as providing development information and operating experience for the fusion program. The development of a safe, low-inventory tritium system is an important project goal.

5.8.2 Tritium Injection Requirements

Pellet injection will be the primary plasma system for fueling the core of the FIRE plasma utilizing both high speed pellets and guided lower speed pellets. Gas injection systems will also be provided for edge fueling. The total number of tritons in the nominal FIRE plasma is:

$$Ne = <ne> Vp /2 \sim 2.25 \times 10^{20} \text{ m}^{-3} \times 18 \text{ m}^3 \sim 5 \times 10^{21} \text{ tritons}$$

The particle confinement in tokamaks is described by $D \sim \chi$, or $\tau_p \sim \tau_E$ which translates into $\tau_p \sim 0.5$ to 0.8 s in FIRE. A fueling rate of $\sim 0.5 - 1 \times 10^{22}$ particles/s would be required to sustain the density with zero recycling. The standard assumption for FIRE and ITER-RC is that $\tau_{He} \sim 5 \tau_E$ which suggests an 80% recycling of helium. We make the additional reasonable assumption that the same recycling applies to the hydrogenic species. Therefore, a net rate $\sim 0.1 - 0.2 \times 10^{22}$ particles/sec would be required to sustain the nominal FIRE plasma.

In present experiments with outer mid-plane pellet fueling, the efficiency is low ~20%. FIRE will be employing vertical launch of high-speed pellets aimed inside the magnetic axis or slower pellets guided by tubes to near the inside mid-plane. The injection geometry will be updated, as more information becomes available from ongoing experiments. A pellet fueling efficiency of 50% is assumed for FIRE. The gross tritium fueling rate for the plasma core is then $\sim 0.2 - 0.4 \times 10^{22}$ particles/s.

5.8.3 Requirements for Potential Pulse Sequences

The total number of injected tritons required for various scenarios involving 10 second long pulses is:

$2 - 4 \times 10^{22}$ T/pulse ; 0.8 - 1.6 kCi (~0.1g) / pulse; 10 s pulse

$2 - 4 \times 10^{23}$ T/day ; 8 - 16 kCi (~1g)/day; 10 pulses/day

$1 - 2 \times 10^{24}$ T/week; 40 - 80 kCi(~5g)/week; 50 pulses/week

(where 2.09×10^{19} T atoms = 1 Ci, 10^4 Ci = 1 g, pulses are 10 seconds long)

The total number of DT pulses in FIRE is limited to < 5TJ of fusion energy, or 2,500 pulses at 200 MW for 10 s, or a tritium fueling throughput of 2 - 4 MCi. There will also be many partial power pulses that will consume tritium while not producing optimal fusion power, therefore the lifetime throughput of tritium is assumed to be increased by ~ 5 to a total throughput of 10 - 20 MCi. Assuming that this program takes place over 5 years would require a tritium throughput capability of 2 - 4 MCi/year.

The fractional tritium burn-up of ~ 5% does not affect these estimates significantly.

5.8.4 Tritium Retention and Inventory

The provisional limit for the tritium site inventory has been set at ≤30 g (~0.3 MCi). According to DOE STD 1027,

FIRE would be classified as a Low Hazard Nuclear Facility. Similar to the TFTR tritium management strategy, the maximum tritium in any on-site tritium system is set at 15 g, 1/2 the site limit. The D-T experiments on TFTR and JET have shown that the use of carbon plasma facing components produced an effective tritium retention rate of ~ 40%. Assuming the annual tritium throughput of 2 - 4 MiCi, this level of retention would cause the FIRE system limit to be exceeded in 1 to 2 months. Therefore, the use of carbon will not be allowed in the FIRE vacuum vessel. The initial materials for plasma facing components and divertor plates will be Be and W.

Cryogenic pumps will be installed in the behind the divertors of FIRE to provide adequate pumping during the pulse. Essentially all of the injected tritium will end up on the cryopumps. The schedule for regenerating the cryopumps will be determined to maintain the tritium inventory < 30g. The tritium inventory for several regeneration schedules is:

1. weekly regeneration: < 5g of tritium on the cryopumps would be transferred to the tritium handling system. The tritium separation systems described below would be able to easily separate the tritium from the deuterium and other exhaust gases in < 2 days, so that tritium could be ready for experiments the following week. Need to estimate the number of deuterium only shots in a run sequence to estimate the total number of torr-liters of gas on the cryopumps to see if this is a reasonable sequence.

2. daily regeneration: < 1g inventory on the pumps, probably not worth the hassle of the regeneration procedure.

3. monthly regeneration: < 20g of tritium on the cryopumps if running continuously with tritium. This level is also expected to satisfy the explosive limits.

A monthly regeneration of the divertor cryopumps would fit naturally with the anticipated experimental schedule.

5.8.5 Tritium Systems for FIRE

The tritium systems will be similar to those used successfully at TFTR, and will include Tritium Storage and Delivery, plasma exhaust cleanup, tritium purification system (for reprocessing the on-site inventory), appropriate room air cleanup systems, tritium exhaust gas processing systems, and tritium monitoring for process control and personnel protection. The block diagram for the tritium system is shown in Fig 5.8.5-1.

The FIRE tritium delivery system will be capable of supplying tritium with a purity > 98%. Tritium will be received from a DOE supplier in hydride transport vessels (HTVs) in quantities up to 25 grams. Tritium inventory will be loaded into the tritium storage and delivery system (TSDS) and will be available upon demand (within 6 hours of when required). The FIRE TSDS will be capable of supplying quantities of tritium up to 3 kCi per pulse via direct gas injection. This capability could be upgraded for the long pulse (~ 40s) pulses in the advanced tokamak phase.

FIRE exhaust gas will be collected in a plasma exhaust tank where it will be stored until processed by the on-site tritium purification system (cryogenic distillation). On-site tritium processing will separate non hydrogen isotopes from the plasma exhaust effluent and cryogenically separate tritium from deuterium and protium, thus producing tritium with a purity of > 98 % purity. Plasma exhaust processing will require ~ 24 hours to be recycled back to the tritium storage and delivery system.

The on-site tritium purification system for FIRE will have a resident tritium inventory of ~ 10 grams of tritium with a throughput of (up to) 50 kCi (5 grams) /

day. ITER had planned to reprocess 164 g of tritium during the 40 minute cycle period for an ITER pulse[1].

Tritium residual gases (in glove boxes and in other small volumes) will be processed, oxidized, and deposited on disposal molecular sieve beds for disposal at an off-site facility.

5.8.6 Options to the Tritium Inventory

The tritium inventory has been set at 30g (~0.3 MCi), to allow sufficient operational flexibility without introducing additional restrictions. However, there is the potential for reducing the inventory to even lower levels. If a tritium reprocessing system is used which is able to recycle the working tritium on a daily basis, then the daily working inventory is = 20 kCi (2g).

As noted above, ITER was planning on reprocessing tritium at the rate of >4 g/minute. If FIRE had a system capable of processing 1g/120 minutes, then the

working inventory could be reduced by an order of magnitude to 2kCi(0.2g). The main contributions to the inventory would now be in residual holdup in various systems including the vacuum vessel. There should be a follow-up study to look at the minimum tritium inventory case.

[1] D. K. Murdoch, "Tritium Inventory Issues for Future Reactors"; Choices, Parameters, Limits. Proc., SOFT 1998


Fig. 5.8.5-1 Tritium System Piping and Instrumentation Diagram (P&ID) for FIRE

5.9   Neutronics and Shielding

5.9.1   Introduction

The FIRE operation schedule includes DD and DT pulses with different fusion powers and pulse widths. DT pulses with widths up to 20 s and fusion powers as high as 200 MW producing a total of 5 TJ of fusion energy are planned. In addition, DD pulses with different widths and fusion powers up to 1 MW are expected to yield a total fusion energy of 0.5 TJ. Neutronics and shielding analyses have been performed. The largest nuclear heating values in the different components were calculated for the 200 MW fusion power DT pulses. During these pulses the average neutron wall loading is 3 MW/m^2 with values at the outboard (OB) midplane, inboard (IB) midplane, and divertor being 3.6 MW/m^2, 2.7 MW/m^2, and 1.8 MW/m^2, respectively. At each of these locations, the appropriate radial build was used along with the corresponding neutron wall loading. The end-of-life magnet insulator dose and helium production in the vacuum vessel (VV) were determined for a cumulative fusion energy of 5 TJ DT and 0.5 TJ DD.

Two design options are considered for the FW/tiles: Option 1 with passive cooling and Option 2 with active water cooling. The FW/tiles on the IB side for Option 1 consist of 0.5 cm Be PFC (90% Be), followed by 4.3 cm Cu tiles (80% Cu) and 0.2 cm gasket (50% SiC). In Option 2, the IB FW/tiles consist of 0.5 cm Be PFC (90% Be), 1.8 cm Cu tiles (80% Cu), 0.2 cm gasket (50% Cu), and 2.5 cm water cooled Cu (80% Cu, 15% water). For the OB side, the same radial build is used except that the total thickness is increased to 10 cm in Option

1. The calculations were performed for both the passively cooled and actively cooled FW/tiles design options. The impact of these design options on nuclear heating in the different components was assessed. The effect on the VV and magnet shielding was also evaluated.

The detailed radial build of the outer divertor plate was used in the analysis. The front layer is a 0.5 cm W Brush (90% W) followed by a 0.1 cm region (84% W, 14% Cu, 2% void) where the W rods are joined to the Cu heat sink. The 1.9 cm heat sink is made of Cu finger plates (78% CuCrZr, 20% water, 2% void). A 3 cm region (47% CuCrZr, 48% SS316, 5% void) represents the mechanical attachment between the Cu finger plates and the backing plate. The SS backing plate (84% SS316, 16% water) is 7 cm thick.

The VV consists of 1.5 cm thick inner and outer facesheets made of 316SS. It is assumed that the space between the VV facesheets (VV shielding zone) includes 60% 316SS and 40% water except in the IB region where 11% 316SS and 89% water is used because of the small thickness. The thicknesses of the VV shielding zone in the IB midplane, OB midplane, and divertor region are 2, 51, and 9 cm, respectively. A 1.5 cm thick layer of thermal insulation (10% Microtherm insulation) is attached to the back of the coil-side VV facesheet. The Cu TF coils are included in the model with Cu at a 90% packing factor. A 304SS coil case is used in the OB region with 4 cm front thickness and 6 cm back thickness. Both the IB and OB regions were modeled simultaneously to account for the toroidal effects.

5.9.2   Nuclear Heating

Nuclear heating deposited in the different components was determined and used in the thermal analysis. The calculations were performed for the DT pulses with 200 MW of DT fusion power to determine the largest nuclear heating generated. Nuclear heating results can be modified for lower power pulses by scaling linearly with the fusion power. For the DD pulses with the largest fusion power (1 MW), nuclear heating values are less than 1% of the values for the 200 MW DT pulses. Table 5.9.1 gives the peak power density values in the different components at the chamber midplane. The results are given for the two FW/tiles design options. The peak nuclear heating values in the FW/tiles are comparable for the two design options. The IB VV and magnet heating values decrease by ~15% in Option 2 because of the added water coolant in the FW and using Cu in the gasket in place of SiC. The OB VV and magnet heating values increase by a factor of 1.5-2 in Option 2, primarily due to the 5 cm reduction in the FW/tiles thickness. The largest power density values in the magnet occur in the IB region at midplane with the minimum being in the OB region at midplane due to the 49 cm thicker VV. Fig. 5.9.1 shows the radial variation of nuclear heating in the IB FW/tiles and VV at midplane for the passively cooled FW/tiles design option. Fig. 5.9.2 gives the nuclear heating distribution in the OB FW/tiles at midplane. Notice the larger drop in nuclear heating at the back of the OB FW/tiles compared to that in

the IB region due to the added 5 cm thickness. Fig. 5.9.3 shows the radial distribution of nuclear heating in the VV components at midplane in the OB region. Nuclear heating drops by an order of magnitude in ~18 cm of VV. Nuclear heating distribution in the IB leg of the TF coils at midplane is given in Fig. 5.9.4. Nuclear heating in the IB magnet drops by an order of magnitude in ~28 cm. This relatively small attenuation is due to the toroidal geometrical effects. Table 5.9.2 lists the peak nuclear heating values calculated in the different components at the top and bottom of the machine. Relatively high nuclear heating is deposited in the W PFC. Fig. 5.9.5 shows the nuclear heating distribution in the outer divertor plate.

Table 5.9.1. Peak Nuclear Heating (W/cm^3) in the Different Components at Midplane

	Option 1 (Passively Cooled FW)		Option 2 (Actively Cooled FW)	
	IB	OB	IB	OB
Be PFC	34.7	36.8	33.3	35.6
Cu Tiles	44.9	43.6	46.9	46.3
Gasket	19.6	11.0	40.6	40.6
Cooled Cu FW	NA	NA	40.2	40.1
H2O FW Coolant	NA	NA	27.6	30.9
SS Inner VV Wall	35.9	19.6	33.8	30.9
SS VV Filer	37.5	20.6	32.9	28.5
H2O VV Coolant	17.5	11.1	14.9	15.5
SS Outer VV Wall	35.1	0.04	30.3	0.07
Microtherm Insulation	11.4	0.01	9.8	0.02
SS Inner Coil Case	NA	0.021	NA	0.038
Cu Magnet	23.1	0.010	19.5	0.019
SS Outer Coil Case	NA	1.5x10^{-5}	NA	2.8x10^{-5}
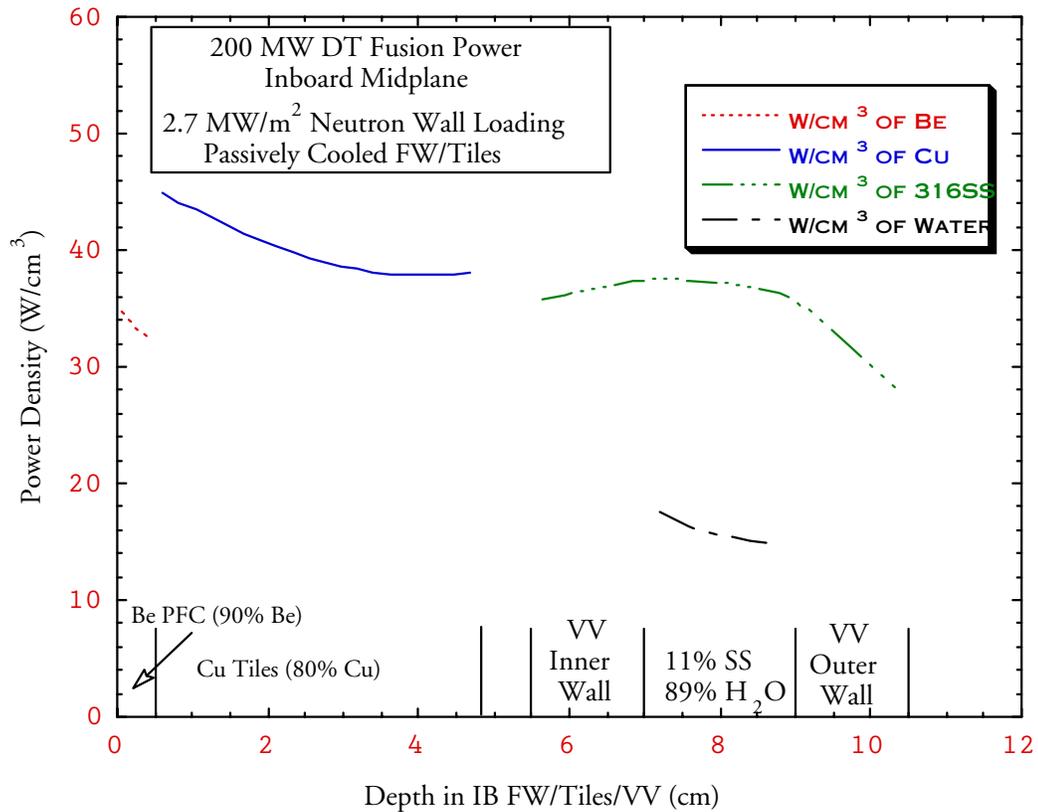
Fig. 5.9.1. Nuclear Heating Distribution in the IB FW/Tiles/VV at Midplane
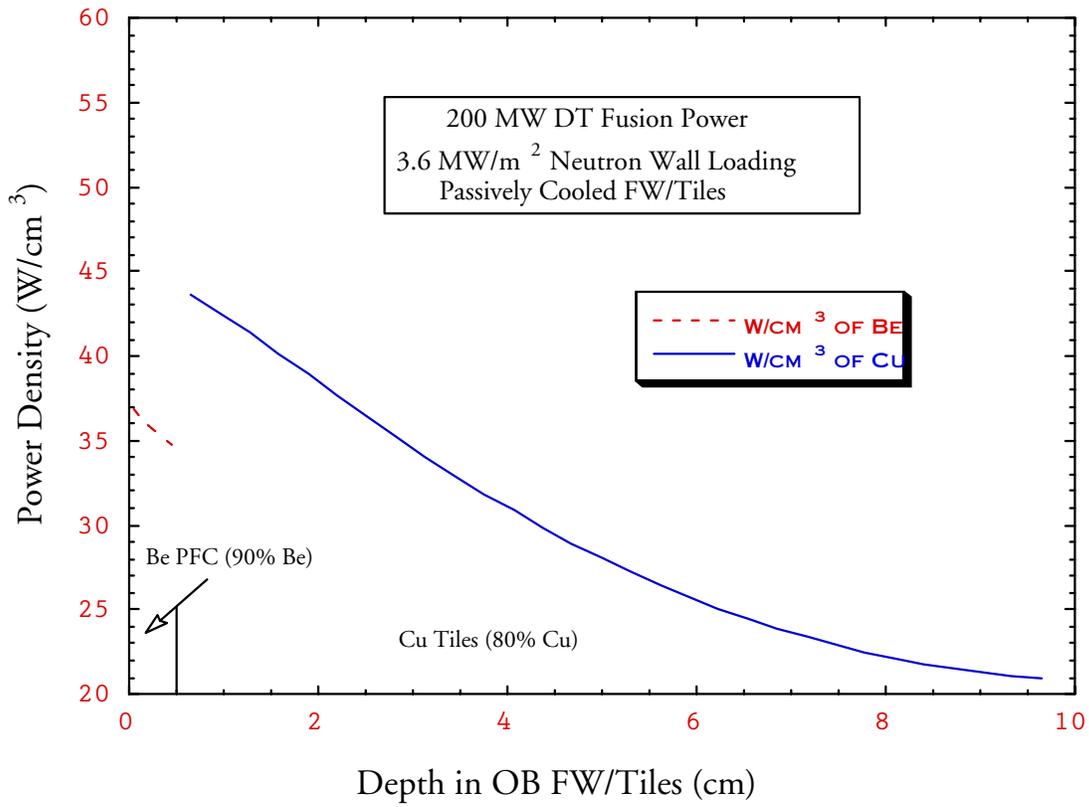
Fig. 5.9.2. Nuclear Heating Distribution in the OB FW/Tiles at Midplane
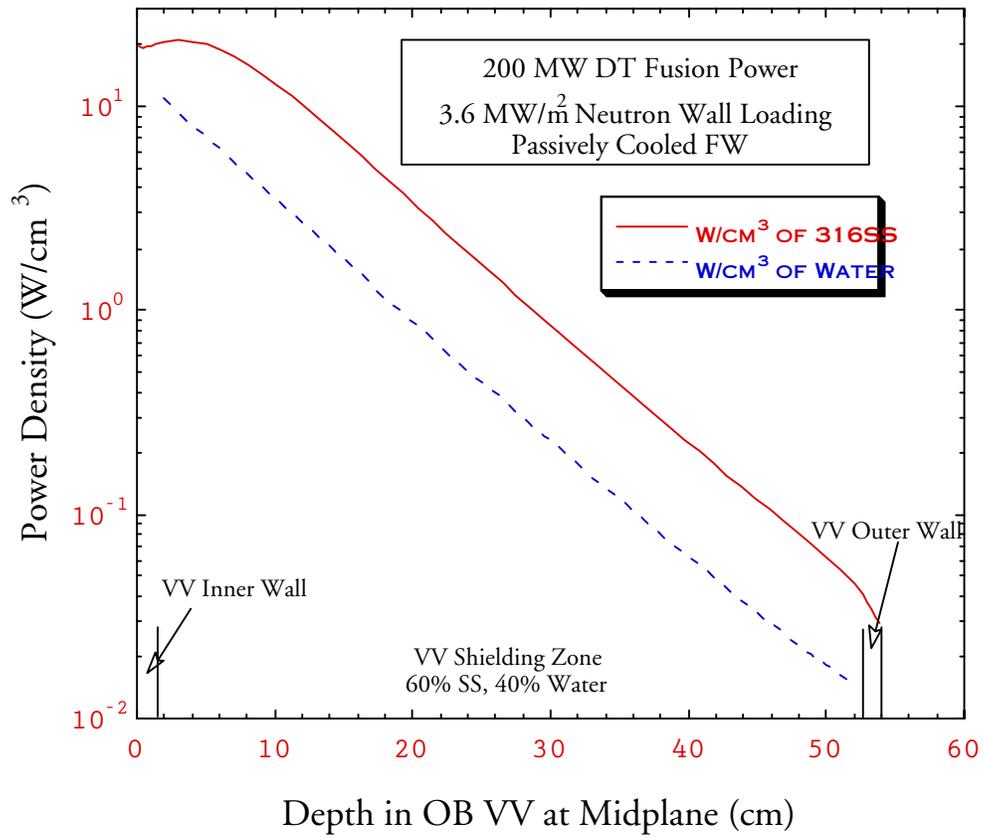
Fig. 5.9.3. Nuclear Heating Distribution in the OB VV at Midplane
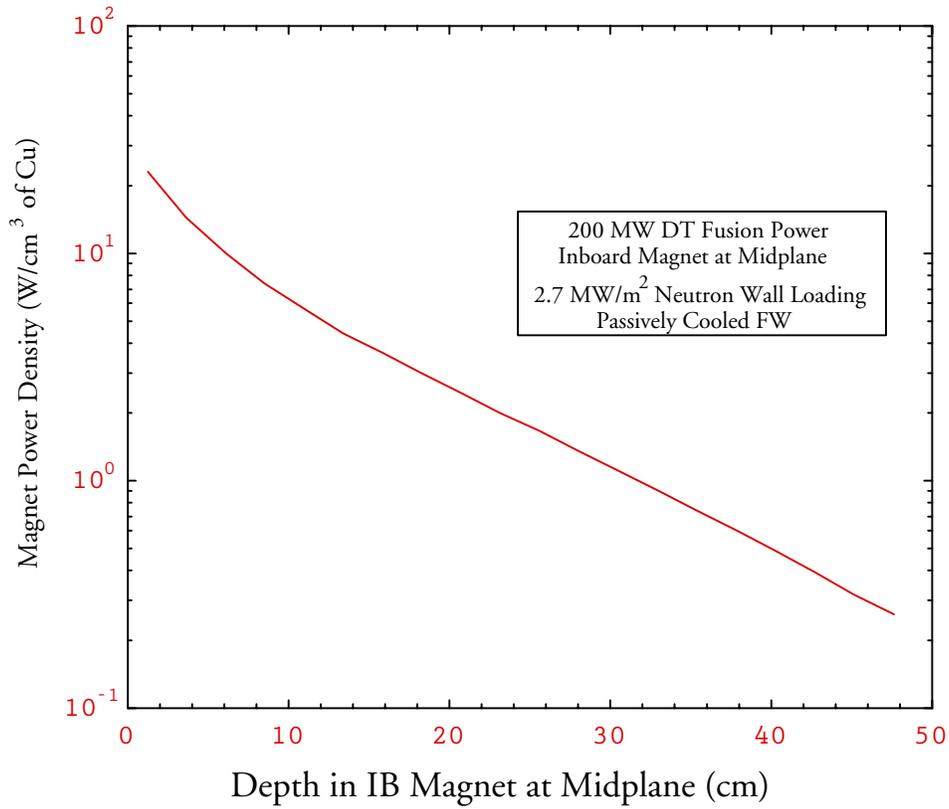
Fig. 5.9.4. Radial Variation of Nuclear Heating in the IB Magnet

Table 5.9.2. Nuclear Heating in the Divertor Region

	Peak Nuclear heating (W/cm^3)
W divertor PFC	49.0
Cu divertor heat sink	17.2
SS divertor structure	14.9
SS VV	6.7
Magnet	1.7
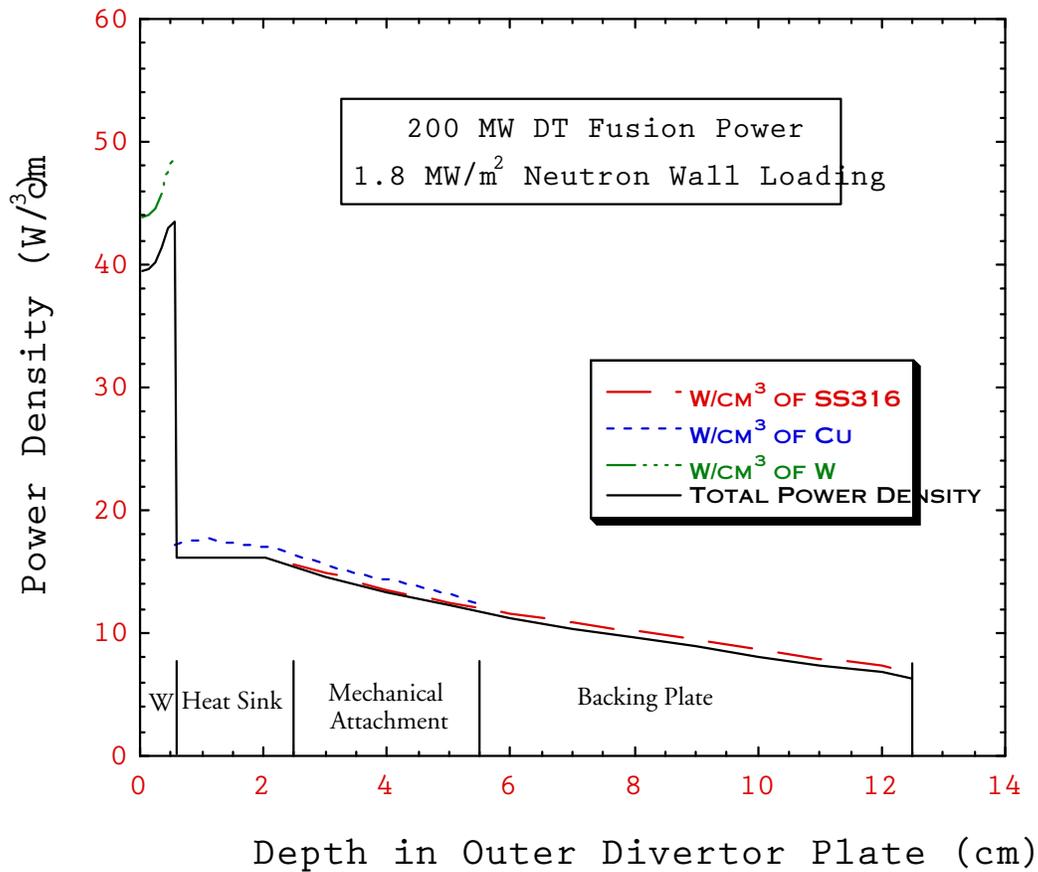
Fig. 5.9.5. Nuclear Heating Distribution in the Outer Divertor Plate

The total nuclear heating in the 16 TF coils for 200 MW DT fusion power was estimated based on the results of the 1-D calculations taking into account the poloidal variation of neutron wall loading, shielding thickness, and magnet toroidal coverage. Table 5.9.3 gives the breakdown of total magnet nuclear heating for the two FW/tiles design options. The total heating is dominated by contribution from the lightly shielded IB legs. The total magnet heating decreases by 14% in Option 2 compared to Option 1 because of the added water coolant in the FW and using Cu in the gasket in place of SiC.

Table 5.9.3. Total Magnet Nuclear Heating

	Magnet Nuclear Heating (MW)	
	Option 1	Option 2
IB region	27	22.9
OB region	0.03	0.05
Divertor region	2.1	2.1
Total	29.13	25.05

5.9.3   Radiation Damage

The peak cumulative end-of-life radiation damage values were calculated for the FW/tiles, VV, divertor, and magnet. Atomic displacement (dpa) and He production rates were determined. For the operation scenario of total DT fusion energy of 5 TJ and total DD fusion energy of 0.5 TJ, the dpa values are very low (< 0.05 dpa) and will not limit the lifetime of these components. Since the VV is protected from the fusion neutrons by the thin FW/tiles, the issue of reweldability was addressed. The end-of-life helium production in the VV structure should be limited to 1 appm to allow for rewelding. Table 5.9.4 gives the cumulative end-of-life peak VV He production at different poloidal locations for the passively and actively cooled FW/tiles design options. The contribution from DD shots is very small (<0.15%). In Option 1, the peak VV helium production occurs in the IB region since the FW/tiles is 5 cm thinner than in the OB region. In Option 2, the FW/tiles thickness is the same in both regions and the higher OB neutron wall loading results in higher VV He production in the OB region. Lower VV He production occurs in the divertor region as a result of shielding by the relatively thick divertor plate. The IB VV He production decreases by 15% in Option 2 because of the added water

coolant in the FW and using Cu in the gasket in place of SiC. The OB VV He production increases by a factor of ~2 in Option 2 due to the 5 cm reduction in FW/tiles thickness. The results imply that reweldability of the VV should not be a concern with both FW/tiles design options.

Table 5.9.4. Peak End-of-life He Production (appm) in VV

	Option 1	Option 2
IB midplane	0.13	0.11
OB midplane	0.07	0.15
Divertor	0.016	0.016

5.9.4   Magnet Insulator Dose

The dose rate to the insulator in the TF magnet was calculated at different poloidal locations. The dose rate was determined at the front layer of the magnet winding pack. For 5 TJ of DT fusion enrgy and 0.5 TJ of DD fusion energy, Table 5.9.5 provides the peak cumulative end-of-life magnet insulator dose at different poloidal locations. The results are given for both FW/tiles design options. Because of the minimal shielding provided by the thin VV in the IB region, the peak value occurs in the IB side at midplane. The dose rate decreases as one moves poloidally from the IB midplane to the OB midplane. The neutron contribution to the insulator dose varies between 50% at the front of the winding pack to 30% at the back.

The relative contribution from DD shots decreases as one moves poloidally from the IB midplane to the OB midplane due to increased attenuation of DD neutrons compared to attenuation of the high energy DT neutrons. The peak cumulative insulator dose decreases by 14% in Option 2 compared to Option 1 because of the added water coolant in the FW and using Cu in the gasket in place of SiC.

Table 5.9.5. Cumulative Peak Magnet Insulator Dose

	Option 1	Option 2	% from DD Shots
IB midplane	1.47×10^{10}	1.26×10^{10}	13%
OB midplane	6.97×10^{6}	1.26×10^{7}	1.6%
Divertor	9.80×10^{8}	9.80×10^{8}	10%

The mechanical strength, dielectric strength, and electric resistivity are the important properties that could be affected by irradiation. Experimental results indicate that the electrical properties are not degraded as much as the mechanical properties. The shear strength is the property most sensitive to irradiation. The commonly accepted dose limit for epoxies is 10^{9} Rads. This is the limit used in ITER. Polyimides and bismaleimides are more radiation resistant with experimental data showing only a small degradation in shear strength at dose levels in excess of 10^{10} Rads. However, they are difficult to process due to their high viscosity and requirement for high temperatures to fully cure. Hybrides of polyimides or bismaleimides and epoxies could provide radiation resistant insulatorswith more friendly processing requirements.

The results presented here were obtained by performing 1-D calculations. Based on previous studies, accurate modeling of the chamber geometry and source profile in a 3-D calculation results in about 20% lower peak IB results. In addition, in the FIRE design, the peak shear stresses occur at the top and bottom of the TF coil IB leg behind the divertor. The end-of-life dose to the insulator at this location is reduced to $\sim 10^{9}$ Rads due to the additional shielding provided by the divertor. The insulator dose decreases as one moves radially from the front to the back of the winding pack as shown in Fig. 5.9.6. The dose decreases by an order of magnitude in ~ 22 cm of the IB magnet. Based on this analysis, it is expected that the magnet insulator will last for the whole device lifetime.
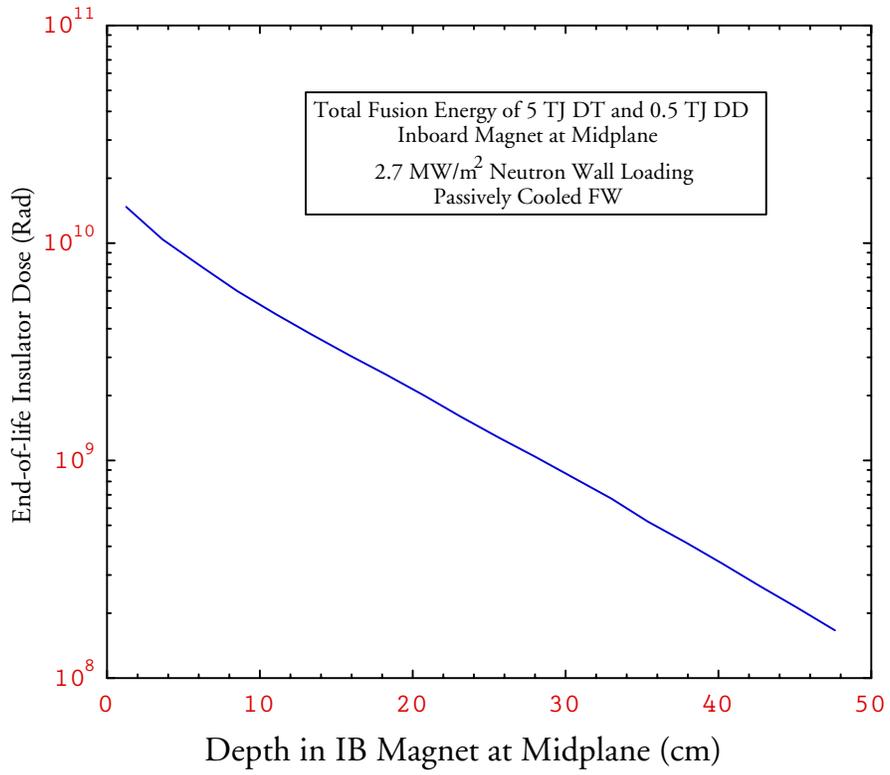
Fig. 5.9.6. Radial variation of insulator dose in the IB magnet

5. 10 Decay Heat, and Radiation Exposure

5.10.1 Introduction

Activation analysis was performed using toroidal cylindrical geometry with the inboard and outboard sides modeled simultaneously. Calculations assumed peak neutron wall loadings of 1.8 and 3.6 MW/m^2 for the divertor and outboard first wall, respectively. The machine is assumed to have an operation schedule of four pulses per day for one full power year (FPY). The total number of pulses is 3000 with a pulse burn of 10 seconds and three (3) hours between pulses. Calculations were performed for D-T and D-D pulses with 200 MW and 1 MW of fusion power, respectively. The analysis was performed for two different first wall/tiles options. The first option is the passive cooling option. In this case the model used includes an inboard first wall which is 5 cm thick and consists of 4.3 cm of a CuCrZr alloy followed by a 0.2 cm SiC gasket and utilizes a 0.5 cm layer of Be coating as a plasma facing component (PFC). The outboard first wall has the same radial build but the Cu layer is 9.3 cm thick. The second option is the active water cooling option. In this case the model used for the inboard and outboard first wall is also 5 cm thick and consists of 0.5 cm layer of Be PFC coating, 1.8 cm of a CuCrZr alloy, 0.2 cm Cu gasket, and 2.5 cm layer of water cooled CuCrZr alloy.

The vacuum vessel structure is made of 316 SS and it uses a mixture of 304 SS and water as a vacuum vessel shield. The vacuum vessel thickness varies poloidally from 4.7 cm in the inboard region to 55.5 cm in the outboard region at the midplane. The magnet winding pack is modeled using OFHC alloy, which is 61.5 cm thick on the outboard side at the midplane. The magnet uses a 316 SS coil case with 4 cm front thickness and 6 cm back thickness. The divertor consists of three layers. The front layer consists of 0.5 cm thick tungsten rods followed by 2 cm of a CuCrZr/water mixture as a heat sink, and a 3 cm thick layer of a mechanical attachment made of CuCrZr/316 SS mixture. Finally, the mechanical attachment connects the heat sink to a 7 cm thick layer of 316 SS/water mixture which is used as a backing plate. The use of a plug (80% steel and 20% water) to stop neutrons streaming through penetrations at the midplane and using an additional shield at the top of the machine were assessed.

5.10.2 Activity and Decay Heat

The neutron flux used for the activation calculations was generated by the one-dimensional discrete ordinates neutron transport code ONEDANT. The activation analysis was performed using the activation code DKR-PULSAR2.0. The code combined the neutron flux with the FENDL/A-2.0 cross section library to calculate the activity and decay heat as a function of time following shutdown. Figures 5.10-1 and 5.10-2 show the specific activity values for the inboard and outboard regions of the option 1 design as a function of time following shutdown, respectively. Figures 5.10-3 and 5.10-4 show the specific activity values for the inboard and outboard regions of the option 2, respectively. Figures 5.10-5 and 5.10-6 show the specific decay heat values for the inboard and outboard regions of option 1 as a function of time following shutdown, respectively. Figures 5.10-7

and 5.10-8 show the specific decay heat values for the inboard and outboard regions of option 2, respectively. Finally, figures 5.10-9 and 5.10-10 show the specific activity and decay heat generated in the divertor. As shown in figures 5.10-1 to 5.10-8, the levels of activity and decay heat generated in the two options are comparable. The plasma facing components, first wall on the inboard and outboard sides as well as the divertor, produce the highest levels of specific activity and decay heat. However, the favorable operational schedule allows for the decay of short-lived radionuclides between pulses resulting in low levels of activity and decay heat at shutdown.
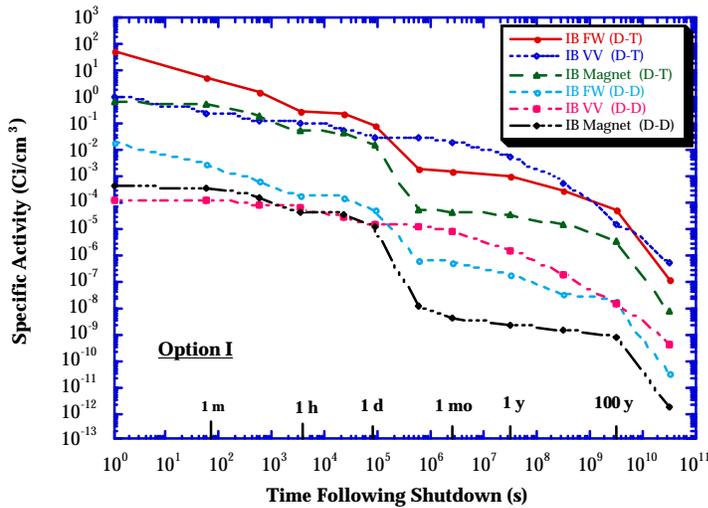
Fig. 5.10-1. Activity induced in the inboard side of option 1.
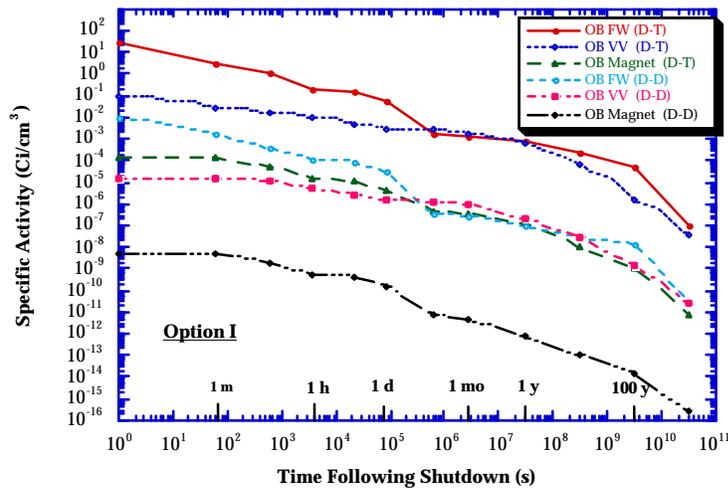
Fig. 5.10-2. Activity induced in the outboard side of option 1.
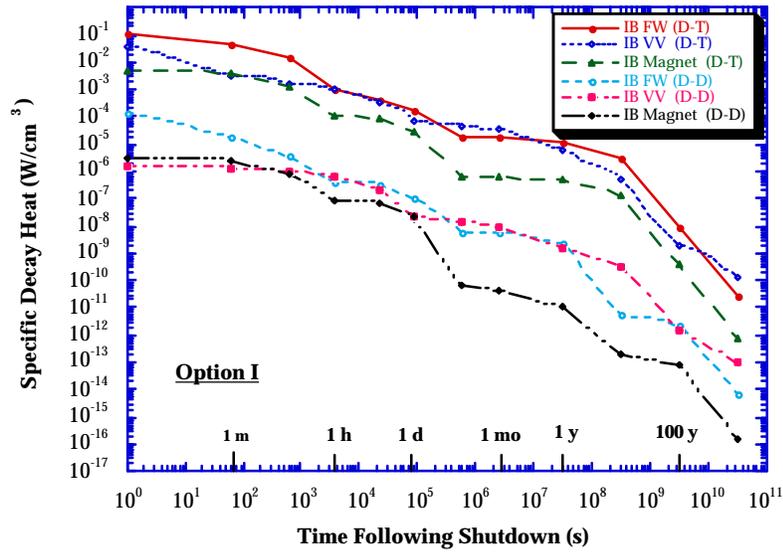
Fig. 5.10-3. Decay heat induced in the inboard side of option 1.
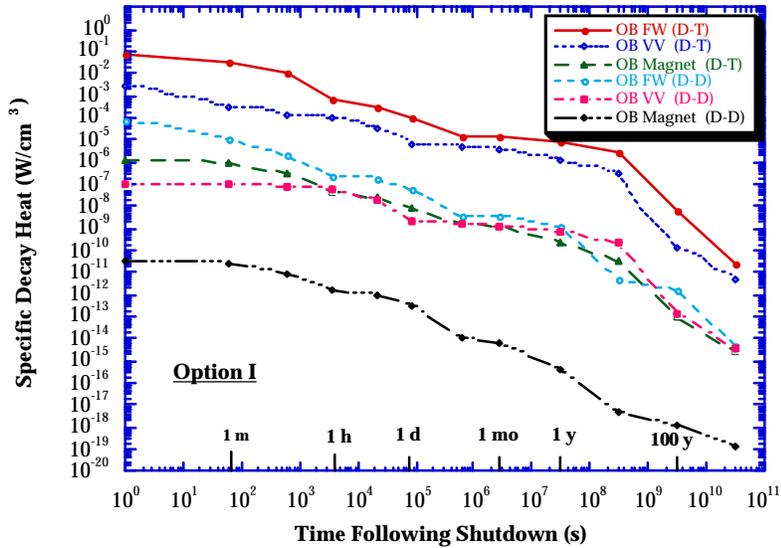
Fig. 5.10-4. Decay heat induced in the outboard side of option 1.
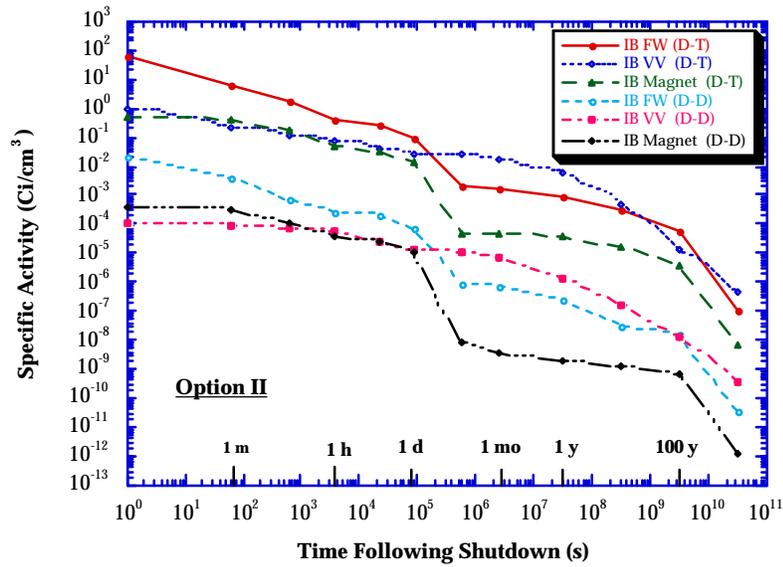
Fig. 5.10-5. Activity induced in the inboard side of option 2.
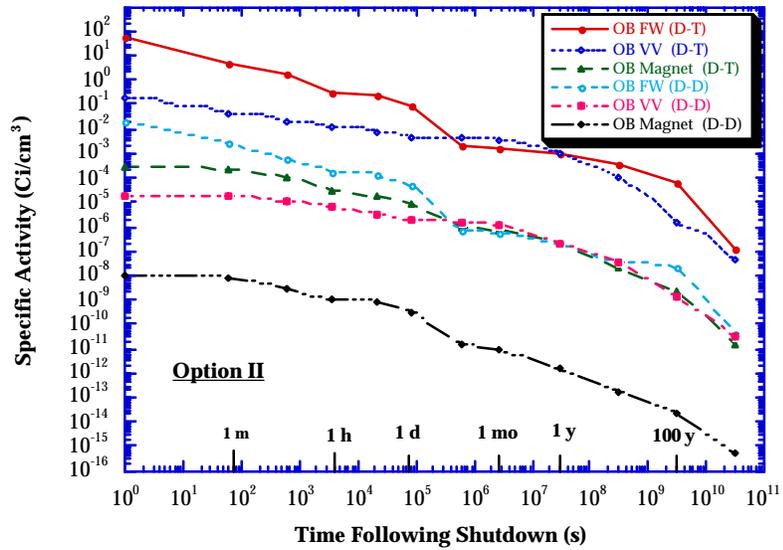
Fig. 5.10-6. Activity induced in the outboard side of option 2.
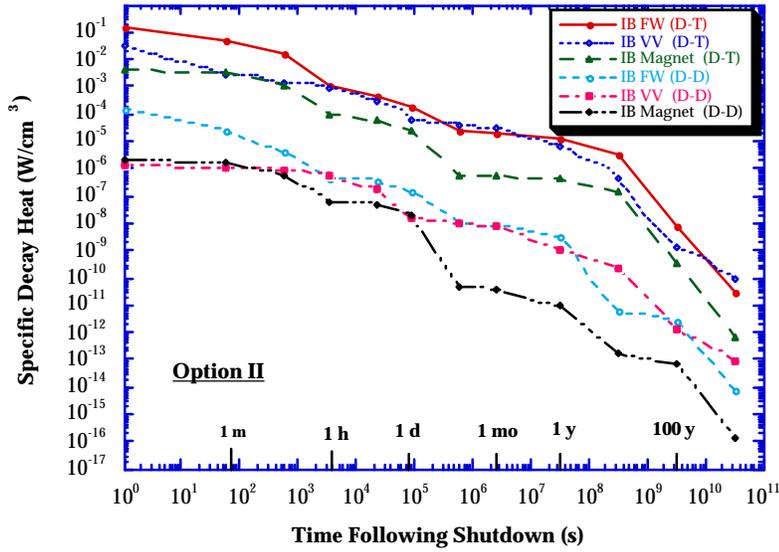
Fig. 5.10-7. Decay heat induced in the inboard side of option 2.
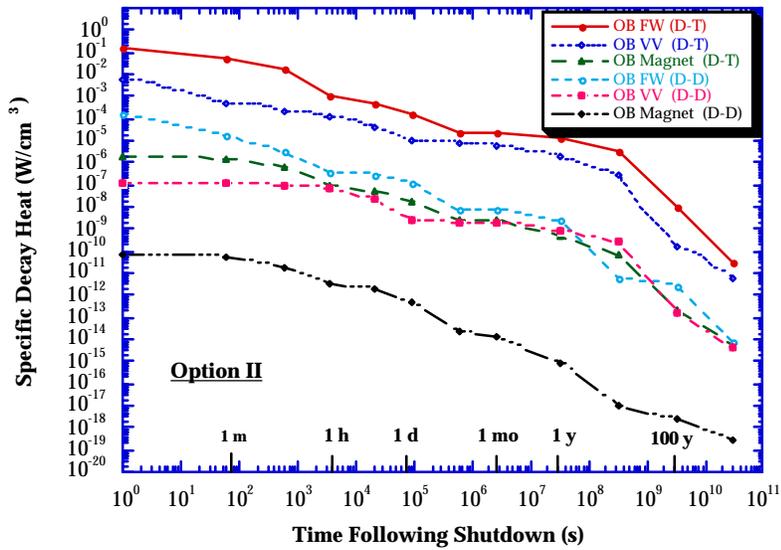
Fig. 5.10-8. Decay heat induced in the outboard side of option 2.
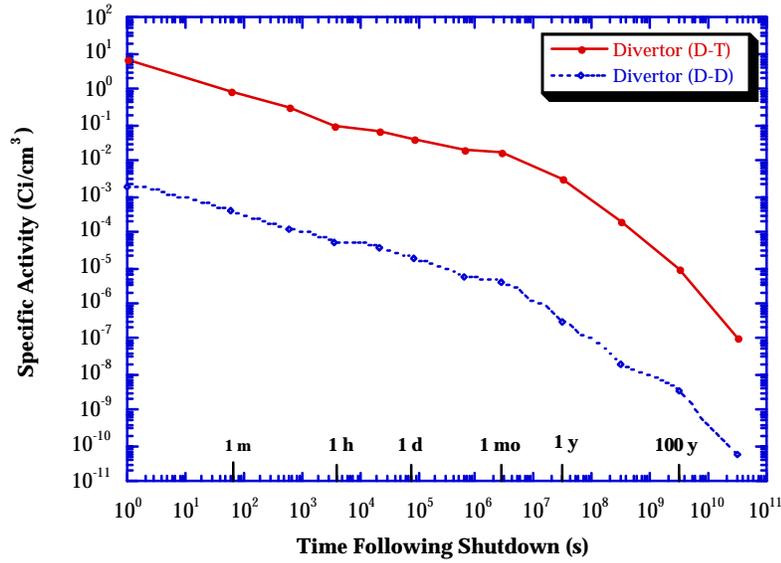
Fig. 5.10-9. Activity induced in the divertor.
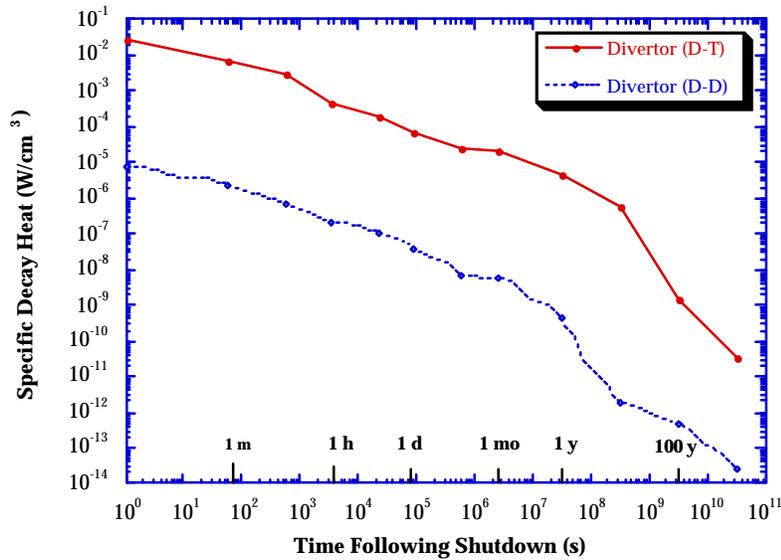
Fig. 5.10-10. Decay heat induced in the divertor.

At shutdown, the decay heat induced in the first wall following D-T shots is less than 0.25% of the nuclear heating generated in the first wall during operation. In the mean time, the ratio between the shutdown decay heat and

nuclear heating generated in the vacuum vessel during operation is on the order of 0.1%. The activity and decay heat generated following D-D shots are more than three orders of magnitude lower than their values following D-T shots due to the lower D-D fusion power and the significant reduction in the number of high energy neutrons.

Table 5.10-I. List of Dominant Nuclides.

Short-term< 1 day		
	Activity	**Decay Heat**
FW	^{62}Cu, ^{64}Cu, ^{66}Cu	^{62}Cu, ^{64}Cu, ^{66}Cu
VV	^{56}Mn, ^{58}Co, ^{51}Cr	^{56}Mn, ^{58m}Co
Mag.	^{62}Cu, ^{64}Cu, ^{66}Cu	^{62}Cu, ^{64}Cu, ^{66}Cu
Div.	^{187}W, ^{185}W, ^{181}W	^{187}W, ^{185}W
Intermediate-term < 1 month		
	Activity	**Decay Heat**
FW	^{60}Co, ^{63}Ni	^{64}Cu, ^{60}Co
VV	^{55}Fe, ^{51}Cr, ^{57}Co	^{58}Co, ^{54}Mn, ^{58m}Co
Mag.	^{60}Co, ^{63}Ni	^{64}Cu, ^{60}Co
Div.	^{185}W, ^{181}W	^{185}W, ^{181}W
Long-term > 1 year		
	Activity	**Decay Heat**
FW	^{63}Ni	^{63}Ni
VV	^{63}Ni	^{60}Co, ^{63}Ni
Mag.	^{63}Ni	^{63}Ni
Div.	^{91}Nb, ^{63}Ni	^{94}Nb, ^{39}Ar

The decay heat induced in the first wall at shutdown is dominated by the two copper isotopes ^{62}Cu($T_{1/2}$ = 9.74 min) and ^{66}Cu($T_{1/2}$ = 5.1 min). The low decay heat induced in the first wall at

shutdown is due to the fact that the short lifetimes of the ^{62}Cu and ^{66}Cu isotopes allow them to decay during the three hours between pulses. The decay heat induced in the vacuum vessel at shutdown is dominated by ^{52}V($T_{1/2}$ = 3.76 min) and ^{56}Mn($T_{1/2}$ = 2.578 hr) isotopes. Due to the short lifetime of ^{52}V, its entire radioactivity also decays between shots, resulting in a low overall radioactivity generated in the vacuum vessel at shutdown. In general, the short-term activity and decay heat values at shutdown are almost fully dominated by activation during the last pulse. Table 5.10-I shows a list of nuclides that dominate the induced radioactivity in the different machine components.

5.10.3 Biological Dose Rates

In order to assess the feasibility of hands-on maintenance, biological dose rates were calculated at different locations following shutdown. The gamma source from radioactive decay was determined at all mesh points and transported, using the ONEDANT code, to calculate dose rate at different locations following shutdown. The dose rates were calculated at the following locations:

➢ Behind the outboard vacuum vessel and magnet at the midplane.

➢ Behind the magnet at the machine top.

➢ Behind the additional shield at the machine top.
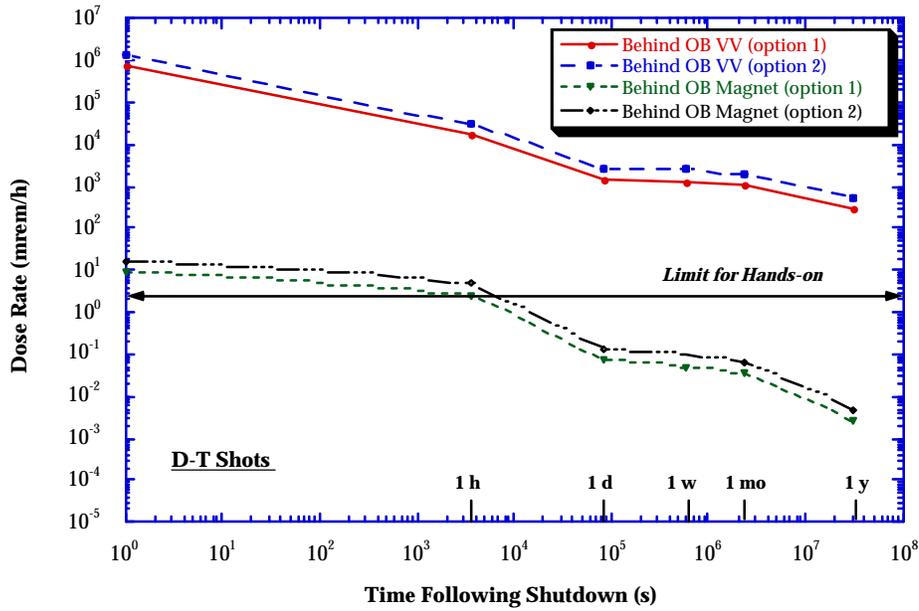
Fig. 5.10-11. Biological dose rates at the midplane following D-T shots.
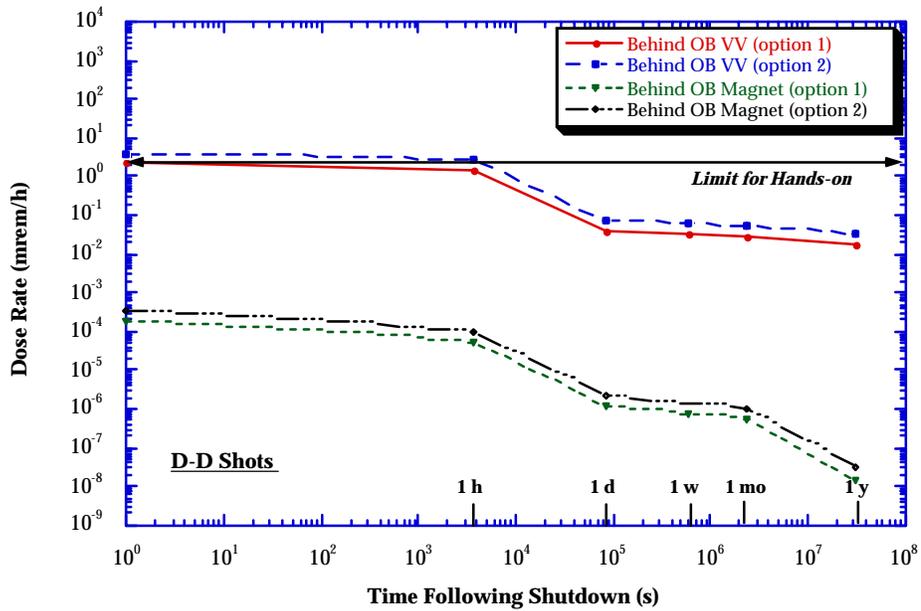
Fig. 5.10-12. Biological dose rates at the midplane following D-D shots.
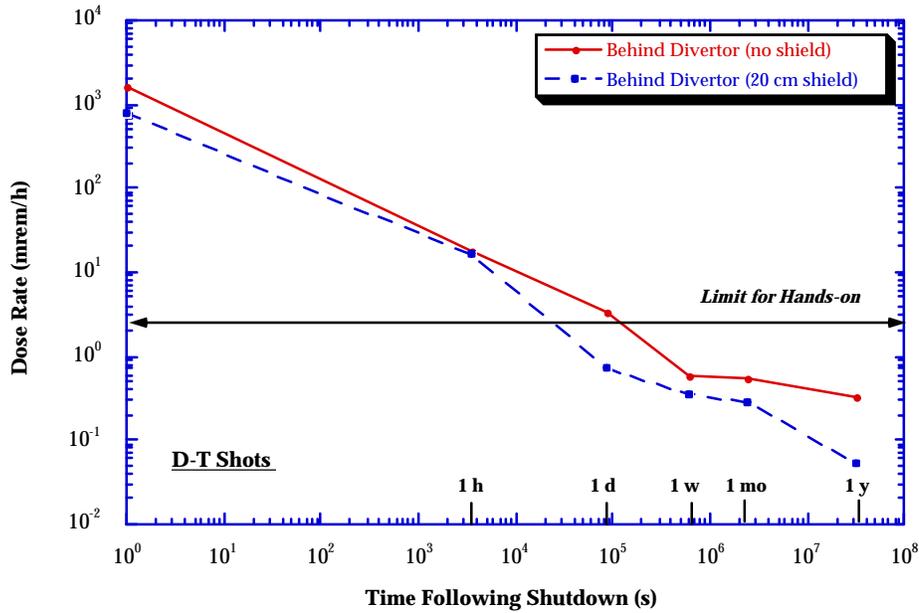
**Fig. 5.10-13.** Biological dose rates at the machine top following D-T shots.
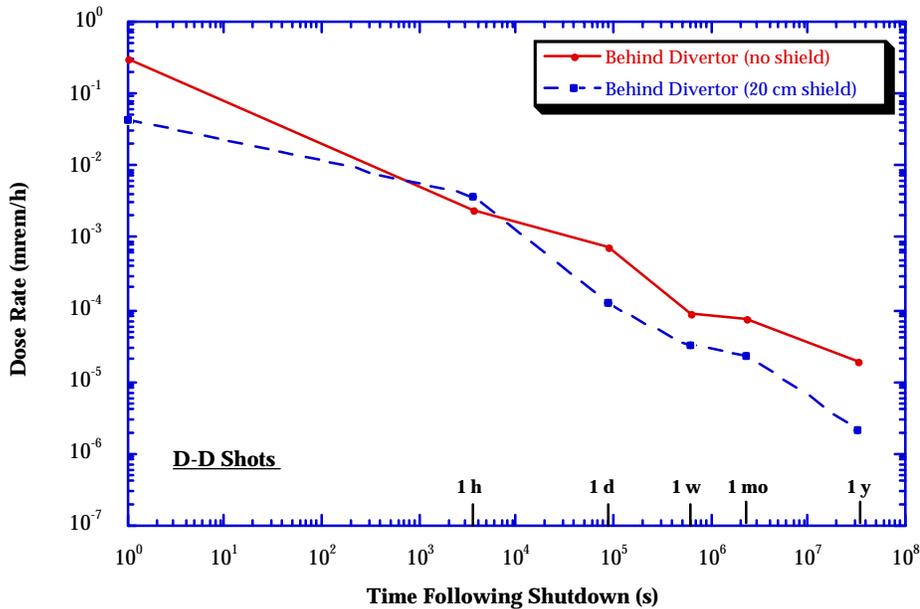
Fig. 5.10-14. Biological dose rates at the machine top following D-D shots.

Figures 5.10-11 and 5.10-12 show the biological dose rates at the midplane as a function of time following shutdown for D-T and D-D shots, respectively. As shown in figure 5.10-11, the biological dose rates behind the vacuum vessel

remain high for many decades following shutdown for D-T shots. On the other hand as shown in figure 5.10-12, in the case of D-D shots, the dose rates behind the vacuum vessel are five order of magnitudes lower than after D-T shots. The significant drop in the dose rate allows for hands on maintenance behind the vacuum vessel following D-D shots. The dose rates behind the magnet and at the midplane are acceptable for both D-D and D-T shots. The thinner outboard first wall in option 2 results in higher neutron flux near the magnet. The higher neutron flux results in dose rates in option 2 that are about twice the dose rates in option 1. Dose rates behind the magnet are caused by the $^{62m}Co(T_{1/2} = 13.9$ min) isotope and are independent on the number of pulses due to the fact that ^{62m}Co decays between pulses. One week following shutdown, the dose rates are dominated by the $^{60}Co(T_{1/2} = 5.27$ yr) isotope. The dose rates caused by the ^{60}Co isotope almost increase linearly with the increase in number of pulses. Using a 110 cm long steel plug at the midplane will stop neutron streaming through penetration and provide adequate shielding that allows for hands-on maintenance.

The dose rates at the top of the machine (at the maximum divertor thickness) following D-T shots (figure 5.10-13), drops to an acceptable level within a day following shutdown. Adding a 20 cm thick POLY/CAST shield at the top of the magnet drops the dose rates on the top of the shield to acceptable levels only few hours earlier. However, since the divertor thickness is much smaller at other locations, it is essential to maintain the same shield thickness to guarantee hands-on maintenance at all locations at the top of the machine. The shield is

composed of a POLY/CAST mix placed inside a steel tank (the tank wall is 1 cm thick). The activation of the outer wall of the steel tank results in the generation of ^{56}Mn. As shown in the figure, the $^{56}Mn(T_{1/2} = 2.578$ hr) isotope results in a slightly higher dose (in comparison to the no shield case) outside the 20 cm thick shield during the first couple of hours following shutdown. As shown in figure 5.10-14, the dose rates at the top of the machine following D-D shots are very low, allowing for immediate access to that space any time following shots.

5.10.4 Waste Disposal Ratings (WDR)

The radwaste of the different components of the machine were evaluated according to both the NRC 10CFR61 and Fetter waste disposal concentration limits. The 10CFR61 regulations assume that the waste disposal site will be under administrative control for 100 years. The dose at the site to an inadvertent intruder after the 100 years is limited to less than 500 mrem/year. The waste disposal rating (WDR) is defined as the sum of the ratio of the concentration of a particular isotope to the maximum allowed concentration of that isotope taken over all isotopes and for a particular class. If the calculated WDR ≤ 1 when Class A limits are used, the radwaste should qualify for Class A segregated waste. The major hazard of this class of waste is to individuals who are responsible for handling it. Such waste is not considered to be a hazard following the loss of institutional control of the disposal site. If the WDR is > 1 when Class A WDL are used but ≤ 1 when Class C limits are used, the waste is termed Class C intruder waste. It must be packaged and buried such that it will not pose a hazard

to an inadvertent intruder after the 100 years institutional period is over. Class C waste is assumed to be stable for 500 years. Using Class C limits, a WDR > 1 implies that the radwaste does not qualify for shallow land burial. Fetter developed a modified version of the NRC's intruder model to calculate waste disposal limits for a wider range of long-lived radionuclides which are of interest for fusion researchers than the few that currently exist in the current 10CFR61 regulations. Fetter's model included more accurate transfer coefficients and dose conversion factors.

The waste disposal ratings for the 10CFR61 and Fetter limits are shown in Table 5.10-II following D-T shots. Results in the table are given for compacted wastes. Compacted waste corresponds to crushing the solid waste before disposal and thus disallowing artificial dilution of activity. The dominant nuclides are given between brackets. At the end of the machine life, all components would qualify for disposal as Class C low level waste according to the two waste disposal concentration limits used in the analysis. As shown in the table, according to Fetter limits, the WDR are dominated by the silver impurities in the CuCrZr alloy and the niobium impurities in the 316 SS and 304 SS alloys. The 10CFR61 limits indicate that the WDR of components made of the CuCrZr alloy are dominated by ^{63}Ni which is produced from copper by the ^{63}Cu(n,p) reaction. On the other hand, the WDR of components made of the steel alloys are dominated by their niobium impurities. Due to the reduced neutron environment following D-D shots, all components will easily qualify for disposal as Class C LLW.

Table 5.10-II. Class C WDR.

Zone	Fetter	10CFR61
IB FW	0.18 (^{108m}Ag)	1.98e-2 (^{63}Ni)
IB VV	5.67e-2 (^{94}Nb)	5.87e-2 (^{94}Nb, ^{63}Ni)
IB Mag.	2.4e-4 (^{108m}Ag)	1.15e-3 (^{63}Ni)
OB FW	0.14 (^{108m}Ag)	1.7e-2 (^{63}Ni)
OB VV	1.84e-3 (^{94}Nb)	2.44e-3 (^{94}Nb, ^{63}Ni)
OB Mag.	1.2e-6 (^{94}Nb)	1.37e-6 (^{94}Nb, ^{63}Ni)
Divertor	3.4e-2 (^{108m}Ag)	1.33e-2 (^{94}Nb)

5.11 Remote Maintenance

5.11.1 Introduction

FIRE in-vessel components will become neutron activated, making it necessary to perform maintenance operations by remote techniques. Components that require remote maintenance include those mounted on the vessel interior and in the ports.

When maintenance is required, the affected components are removed from the vessel and transferred to the hot cell where they are refurbished or processed as waste. They are then replaced in the vessel by the refurbished units or a spare.

First wall (FW) and divertor modules are accessed through any of the 16 midplane ports and are handled with a cantilevered boom. Port mounted assemblies such as heating systems and cryopumps are replaced by remote handling (RH) equipment operating on the outboard end of the related port.

The strategy for FIRE ex-vessel maintenance is to employ hands-on techniques to the fullest extent possible. The FW, VV and external structures, including the magnets, are designed to provide sufficient combined shielding to allow controlled access and hands-on maintenance on the complete exterior of the machine. This includes the outboard end of the VV ports for removal of service connections in advance of removing port-mounted systems, and access to other ex-vessel areas for maintenance of services and components such as magnet current and coolant feed lines.

5.11.2 Remote Maintenance Requirements and Classification of Components

FIRE systems and components are designed to minimize remote maintenance requirements where possible. When remote maintenance is required, component modularity, standardization and segmentation are implemented to reduce costs, risks and maintenance time. Design features facilitating RH are standardized to minimize the number and variety of handling equipment and tools. Handling equipment is designed for ease of decontamination to allow hands-on reconditioning and repair.

Machine availability should not be compromised by maintenance operations, especially by those that are regularly required. For this reason, components that require regular remote maintenance (e.g., divertor modules and access port assemblies) are designed so they can be replaced in a relatively short time period.

In-vessel component designs should be optimized towards maximum verification of component performance prior to installation in the VV. This leads to the general requirement that components are fitted and withdrawn for maintenance as much as possible in one piece, avoiding or minimizing the cutting and rewelding of functional elements.

All components are classified according to their RH requirements by the following scheme. Classification is based on the need for scheduled or unscheduled maintenance or modification, the likelihood of maintenance, and on the impact of the maintenance procedure on machine operations and availability.

Once a component's classification has been determined, the type of RH equipment required, the guidelines for component design, and the program to assure RH compatibility is established. Components that obstruct access are given at least the same classification as the component to which the access is blocked, provided they require RH.

Class 1

The first category includes components that require several regularly scheduled maintenance or replacement operations (e.g., divertor). The component designs and the associated RH equipment and service procedures are optimized to ensure task completion within a specified time. All RH equipment for Class 1 components will be designed in detail during the design phase of the project. The feasibility of Class 1 maintenance tasks are to be verified during the design phase, or prior to final fabrication and may involve the use of mock-ups. Further demonstration using real components during initial assembly is highly desirable.

Class 2

The second category contains components which do not require scheduled maintenance but are likely to require a few unscheduled maintenance or removal operations (e.g., FW modules). These components are designed for full remote repair or replacement, but minimization of repair and replacement time is subordinate to consideration for the component's design, such as nuclear performance and operational reliability. RH equipment for Class 2 components will be designed in detail during the design phase of the project. The feasibility of Class 2 maintenance tasks will be verified where deemed practical and necessary and may

involve the use of mock-ups. Demonstration using actual components during initial assembly of the machine is very desirable.

Class 3

The third category of components are not expected to require maintenance, such as a VV segment and toroidal field coil. These components are expected to last through the operating phase, and major maintenance or upgrading is not anticipated. If major maintenance operations should be needed, they will require substantial disassembly of at least part of the tokamak and the projected maintenance time may be long. Although these components must be designed to make disassembly and replacement feasible by RH means, their design emphasizes reliability and performance optimization. The procedures for maintenance of selected Class 3 components will be defined during the design phase.

Class 4

The fourth category of components do not require remote maintenance or are non-essential to continued operation. Class 4 includes components that:
- are hands-on accessible and maintained;
- are non-essential to FIRE operation and are considered expendable in the event of failure; or
- have negligible risk of failure.

The RH classification of major FIRE components is presented in Table 5.11.2-1. Auxiliary systems such as diagnostics and heating systems are not specifically listed. They are housed in standard port assemblies.

Table 5.11.2-1   Remote Handling Classification of Major FIRE Components

Class 1	Class 2	Class 3	Class 4

Divertor Modules
 	
Limiter Modules
 	
Midplane Port Assemblies
  - RF heating
  - diagnostics
	First Wall Modules
	
	Upper and Lower Horiz. Auxiliary Port Assemblies
	   - cryopumps
	   - diagnostics
		Vacuum Vessel Sector with Toroidal Field Coil
		
		Passive Plates
		
		In-Vessel Cooling Pipes
		   - divertor pipes
		   - limiter pipes
			Toroidal Field Coil Connections
			
			Poloidal Field Coils
			
			Central Solenoid
			
			Magnet Structure

Additional information regarding the anticipated frequency of component maintenance and maintenance time estimates is contained in the appendix.

5.11.3 Remote Maintenance Approach

In-vessel components will generally be removed as integral assemblies and transferred to the hot cell where they will be repaired or processed as waste. In-situ maintenance operations will typically be limited to inspection (viewing and metrology), vacuum window replacement and leak testing.

Containment and transfer of in-vessel components

In-vessel interventions are carried out with the VV cooled and vented. At least one containment barrier is required during openings to prevent the release of hazardous material (i.e., activated dust, tritium and beryllium). For this reason, in-vessel interventions will be performed from sealed transfer casks that dock to the VV ports and that contain the required RH equipment. Cask docking interfaces at the ports and hot cell utilize

"double seal doors" to keep the exterior surfaces of the port and cask doors clean.

Component transfer casks are not shielded due to the resulting excessive weight and size. When VV ports are open for extended periods, e.g., during in-vessel interventions involving the removal of several in-vessel components, a shielded enclosure will be installed at the port opening / cask location so that personnel access to other ex-vessel regions of the machine is possible.

Transfer routes between the VV and hot cell will be evacuated of personnel when a cask containing activated components is moved. This would typically be performed during off-shift hours to minimize interruptions to machine access. Casks will be moved by either the facility overhead crane or a separate vehicle such as an air cushion transporter.

Port-mounted system maintenance and handling

Port-mounted systems are housed in a standard integrated assembly that

includes shielding for the port opening. Auxiliary heating systems are mounted in midplane ports, diagnostics utilize all port types and cryopumps are mounted in the upper and lower auxiliary ports. Midplane port assemblies are removed to either maintain the system assembly or to gain access to the in-vessel plasma region.

Port assembly design details will vary depending on the system, but the space envelope, port attachments and handling techniques are standardized. The assembly is mechanically attached and vacuum seal welded at the vacuum closure plate located at the outboard end of the port. Prior to cask docking and removal operations, the system services (e.g., cooling water pipes, waveguides, transmission lines, etc.) feeding through the port interface in the ex-vessel region are hands-on removed. Remote operations begin with the disassembly of the VV closure plate.

Port assembly handling equipment includes a cask, double seal door and handling vehicle. A transfer cask and RH equipment are provided for each type of port (i.e., midplane port and upper & lower horizontal auxiliary port). The handling vehicle attaches to the assembly's vacuum closure plate. A manipulator is included onboard the vehicle for handling tools and performing closure plate bolting and vacuum seal cutting and welding operations. After disconnection from the port, the assembly is withdrawn to the cask and is transferred to the hot cell for repair or replacement of any faulty components. Installation is performed by a reversal of these operations.

Divertor, first wall and limiter module maintenance and handling

These components are accessed and handled through the midplane ports. At least one port assembly must first be removed using the equipment and procedures discussed in the previous section. The handling system consists of a cantilevered articulated boom operating from a transfer cask docked to the VV port as shown in Figure 5.11.3-1.

The boom reaches one-quarter of the in-vessel surfaces from a single port so localized module replacements can be performed through one or more ports and the complete in-vessel region can be accessed from 4 of the 16 midplane ports. The boom is equipped with an end-effector to position and handle either the divertor, FW or limiter modules. Different end-effectors specific to each of the module types is necessary. In addition, a general purpose manipulator end-effector may be required to provide adaptable handling capabilities and to perform certain component maintenance operations.

Prior to removal, coolant pipes to the divertor and limiter modules must be cut. This is performed with pipe bore tooling that is hands-on deployed inside the coolant pipes where they enter the upper and lower horizontal ports. The pipes are then rewelded to the modules and leak checked during the installation process.

Once disconnected from the VV, a module, or modules, are removed to the cask and transferred to the hot cell for repair operations such as surface refurbishment.

Transfer Cask

Articulated Boom

Boom End-Effector

Midplane Port Assembly
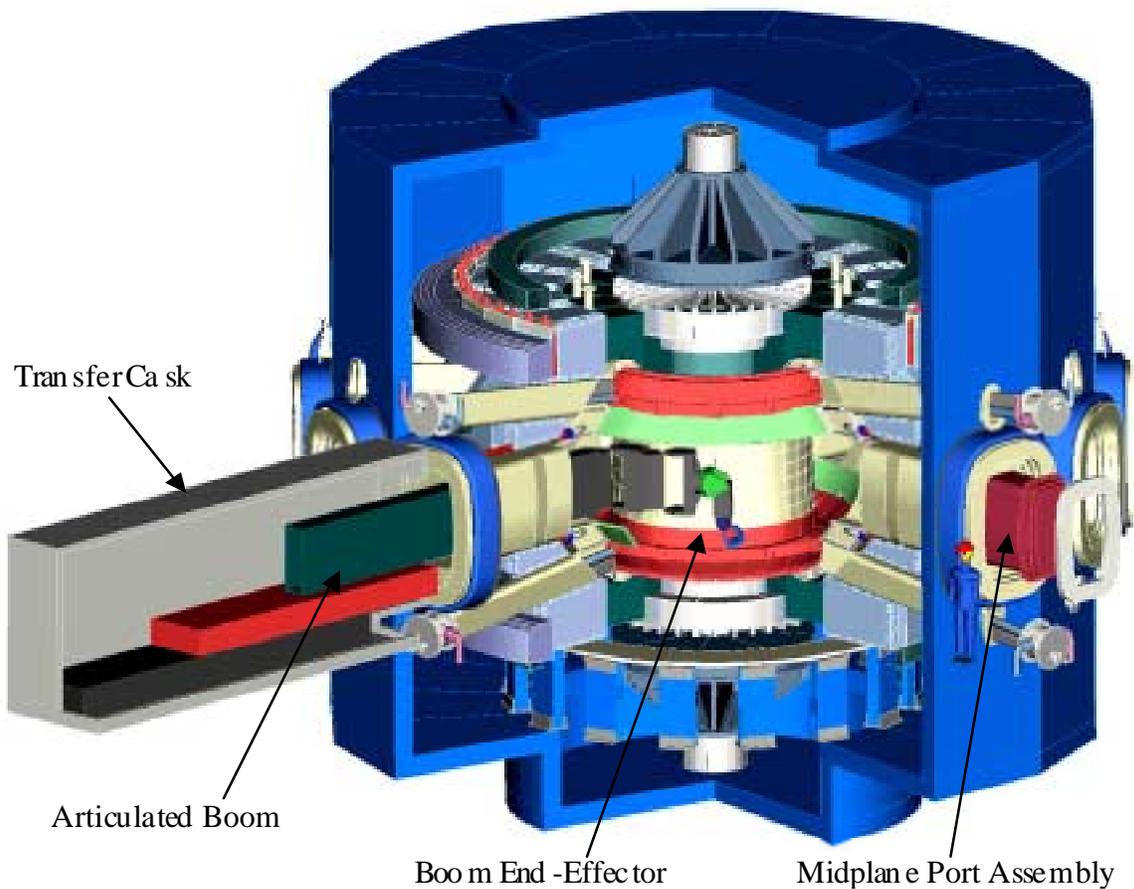
Figure 5.11.3-1 In-vessel transporter deployed inside the vacuum vessel

Inspection of Plasma Facing Surfaces

Plasma facing surfaces must be periodically inspected to verify alignment, quantify erosion and perform visual inspections. Viewing and metrology inspection is performed with vacuum compatible probes that are inserted through an upper vertical port to the plasma region of the vessel. Inspections are conducted between plasma shots with the vessel at vacuum and bakeout temperatures, or during maintenance campaigns with the vessel cooled and vented.

Metrology measurements of sub-millimeter accuracy are required and achieved with a frequency-modulated coherent laser radar based sensor. Viewing is performed with conventional camera (video) based systems. Both inspection systems utilize a common vacuum compatible deployment probe design.

5.12 Magnet Power Supplies

The conceptual design of power supplies for FIRE magnet systems seeks to minimize capital cost by leveraging existing capabilities of the local electric utility, which are assumed to be robust. Therefore, all of the FIRE device's time-varying power (peak demand of 800MW for 10T) for TF and PF magnets as well as the RF systems are provided directly by the utility's "stiff grid" without requiring any power demand ramp rate limiting equipment, or energy storage equipment, at the FIRE device site. However, provision for reactive power (MVA) support up to 300MVA is included in the design baseline. The grid's ability to supply the required time varying active and reactive power demand will be evaluated when a specific FIRE site is chosen and the above assumptions adjusted as necessary.

FIRE Magnet Power Supplies equipment includes:

•2-quadrant thyristor rectifiers converting power between the 60 hertz 3-phase ac line and the controlled dc needed by the magnets, along with their associated transformers, circuit breakers, and other equipment,

•resistor banks and associated interrupter /switching circuits (e.g., for plasma initiation).

<u>TF System</u>

The TF electrical power circuit consists of thyristor rectifier modules interposed between the local electric utility company's ac line power "source" and the TF magnet "load". Figure 5.12-1 schematically depicts two such 6-pulse bridge modules sharing a rectifier transformer.

Figure 5.12-1: Two Thyristor Rectifier Modules
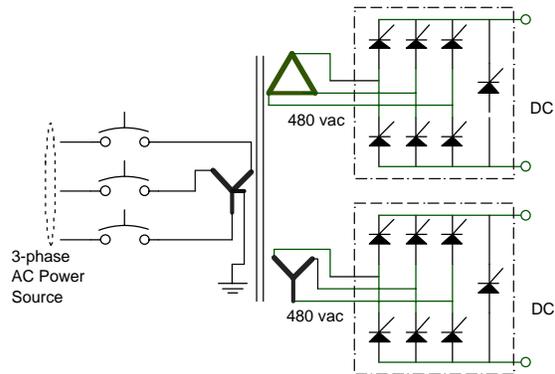
Each 6-pulse bridge module includes 6 thyristor 'valves' and their controls (not shown) connected between a 480 vac 3-phase floating transformer secondary and its DC load circuit, and another 'bypass' thyristor connected across the load. Each TF module's output current ranges over 0-59.5 kA DC while its output voltage ranges over ±650 volts. If the two modules shown are connected in series and also controlled identically, the resulting 12-pulse rectifier develops ±1.3 kV while introducing less harmonic noise to the ac power grid. Using abbreviated symbols, Figure 5.12-2 shows the planned DC circuit connection of fourteen of these modules providing up to 417 kA, ±1.3 kV to power the TF coils.
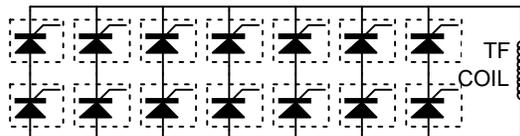
Figure 5.12-2   DC Modules in TF System

The TF circuit operates in three successive phases during each pulse. During the TF ramp-up phase, the maximum possible TF forcing voltage, equal to the TF system's open-circuit

voltage minus its regulation droop (proportional to TF current), is supplied to charge the TF electromagnet. During the TF flattop phase, the TF voltage is feedback controlled to match resistive losses and thus maintain the TF current at its desired value. During the TF shutdown phase, the TF voltage polarity is either "crowbarred" to zero volts or is reversed by operating the thyristor rectifiers in their inversion mode to rapidly remove some of the stored magnetic energy and return it back to the electric utility's ac power line.

The key TF electrical power system design parameter which can be varied is the open-circuit volts/turn. With no need for local energy storage, TF power system cost varies directly with its MVA rating. Higher volts/turn values require a higher MVA rating for the power system and would draw more peak power from the line, but yield faster TF coil charging which reduces TF coil energy consumption and heating during the ramp-up phase. This relation defines a tradeoff optimization between TF power system cost and TF flattop duration. The tradeoff result chosen for this design selects an open circuit volts/turn value of 5.42 v/t. This value requires a TF system pulse rating of 542 MVA, but yields a 19 second time for the nonlinear TF ramp-up waveform to reach the full 10 Tesla design field.

The 542 MVA TF power system pulse rating is set by the expected maximal TF waveform, which has an equivalent square wave duration of 36 seconds. However, the FIRE device may have a complementary long pulse mission requirement of providing 4 Tesla, 2 MA advanced tokamak plasmas for several minutes duration. If so, the continuous

rating for the TF power system is 217 MVA.

The TF loop voltage and the number of turns per TF coil were chosen together to permit use of power supply equipment with an industrial standard as its operating voltage and to allow a TF coil turn size convenient for manufacture. If it becomes necessary to change the TF design to a non-standard voltage, a cost increase would be expected. With 15 turns in each of 16 TF coils, the full 10 Tesla current per turn is 417 kA and the total TF open circuit loop voltage is 1300 volts. Since 6-pulse thyristor rectifier bridge circuits operating from standard 480 vac 3-phase power produce an open circuit voltage of 650 volts, the dc output sides of 6-pulse bridge modules powered from 480 vac Y-Δ rectifier transformer secondary windings are connected in series pairs to form 1300 volt 12-pulse rectifiers. Multiple 12-pulse rectifiers are connected in parallel to provide the full 417 kA pulsed output current. Current sharing between rectifiers is enforced through a passive interconnecting network for high frequency imbalance components and through active feedback control of thyristor firing angle differences for low frequency imbalance components.

During the TF flattop phase, the TF power supply output voltage necessary to counteract resistive losses will vary from about 600 to 800 volts as TF circuit resistance increases due to conductor heating. This reduced flattop voltage will be developed by retarding rectifier firing angles as needed to maintain the total 417 kA TF current.

During a TF shutdown using inversion, the TF power supply voltage will be adjusted to -1000 volts by retarding the

firing angle maximally without incurring commutation failures. Commutation failures have increased likelihood during such inversion operations. The negative voltage removes some of the TF coil's 3.8 Gigajoules of magnetic energy and returns it to the electric utility power line as a negative power load, initially -417 MW and then increasing to zero. Combined with the effect of the TF circuit's resistive voltage drop, this produces a nonlinear TF ramp-down waveform with coil heating intermediate between a 10 second linear ramp-down and a "crowbarred" shutdown. However, the zero volts situation will unavoidably result on rare occasions whenever inversion commutation failures occur, so the TF flattop pulse duration's will need to be restricted to limit end-of-pulse TF coil temperatures for those occurrences. No flattop extending benefit derives from inversion unless a higher non-repetitive peak coil temperature can be permitted for rare commutation failure events than can be permitted for repetitive pulses.

Waveform plots calculated for a TF pulse with "crowbarred" shutdown are shown in Figures 5.12-3 (a) and (b)

If the local utility company is not willing to accept the -417 MW pulsed inversion load, it still would be possible to operate the FIRE device by "crowbarring" the TF power supply circuit to zero volts and reducing the flattop duration to accommodate the additional repetitive rampdown heating. Alternatively, to avoid TF flattop reduction it would become necessary to include a resistor bank and its associated dc interrupter power transfer circuitry and switching to repetitively absorb some of the TF energy.

The TF coil system stresses may permit an extension of operations up to 12 Tesla. If 12 Tesla operation were pursued as a mission-extending enhancement, it would be necessary to upgrade the TF power system. Possible options for this upgrade have not been fully evaluated but are discussed here. Additional paralleled thyristor rectifier units (108 MVA) would be needed to provide the total 500 kA TF current for 12 Tesla operation. Although the total stored TF magnetic energy would increase to 5.5 Gigajoules, the total dissipated resistive energy per pulse

(a) Toroidal Coil Field   (b) Power Supply and Coil Terminal Voltage

Fig. 5.12-3. FIRE TF Coil Field and Power Supply Voltage Waveforms
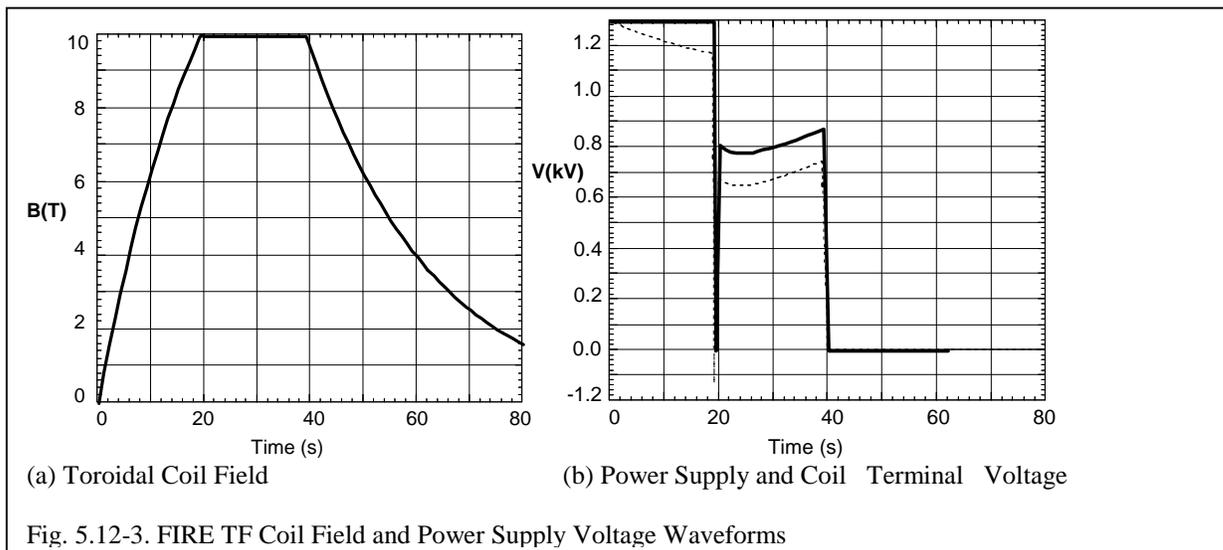
must not be permitted to increase (because of TF coil temperature limits). The TF voltage could be left at its 1300 volt design value (which would restrict the extended TF system rating and electric utility line demand by the TF system to 650 MVA), but the resulting flattop time at 12 Tesla would be very short. To extend the flattop duration at 12 Tesla, additional rectifier modules would need to be added in series connection to boost the TF voltage during the ramp-up phase. Doubling the TF open circuit voltage by inserting in series an additional 650 MVA parallel connected set of identical 12-pulse rectifiers would extend the allowable 12 Tesla flattop duration by reducing the 12 Tesla ramp-up time to less than 10 seconds, but would also increase the total TF system pulse rating to 1300 MVA. If this extended power load were not acceptable to an electric utility, an option would be to install a 1.7 Gigajoule variable frequency Motor-Generator-Flywheel for auxiliary energy storage and for powering the additional 650 MVA of rectifiers. Another option to consider for extended 12 Teslaoperation is an energy dump resistor bank.

CS/PF System

The CS/PF system must provide a more complicated and diverse set of waveforms than the TF system. Plasma simulation TSC computer runs have produced one optimized set of CS/PF waveforms for a 21 second, 6.44 MA, Q=10 burning plasma, consistent with use of OFHC copper for all CS/PF coils. It models a twenty volt plasma breakdown as consuming 2 Webers of flux in 0.1 seconds. These waveforms have been used along with the PF/plasma inductance matrix and coil heatup algorithms to evaluate minimum CS/PF power system requirements. Although the entire waveform set would require 1297 MVA of thyristor rectifier equipment acting alone, only 412 MVA of thyristor rectifier equipment is required if resistor banks are used to augment coil resistance and rectifier equipment for plasma breakdown. Key waveform parameters derived from the waveforms are listed in the Table 5.12-1, and the waveforms themselves are plotted at the end of this section.

Table 5.12-1. Key Waveform Parameters for the FIRE Poloidal Field Coils

Coil Name	Applied Voltage Range (volts/turn) (excluding breakdown)		Current Range (Mega-ampere-turns)		Rectifier MVA rating	Applied volts/turn during breakdown	Proposed Number of Turns	Maximum Absolute Current (kA)
	Minimum	Maximum	Minimum	Maximum				
CS1 U	-3.93	2.92	-11.97	8.45	47.0	-15.57	200	59.9
CS1 L	-3.93	2.92	-11.97	8.45	47.0	-15.57	200	59.9
CS2 U	-1.90	3.00	0.00	5.93	17.8	-15.62	100	59.3
CS2 L	-1.90	3.00	0.00	5.93	17.8	-15.62	100	59.3
CS3 U	-1.04	2.30	0.00	3.01	6.9	-12.71	100	30.1
CS3 L	-1.04	2.30	0.00	3.01	6.9	-12.71	100	30.1
PF1 U	-1.77	2.79	0.00	4.75	13.3	-15.29	80	59.4
PF1 L	-1.77	2.79	0.00	4.75	13.3	-15.29	80	59.4
PF2 U	-2.22	4.68	0.00	4.75	22.2	-24.20	80	58.5
PF2 L	-2.22	4.68	0.00	4.75	22.2	-24.20	80	58.5
PF3 U	-10.91	5.94	-3.36	0.45	36.7	-18.94	60	56.6
PF3 L	-10.91	5.94	-3.36	0.45	36.7	-18.94	60	56.6
PF4 U	-15.67	14.84	-3.96	0.17	62.1	-19.98	60	66.0
PF4 L	-15.67	14.84	-3.96	0.17	62.1	-19.98	60	66.0

With these numbers of turns per coil, maximum rectifier module currents in 6 of the 7 CS/PF circuits closely match each other and also the module current rating chosen for the TF system.

The CS1, PF3, and PF4 coil current waveforms are bidirectional, but their numbers of current reversals in this set of waveforms are only 2, 1, 1, respectively. For these coil circuits, power supplies include rectifier dc reversing switches, which operate near zero current, along with associated passive networks, switching, and controls. The CS2, CS3, PF1, and PF2 coil current waveforms are unidirectional.

Figure 5.12-3 depicts the CS1 coil circuit which includes both a resistor bank used for plasma initiation, Ri, and the reversing switch feature which requires resistor Rr. The figure uses magnetic relay symbols for the high ampacity swiches S1-S3, but they may instead be controlled by other methods (e.g., pneumatics). Plasma initiation is accomplished as follows. Prior to plasma initiation, current flows through

rectifier modules, M1-M3, through the closed switch S1, through S2, and through the CS1 coils. Shortly before plasma initiation, the fast vacuum switch, VS, is closed and S1 is then opened. Thyristor Q1 fires to discharge the counterpulse capacitor bank, C1, while simultaneously vacuum switch VS reopens. Coil current is then commutated to flow through the resistor bank, Ri, which augments the voltage produced in the rectifier modules and causes plasma breakdown. The high resistor bank voltage continues until VS recloses. Subsequently, S1 recloses and remains closed for the remainder of the pulse.

By comparison, this interrupter configuration has advantages over TFTR's, which required high voltage
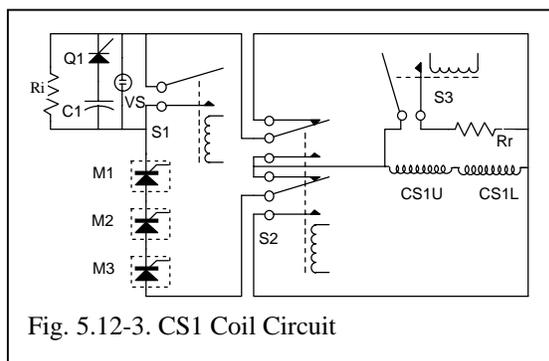
Fig. 5.12-3. CS1 Coil Circuit

blocking diodes and which limited joint rectifier/interrupter operations.

Current reversal is accomplished as follows. As CS1 current approaches zero, switch S3 closes to insert resistor Rr in parallel with the CS1 coil. Output voltages from rectifier modules M1-M3 are then adjusted so that the CS1 coil current flows entirely through Rr and not through the S2's switch contacts or the rectifier modules. The position of S2 is then reversed. Next, rectifier voltage is increased in order to drive coil current through zero. Finally, the rectifier voltage is adjusted so that resistive current through Rr and the S3 switch contacts is zero, and switch S3 is reopened. By comparison, this current reversal configuration has advantages over TFTR's, which did not allow all of the rectifier modules to conduct both

before and after current reversal. The CS/PF circuit is depicted in Figure 5.12-4. Eight of the fourteen CS/PF rectifier modules can be connected as 12-pulse systems.

The cumulative energy injected into the CS/PF coils during this waveform set reaches a 2.11 Gigajoule peak, although the net dissipated energy at the end of pulse is only 1.8 Gigajoules. In the event that FIRE is sited in a location where the local electric utility. .   company cannot support the 412 MVA power demand profiles expected for each FIRE pulse, it would be necessary to provide a local Motor-Generator- Flywheel energy storage system sized to provide at least 2.11 Gigajoules and 412 MVA.
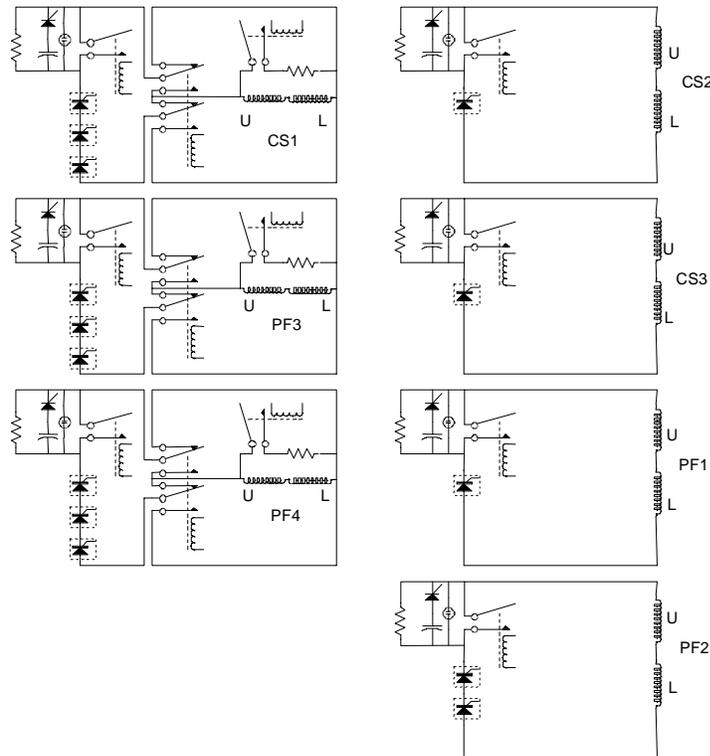
Fig. 5.12-4. CS/PF System

CS1 CURRENT

CS1 VOLTAGE

CS1 TEMPERATURE

CS2 CURRENT

CS2 VOLTAGE

CS2 TEMPERATURE

CS3 CURRENT

CS3 VOLTAGE

CS3 TEMPERATURE

PF1 CURRENT

PF1 VOLTAGE

PF1 TEMPERATURE

PF2 CURRENT

PF2 VOLTAGE

PF2 TEMPERATURE

PF3 CURRENT

PF3 VOLTAGE

PF3 TEMPERATURE

PF4 CURRENT

PF4 VOLTAGE

PF4 TEMPERATURE
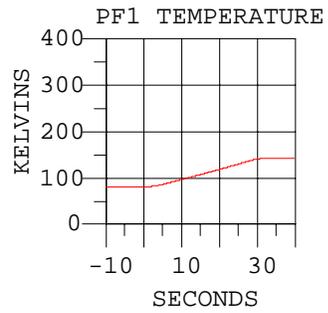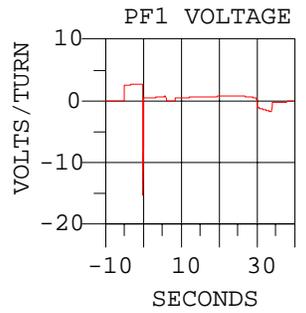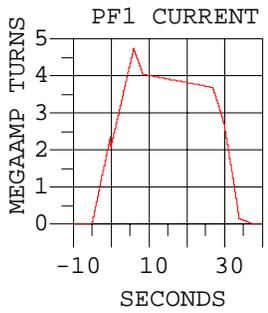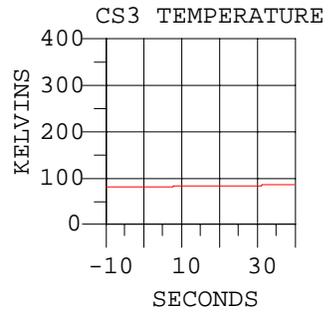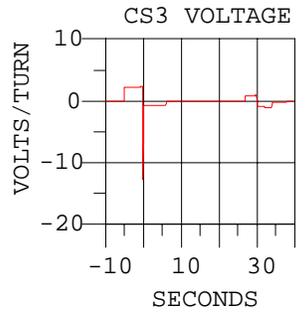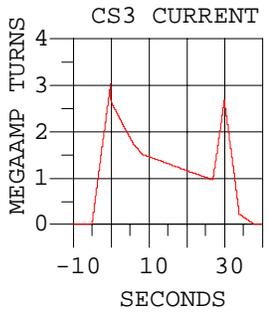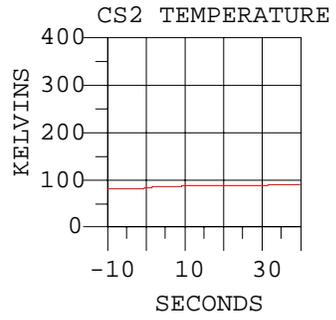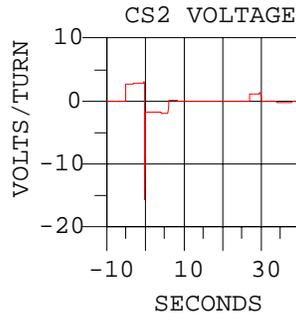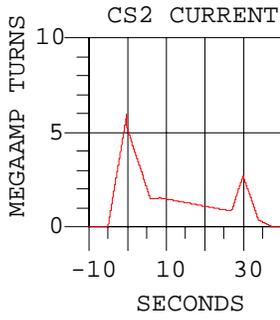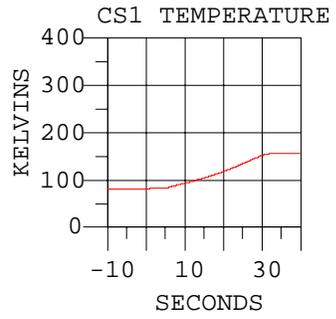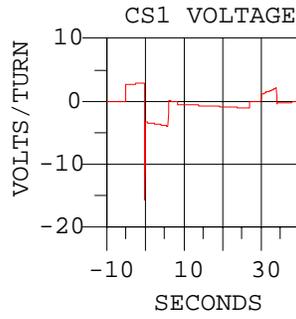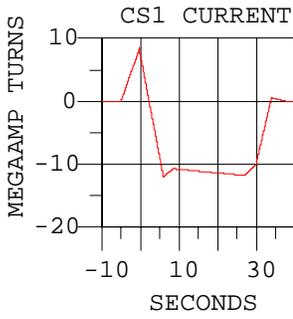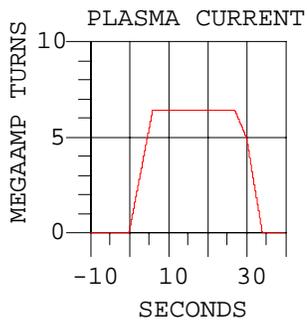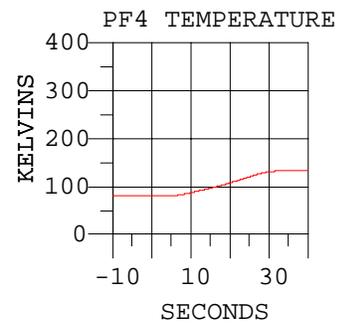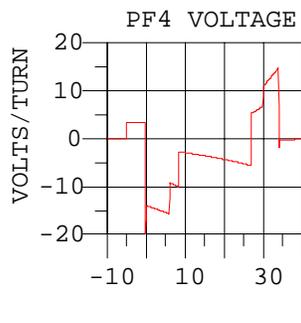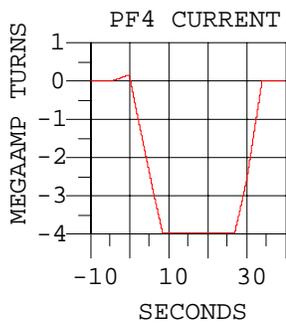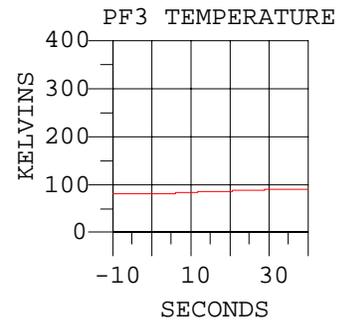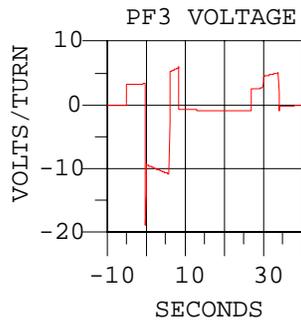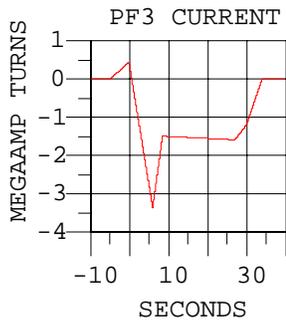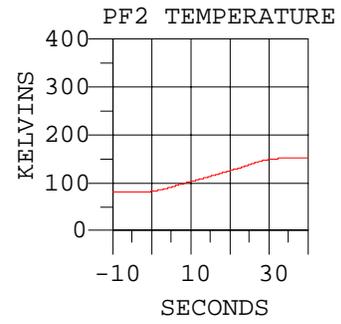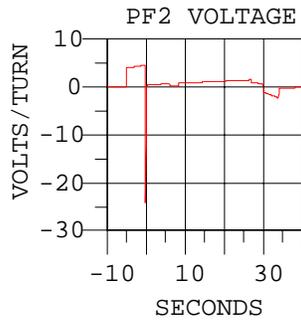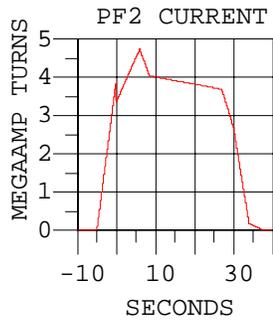
PLASMA CURRENT

5.13   Cryoplant

5.13.1   Introduction

The FIRE cryoplant and nitrogen distribution system provides liquid nitrogen to the TF and PF magnet systems to recool the magnets after pulses and for cooldown from room temperature. The magnet system is flushed out with helium, immediately before each pulse, in order to prevent the formation of radioactive N13.   This section describes the magnet cooling circuit, the overall cryoplant topology, the cryogenic loads, and the sizes of the cryoplant components.

5.13.2   Magnet Cooling Circuit

The magnets are cooled by circulating liquid nitrogen through cooling lines (TF), and radial flow through magnet interpancake space (CS and PF coils). Liquid nitrogen is blown out and replaced by pressurized helium, before pulses, in order to eliminate the creation of N13 through neutron irradiation.   A negligible amount of N13 is still formed in the shielded nitrogen atmosphere of the nuclear island, but it is sufficiently low that no nitrogen holdup system is required .

The TF inside and outside legs are cooled separately by cooling lines that are fed through adjacent holes in each of the TF coil turns. One set of lines turns inwards and cools the TF inside leg and the inner halves of the upper and lower legs, the other cools the outside leg and the outer halves. The line inlet and outlet points are located at the high and low points of the coil profile to facilitate draining of liquid nitrogen prior to a pulse.

The central solenoid and poloidal field coils are cooled radially between double pancakes. As in CIT, the flow direction is from the outside to the inside to prevent outer layer heating and turn-turn delamination. A can around the outside of the Central Solenoid acts as a distribution header. The pancakes are individually insulated, but there is no ground wrap around the entire coil, because of the need for radial flow.

5.13.3   Heat Load Assessment

Cryogenic heat loads, requiring the circulation of liquid nitrogen, include the following:

1) Radiation from the inner vacuum vessel warm surface to the inner magnet surface
2) Radiation from the outer magnet surface to the cryostat walls and the ducts
3) Radiation from the transfer lines to its cryostat walls
4) Conduction through cold mass supports
5) Joule heating of the TF and PF coils during full-power and 2/3 power pulses
6) Neutron and gamma heating of the TF and PF coils during pulses
7) Heat conduction and Joule heating in the high-current leads
8) Cold   mass   cooldown   from   room temperature
9) Removal of nuclear after heat

The load parameters that are most relevant to assessing these loads are accumulated in Table 5.13-1. The dominant load is the ohmic dissipation of the TF coil.

The nitrogen storage tanks are sized for a two-day supply of nitrogen at 4 shots/day.   The energy needed for cooldown from room temperature was calculated to be equal to 12 days of idling losses. Therefore, the magnet system is kept cold over a weekend and there are only 50 room temperature cooldowns during the machine life.

5.13-4a Cryoplant Topology

The overall cryoplant design of FIRE was originally based on those of CIT[1] and BPX[2]. Major design features include the following:

1)   Large liquid nitrogen storage tanks and fill stations are used, instead of a closed-cycle nitrogen refrigerator. However, in FY99, FIRE studies agreed with CIT, BPX, and Alcator that truck deliverires from a commercial air liquefaction plant must be most economical, because of the pulsed nature of the load. This was reviewed in FY00 and both BOC/AIRCO and Air Liquide recommended the

[1] R.B. Fleming and G.D. Martin, "Liquid nitrogen cooling for the Compact Ignition Tokamak," Knoxville, SOFE 13, 1989
[2] R.B. Fleming and G.D. Martin, "System Description, Cryogenic System, WBS Q: BPX Design Description Document," Feb 13, 1991

construction of a dedicated on-site or near-site nitrogen plant. The design still includes on-site liquid nitrogen storage.

2) FIRE uses the Alcator C-Mod method of one pump and individual regulator valves for each flow circuit. This provides close to optimized cooldown and has proven to be very reliable.

3) A subcooler is used, as in the BPX and CIT designs, in order to provide 80 K liquid nitrogen to the coils. The boiling temperature of nitrogen at 10 atmospheres is 105 K.

4) The secondary circuit of CIT was eliminated by BPX and FIRE. One difference was that sites other than PPPL, such as ORNL, were considered with large distances to the site boundaries, so that even without holdup, the nitrogen-13 discharge could be within allowables[3]. The FY99 cryogenic system provided one day's holdup for nitrogen-13, which has a half-life of ten minutes.

The refrigerator is not sized for daily cooldown from room temperature. The magnets are kept cold overnight and weekends, and only warmed up to room temperature during maintenance periods. Despite the increase in the peak temperature to 370 K at the end of a pulse, the energy required for cooldown of the system is nearly five times higher than that for recool of the coils, and it would take 12 days for heat leakages to warm the magnets to room temperature. Heaters are used on vent lines to prevent condensation plumes of liquid nitrogen.

5.13-4b Design Trades

In the 1999 study, the nitrogen gas holdup system at the outlet cost several million dollars and required more space than the rest of the magnet cooling system. In this year's design study[4], it was established that the previous design, which eliminated N13 release by holding-up the outlet nitrogen vapor overnight, before release to the atmosphere, was too conservative. Four new design options were studied with the goal of further reducing or eliminating the need for N13 holdup systems at a reasonable cost or overall cost savings, as illustrated in Figure 5.13.

For siting at PPPL, it is only necessary to delay the release of N13 for somewhat over an hour. Therefore, the nitrogen can be released between shots, which are no closer than 3 hours apart for full-power pulses, and the temporary storage system need only store the nitrogen used in one shot. Option 1 included the 1999 Reference Design and added a postpulse purge by compressed nitrogen to the 1999 Reference Design. The magnets are purged both before and after a shot, valving off a second release line, so that the nitrogen used for magnet recool that is never irradiated doesn't need to be held-up. This has the advantage of a large reduction in the nitrogen accumulator requirements. It has the disadvantage of a further increase in the recool time, after a pulse. The cost of the additional valve and outlet line is small compared with the savings in storage.

Option 2 was an open nitrogen loop with a helium purge before the pulse. The advantage is that essentially no radioactive gas is generated by the pulse, neglecting any imperfectly shielded nitrogen atmosphere in the cell. There is also no need to purge the magnet vapor after a shot and recool can begin immediately with no temporary storage. The disadvantage is that pressurized helium storage and a helium-nitrogen heat exchanger have to be added to the cryogenic system. There is also a modest amount of helium that is vented and has be to be purchased. The study showed that the cost of the helium cooldown system was small, because the amount of helium needed to purge the magnets is tiny in comparison with the amount of nitrogen needed for cooldown.

Option 3 was a closed-loop secondary lN2 circuit, similar to that used in the original CIT/BPX cryogenic circuit[5]. The disadvantage is that it requires a primary/secondary loop heat exchanger and an emergency nitrogen holdup system in the case of a fault.

Option 4 was a closed-loop helium secondary that would eliminate the need for an emergency holdup system and would presumably have the smallest generation of N13 through parasitic effects. It

---

[3] H. Khater, Sec. 5.8, this report

[4] Joel H. Schultz, "Design of the Cryoplant for Specified Release of N13," Fire No WBS7_000217_Design of the Cryoplant for Specified Release of N13," March 8, 2000

[5] R.B. Fleming and G.D. Martin, "Liquid nitrogen cooling for the Compact Ignition Tokamak," Knoxville, SOFE 13, 1989

would have the disadvantages of requiring a helium-lN2 heat exchanger, high-pressure helium storage, a high-pressure helium compressor. It would have the advantage over Option 2 that the helium isn't released to the atmosphere, so that the cost of helium isn't a factor. Another disadvantage is that it would be harder to recool the magnets with gaseous helium than with liquid nitrogen.   The need for high pressure helium storage and pumping made this the most expensive of the options.

Option 2 was selected as the new reference design, because it had the best overall combination of low cost, radioactivity, and recool time, as shown in Table 5.13.4-I.

5.13.5 Summary

The 1999 Reference Design has been changed so that it is less expensive and no longer generates radioactive N13.

Nitrogen deliveries have been replaced by pipeline delivery from a new air liquefaction plant.

A helium purge has been added to each pulse, eliminating N13 generation and the need for an outlet gas holdup circuit.

Option 1a with nitrogen purges before and after the shot has been retained as an alternative design, because of the cost uncertainties in component and gas prices.
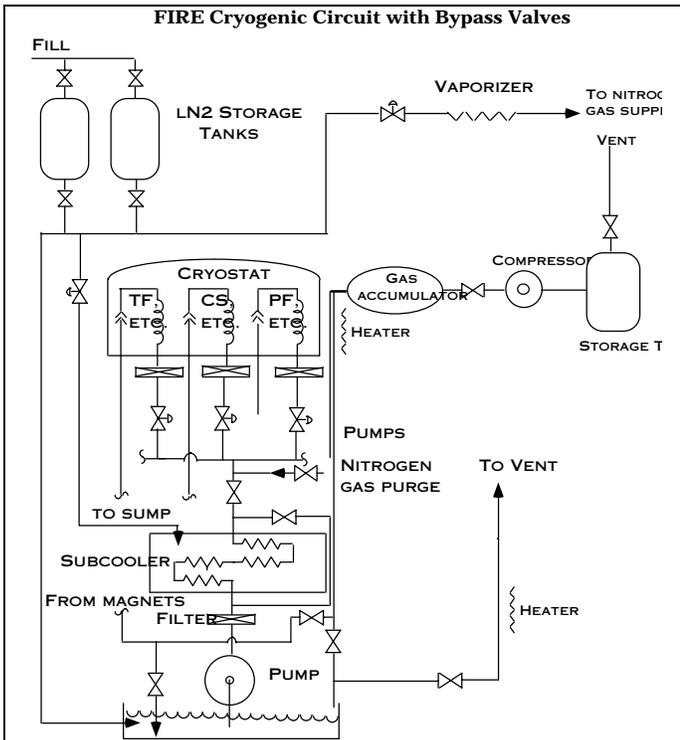
Figure 5.13.1: Option 1: Temporary Storage of Irradiated Gas after Pulse, Open Secondary
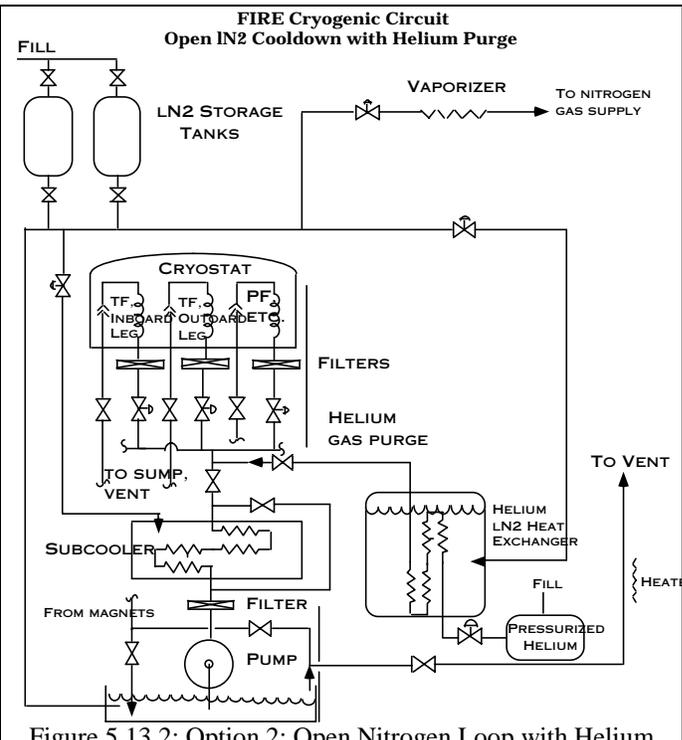
Figure 5.13.2: Option 2: Open Nitrogen Loop with Helium Purge
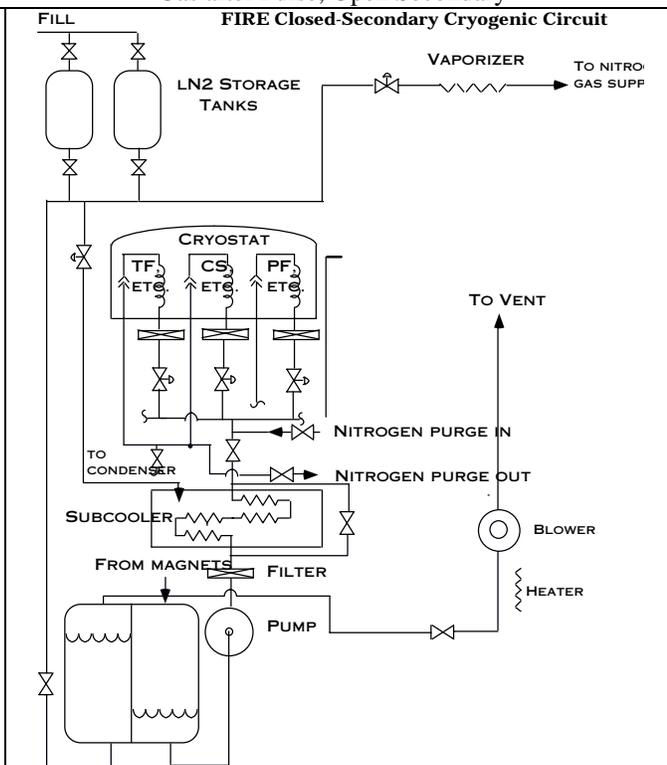
Figure 5.13.3: Option 3-Closed-loop Secondary N2 Circuit (BPX/CIT)
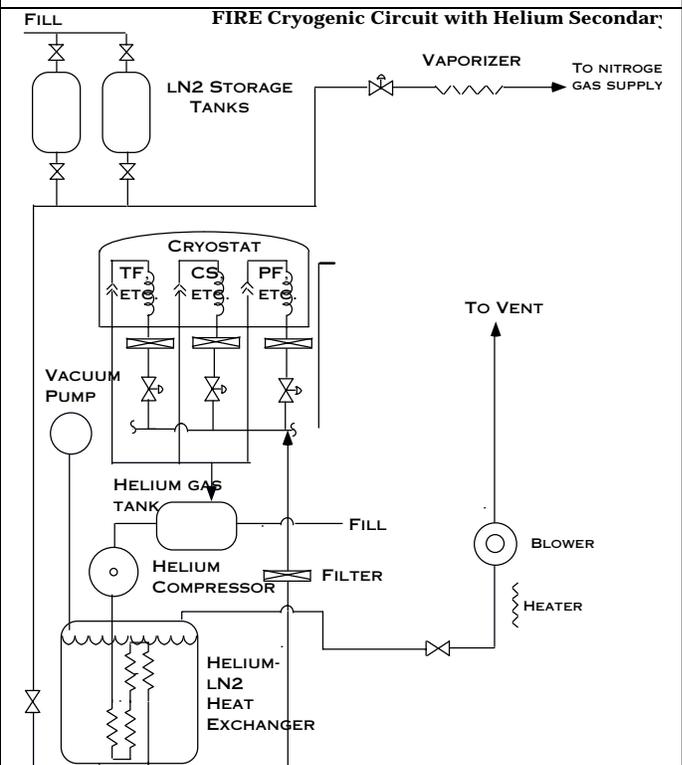
Figure 5.13.4: Option 4: Closed-Loop Helium Secondary

Figure 5.13: Four Cryogenic Refrigerator Topology Options

Table 5.13.4-I Relative Ranking of Refrigerator Options

Refrigerator Option	Cost	N13 Generated/Released	Recool Time
1a Open N2, Holdup all N2	4	3	2
1b Separate holdup streams	2	4	5
2 Open N2, He purge	1	2	2
3 Closed-loop lN2 Secondary	3	5	1
4 Closed-loop He Secondary	5	1	4

The refrigerator components required by the Option 2 design are sized in Table 5.13.4-II.

Table 5.13.4-II: Component Sizes of Option 2 with an Open Nitrogen Loop, Helium Purge, and without Temporary Storage

Parameter	Units	Value
lN2 Storage tank requirement	(kgal)	519.6
nstorage tank 12" shutoff valves		4
Nitrogen Supply to Magnets		
Lcold nitrogen piping	(m)	200
L 8" lN2 vacuum-jacketed pipe	(m)	100
Average nitrogen pumping reqmnt	(kg/s)	13.23
Peak nitrogen pumping reqmnt	(kg/s)	26.45
nRegulator valves to magnets		3
Dregulator valves to magnets	(in)	10
nfilters		4
Total gpm, premagnet filters	(gpm)	519.56
no 12" shutoff valves		6
Purge requirements		
Flush cycles		4
Flush length	(m)	50
Di, flushed pipes	(in)	12
V, total flushed volume	(m^3)	4.65
M, He gas purges	(kg)	197
nshots/Pressurized He tank capacity		4
Volume, 18 atm pressure vessel,supply	(m^3)	272
Di, shutoff valve, He purge stream	(in)	12
L,addit'l pipe, separate flush exhaust	(m)	100
Di, regulator valve, He purge stream	(in)	12
Total flush time	(s)	600
Average mass flow, flush stream	(kg/s)	0.328
Q,He-lN2 heat exchanger	(W)	1908
Blower capacity	(kg/s)	238
Blower power	(hp)	2730
L exhaust pipes	(m)	200
Di exhaust pipe	(in)	16
n,vent valves x Di,vent valves	(in)	2x12
Peak mass flow through gas storage line	(kg/s)	26.455
Heater power	(kW)	5652.6

5.14   Facilities and Siting Requirements

5.14.1   Introduction

FIRE will utilize a significant on-site tritium inventory, and will be a major consumer of electrical power and liquid nitrogen. As a burning plasma experiment, FIRE will cause both direct radiation and induced radioactivity in its materials, resulting in a need to design for the safe handling of radioactive material. FIRE will therefore need to be licensed by the Nuclear Regulatory Commission, although it is expected that it will qualify as a "low hazard facility". The design of facilities and discussion of siting requirements have been approached assuming that FIRE might be constructed at a new, undeveloped site, where there are no constraints on the orientation and interaction between buildings and systems.

5.14.2 Functional Requirements

Generally, the various buildings and site infrastructure comprising the FIRE facilities must be designed to enclose, protect, support, and provide key services to the systems and components which are located within each building or structure. The facilities are also assigned the functional requirements to protect workers and the public from radiation or toxic hazards associated with FIRE operation. Spatial and geometric requirements include space for the tokamak itself, and space to perform assembly, operation, maintenance, and future decommissioning functions. Because of containment and shielding needs, some FIRE maintenance activities will involve the use of robotic remote handling equipment. The FIRE test cell, hot cells, and remote maintenance systems facilities must be large enough to house and shield the remote handling equipment that performs these functions.

FIRE is designed to provide sufficient self-shielding so that the exposed parts of the machine can be approached during shutdown by maintenance workers. However, when operating, the tokamak cannot be approached, and a suitable shielding boundary must be established around the machine. This boundary must include labyrinths and access control features to prevent unplanned worker exposure. In addition, FIRE must be designed against certain accident events (see Section 5.15). To prevent the uncontrolled spread of radioactive material, the tokamak building must include a confinement boundary. This boundary must include features such as airlocks, depressurization, exhaust filters, and perhaps water removal systems to capture tritium, so as to mitigate the consequence of any accidental releases. When radiation sources are enclosed inside the tokamak vacuum vessel, it provides their containment. Whenever objects or materials are removed from the tokamak, the confinement function must be maintained. However, it is not desirable to permit radioactive materials to contaminate the test cell. To deal with radioactive materials and components, the facilities must include one or more hot cells where objects can be maintained or processed as waste. The remote handling system must be configured so that it can transport objects between the tokamak and the hot cell without losing the containment function.

The buildings and structures must be designed to resist all appropriate forces, including gravity, seismic events, wind and extreme weather loads, maintenance loads, and any dynamic loads imposed by operating systems. The various buildings are categorized as either safety related, or non-safety related, depending on the systems and materials they contain, and the functions they are assigned. Safety related buildings are designed and constructed so that they will not lose their functionality during any event included within the design basis. Non-safety-related buildings are designed so that they might fail to perform all their functions during extreme events, however, they are always designed to protect the health and safety of workers.

Figure 5.14.2-1 shows a generic site plan and includes a legend indicating conceptual buildings and structures.

5.14.3 Design Descriptions

5.14.3.1 Tokamak and Hot Cell Building

The tokamak and hot cell building is a two-level reinforced concrete structure. The building outside dimensions are 39 m wide at the south end, 59 m wide at the north end, and 98 m long. An overhead bridge crane serves the tokamak test cell and an

adjacent space on the north side of the test cell (used for remote handling cask operations).

Switch Yard

Cooling Tower

North

15

14 12

23

22

21

25

24

27

28

26

Liquid Nitrogen Storage

50 m

Legend:

Safety Related Buildings
11 - Tokamak and Hot Cell Building
12 - Radioactive System Support Building
14 - Radwaste Systems Building
15 - Emergency Power Supply Building

Non-Safety Related Buildings
21 - Assembly and Mock-up Hall
22 - Magnet Power Conversion Building
23 - Cooling Systems Building
24 - Cryogenic System Building
25 - ICRH Power Supply Building
26 - Laboratory Office Building
27 - Control and Operations Building
28 - Utility Services Building

Figure 5.14.2-1 – FIRE Conceptual Site Plan

The rails for this crane also continue over the assembly and mockup building at the south end of the test cell. The tokamak test cell and remote maintenance area are enclosed by 1 m thick concrete walls and a 60 cm thick roof. These structural elements form a shielding and confinement envelope around the tokamak and some of the remote handling operations. The crane bay is approximately 20 m high. Other parts of the building, which wrap around the remote handling area, contain hot cells and remote handling tools service areas. These parts of the building are approximately 10 m high. The below grade basement level of the building has an internal height of 5 m, and the basemat is 3 m thick. The building is arbitrarily oriented on the site with the longest side of the building in the north-south direction.

The wall at the south end of the test cell is equipped with a large movable section that can be raised to allow the crane to also serve the assembly and mockup building. A similar movable shield wall is provided at the north wall of the test cell. Both the north and south walls of the test cell also have large door sections that can be moved horizontally to allow the crane to carry loads from the assembly and mockup area to any point in the test cell or remote maintenance operating area. The horizontal and vertical shield wall sections at the south end of the test cell are also equipped with inflatable seals, since they form part of the confinement boundary.

Figure 5.14.3-1 shows an east-west elevation view, or cross-section of the tokamak building. The tokamak is located so that its vertical centerline is in the center of the test cell, and its horizontal centerline is 4.2 m above the operating floor. This elevation is chosen to allow space around the tokamak for the operation of remote handling casks. This view also shows the approximate location of waveguides for the ICRF system, magnet busbars, and the minor structures located east and west of the test cell to facilitate horizontal entry to the test cell basement from the adjacent buildings. Services such as ICRF waveguides, cryopumping, diagnostics, and divertor cooling will connect to the tokamak via vacuum vessel ports. The current test cell layout strategy calls for services that will connect to ports to be routed

through the test cell basement and penetrate the test cell through the operating floor. Because port closure assemblies (except one blocked by a diagnostic neutral beam) are designed to be replaceable, the space immediately in front of each port must be kept clear of permanent installations. Penetrations through the floor must be located in areas aligned with the magnet centerlines, and de-mountable sections of piping, waveguides, or other systems used to complete the connection to the ports.

Other services, such as magnet power leads, magnet pre-cooling and vacuum vessel cooling, will connect to the tokamak at locations other than the ports. The current layout strategy calls for these connections to be made through the test cell basement and to penetrate the tokamak pedestal or test cell floor in the space below the cryostat. This area will be congested because of the tokamak support system. The current concept for these supports is a ring of flexing columns located below each TF coil. Because of space constraints, the tokamak support system must be integrated with the clamps for PF coil 3L.

Figure 5.14.3-2 shows an above grade plan view and North-South elevation view of the assembly, tokamak and hot cell buildings. The test cell size is determined by the space required to maneuver and dock remote handling casks at ports. Because of the length of the port closure assemblies, remote handling casks are expected to be approximately 8 m in length and about 1.9 m in width. There are several strategies under consideration for the design of remote handling cask vehicles. Casks could be transported between the tokamak and the hot cell using the building overhead crane, or they could be designed to move on the building floor using either wheels or air cushion supports. Because of the expected weight of these objects, it is likely that air cushions will be superior to wheels. A strategy for cask access to the inclined upper and lower horizontal ports has not yet been determined, however, the facilities layout assumes that casks for each of the three horizontal locations will be mated with a vehicle designed to support the cask at the correct level from the floor. A floor-supported vehicle will move the cask to a pre-determined position in front of the port established by guide pins or stops. The vehicle

39.0 m

22.6m

TF Busbar Array

CS Busbar Array

5.8 m

3.0 m

4.595 m

Grade
Ele. 0

Building 11 - Tokamak and Hot Cell Building

Fig. 5.14.3-1.
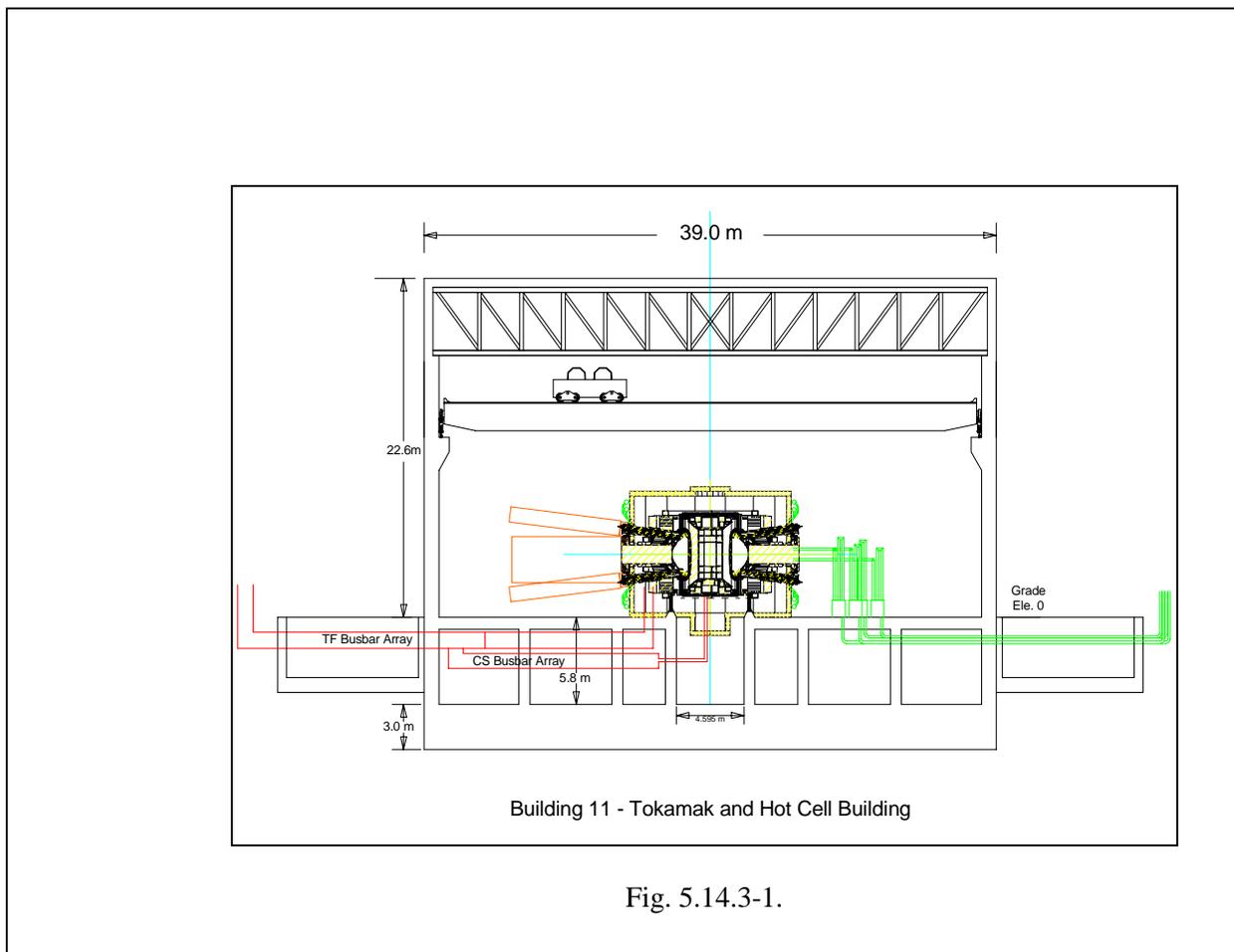
frame system will provide the final motion along the axis of the port.

When port inserts are removed from the tokamak they need to be transported to and transferred into one of the hot cells. It is expected that the radioactivity level of these components will require enough dose attenuation to make it impractical for the casks and remote handling vehicles to include shielding. Therefore, object transfer operations are planned as remote handling activities. When radioactive sources are being moved between the tokamak and the hot cells, the test cell and remote handling vehicle areas must be made inaccessible to workers. The test cell will also be inaccessible whenever a port insert is removed and not replaced by a new insert or a dummy shield. It should be possible to restrict all transfer operations to night shifts.

It will also be necessary to maintain the divertor and first wall. To access these components, an in-

vessel manipulator is proposed. This device should be capable of being inserted through any port (except the port blocked by the DNBI cell) and able to reach one eighth of the vessel in either direction. The in-vessel manipulator may be mounted at a port for an extended time, and there are several potential strategies for re-closing the tokamak shield to make the test cell accessible. These include movable shield walls that could be erected around the manipulator cask, or shielding within the manipulator or cask that prevent radiation streaming from reaching unacceptable levels. Figure 5.14.3-3 is a plan view in the basement of the complete building. Space is available for the roughing vacuum pumping system and for the tritium processing systems. In earlier FIRE reports, these systems were located in a dedicated Vacuum Pumping and Tritium Building, which has now been eliminated.

Assembly Hall, Tokamak Building, and Hot Cell - NS Section

Assembly Hall, Tokamak Building, and Hot Cell - Plan View
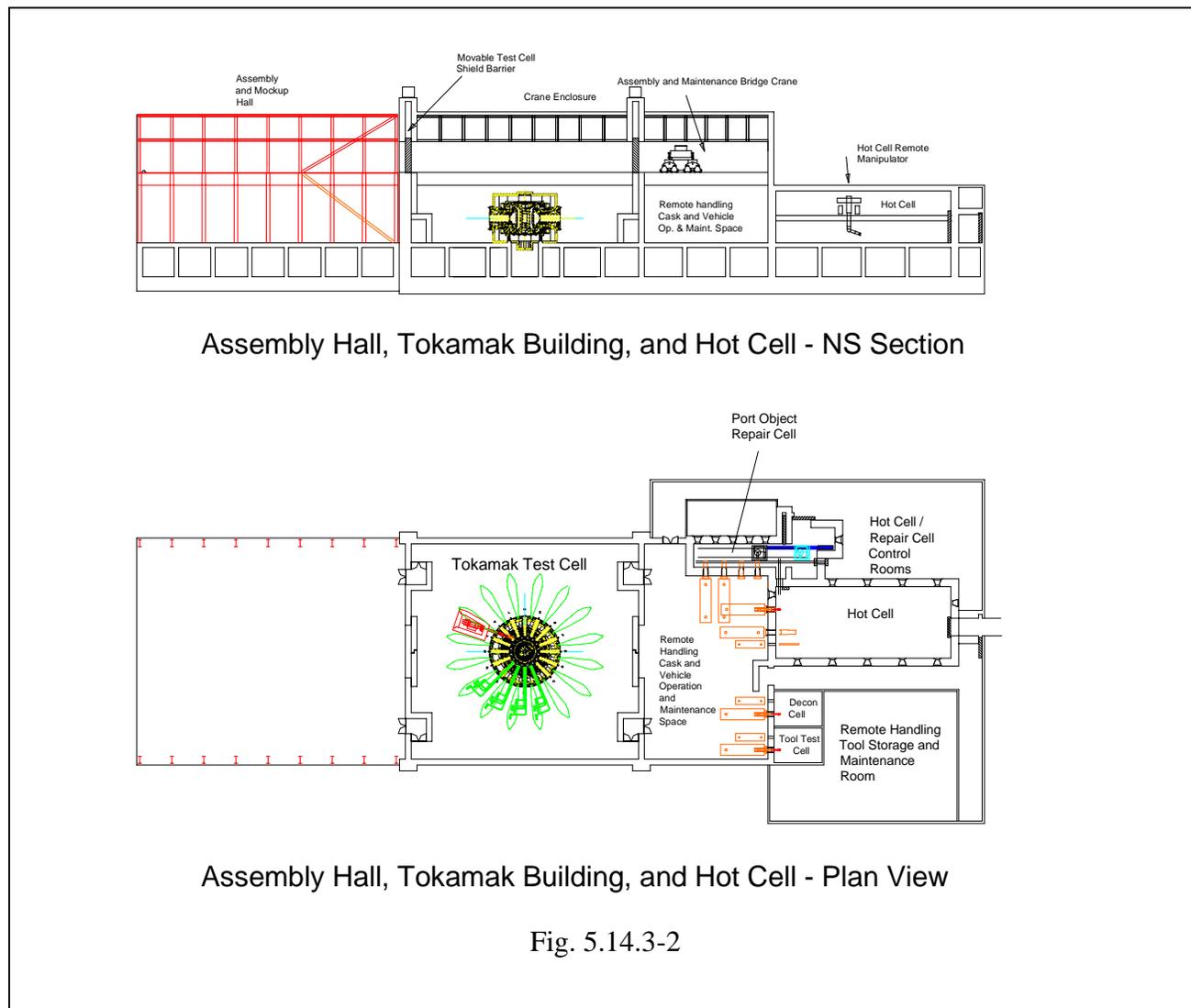
Fig. 5.14.3-2

Figure 5.14.3-2. It is expected that cryopumps located in upper and lower horizontal ports will operate during tokamak pulsing. Between pulses (three hours), cryopumps will be warmed and regenerated back to the vacuum vessel, which will be pumped using mechanical vacuum pumps located in the outer part of some of the mid-plane ports. Because of the high magnetic field, these mechanical pumps will only operate between pulses. The mechanical pumps will exhaust to roughing pumps located in the tokamak building basement. This area will also contain fuel gas purification systems and isotopic separation systems. Tritium and D-T mixtures recovered from the fuel gas will be stored on hydride beds in a secure vault. All tritium processing equipment will be housed in glove boxes. The hot cell

concept is based on the expectation that some port mounted objects can be repaired and returned to the tokamak. To facilitate this, part of the hot cell system will allow port objects to be placed into a cell wall penetration that is physically identical to the tokamak port. Inside the cell, which provides shielding and containment, a remotely controlled work center will be provided, which can perform repair operations on plasma facing components. Meanwhile, the outboard end of the port assembly remains accessible for hands-on work. Divertors and plasma facing objects that cannot be repaired will be transferred through a docking port into a second, larger hot cell. This hot cell will house remotely controlled equipment and workstations used to remove and replace the
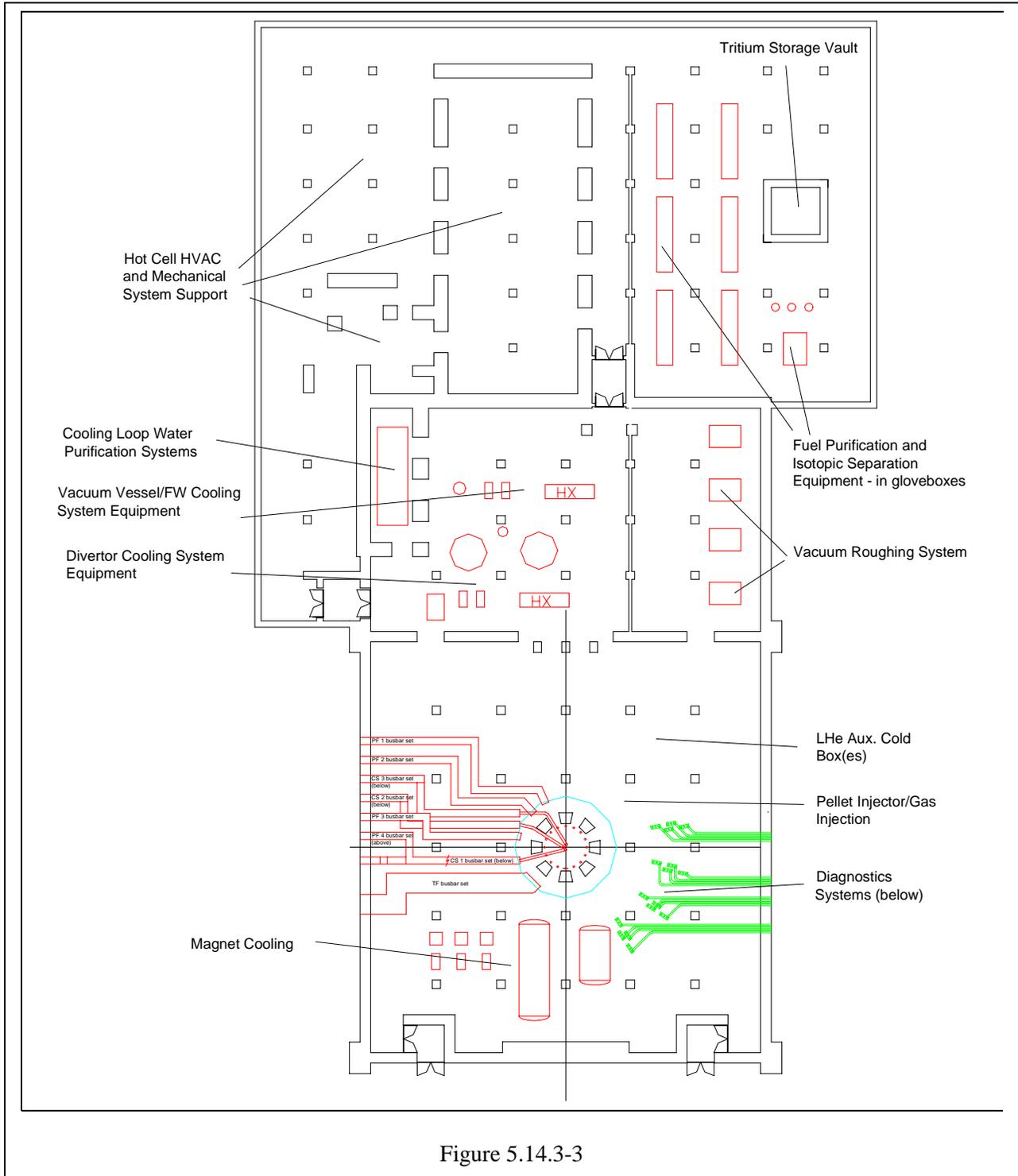
Figure 5.14.3-3

finger elements on divertor modules, which will then be returned to service in the tokamak. Discarded divertor fingers and other irradiated components will be stored and eventually processed for disposal. The extent and nature of

these hot cell processes are not yet well developed, but it is expected that they will include divertor repair (replacement of individual finger-tiles), tritium recovery from beryllium, size reduction by sawing or cutting, and encapsulation of radioactive

material for subsequent shipment to a waste repository.

The tools that operate within the remote handling casks are likely to become contaminated with tritium or radioactive dust, but are unlikely to become radioactive sources. They will need development and periodic maintenance and testing. To serve these functions, facilities are provided where remote handling casks can dock and discharge tools to a decontamination facility. Tools are subsequently moved to a storage and repair facility.

5.14.3.2 Other Safety Related Buildings

The tokamak and hot cell building, and other safety related buildings will generally be constructed using cast-in-place reinforced concrete. They will be designed to resist seismic forces and extreme weather hazards such as tornado missiles. For the tokamak and hot cell building, which is also assigned a shielding function; the thickness required for shielding is generally more than the thickness required to resist tornado missiles.

The radioactive system support building (Building 12) will be used to provide locker and change facilities for workers entering radiation controlled areas and to support systems used in remote repair and processing in the hot cell. This building will also provide space to store materials and supplies used by radwaste encapsulation systems, tritium recovery systems, and waste shipping to offsite disposal locations.

The radwaste systems building (Building 14) will be used to house treatment systems for water which has become contaminated with tritium or activated corrosion products. All floor drains and other intentional drainage from cooling systems which could be contaminated will be processed in this building to remove particulate and ionic activity. Water which is contaminated with tritium or which is recovered from atmospheric detritiation units in the plant HVAC systems will be treated in a water detritiation system. This system will use established technology including vapor phase catalytic exchangers and a tall distillation column.

The emergency power supply building (Building 15) will be used to house a backup power generating system. Presently, the need for safety related backup power is not well known, but the loads are likely to include the HVAC systems and any other loads associated with maintenance of the confinement function. If these loads are small, the safety related power supply system could consist of two small auto-start diesel generators. Some systems will require battery powered un-interruptable power supplies, which could also be located in this building, or which could be distributed on the site.

5.14.3.3 Non-Safety Related Buildings

Non-safety related buildings will generally be constructed using the lowest cost building technology that is suitable for their purpose. This usually means a steel-framed structure built on a concrete slab foundation at grade. The assembly and mock-up hall (Building 21) is provided to facilitate assembly and maintenance functions. The width of this building is set so that the overhead crane used in the test cell and remote handling staging area can also operate here. The assembly and mockup hall will have a below grade level dedicated to diagnostic signal acquisition and processing, and will be built from reinforced concrete below grade. The floor loading capability of the assembly hall will be the same as the tokamak and hot cell building, tentatively 20 tons/m^2. The above grade portions of the building will be steel framing with architectural siding and roofing.

The magnet power conversion building (Building 22) will be used to house the indoor portions of the magnet power supplies. Transformers will be kept outdoors as a safety measure, and rectifier sets and power conditioning and switching apparatus located indoors. This building will be a single floor, steel frame on concrete slab structure. To minimize the length of busbars and cables, the shape proposed for this building uses a main corridor and three transformer-rectifier bays.

The cooling system building (Building 23) will be used to house the indoor parts of the heat rejection system, which provides secondary coolant to the divertor and vacuum vessel cooling systems.

Under present site assumptions, secondary coolant is pumped to cooling towers and rejects heat to the atmosphere. This building will also house the plant component cooling water system, which provides water cooling to many of the plant's power supply and plasma heating systems.

The cryogenics systems building (Building 24) is used to house indoor parts of the liquid nitrogen system used to pre-cool FIRE magnets. Liquid nitrogen storage tanks are located outdoors. Because FIRE will consume large amounts of liquid nitrogen for magnet pre-cooling, it has been proposed that FIRE should be co-located with a commercial air liquefaction plant. Under ideal circumstances, the liquid nitrogen system could be filled by pipeline. Building 24 also houses a liquid helium refrigerator that provides liquid helium to the vacuum vessel cryopumps. Other liquid helium users will be the diagnostic neutral beam, and the isotopic separation system in the fuel process. These systems are not yet well developed, and the size of the system components and building are very preliminary.

The ion cyclotron heating system power supply building (Building 25) will be similar in design and construction to the magnet power supply building. It will house the indoor portions of the ICRH system, including power supply cubicles, and tetrode signal generator modules. The ICRH system will deliver 30 MW to the plasma via 16 trains; hence each train will be sized for about 2 MW. Waveguides from the ICRH building and busbars from the power supply building will be routed through access structures on the east and west sides of the tokamak building, so that they can enter the tokamak building below grade.

The laboratory office building (Building 26) and the control and operations building (Building 27) will be designed and constructed to conventional office building standards. The laboratory office building will be sized for 500 to 700 scientists, engineers, administrators, and other site workers. The LOB will be located near the perimeter of the FIRE site, to permit relative freedom of public access. The control and operations building, on the other hand, will be located as close to the tokamak buildings as reasonably possible, to facilitate easy physical access to FIRE facilities. The control and operations building will include facilities for operator interface with all FIRE control systems, and will include space dedicated to management of abnormal events.

The utility systems building (Building 28) will be dedicated to necessary site infrastructure, and will house compressed air systems, potable and demineralized water treatment systems, site central heating and chilled water systems, and storage of clean parts and supplies.

5.14.3.4 Site Improvements and General Arrangement

In addition to safety and non-safety-related buildings, the FIRE site will include improvement needed to meet the functional requirements of outdoor equipment. The switchyard to receive grid power and step it down to voltages suitable for FIRE systems must be capable of handling approximately 1000 MW. Cooling towers will be required to reject heat from the divertor and vacuum vessel cooling systems. If the heat rejection system is able to average the heat load, the total capacity of the cooling towers could be quite small. Magnet pre-cooling will use liquid nitrogen, supplied by pipeline from a commercial on-site plant or a nearby offsite plant. Because FIRE will be a licensed nuclear facility, perimeter fencing and multiple levels of access control will be required. These features will be further developed in future work.

5.14.5 Site Selection Process

The FIRE design process has been based on the assumption that the experiment will be sited at a new, undeveloped location - a "greenfield" site. This assumption presents the minimum set of design constraints. However, it is likely that several current experimental sites could also provide a good basis for design. The following key criteria are expected to be important to the process of selecting a site for FIRE:

- *Availability of land.* Since FIRE will be a licensed nuclear facility, it will be necessary for the operating organization to be able to control land use within a distance of 500 to 1000 meters from the tokamak building. This exclusion distance is related to the analysis of

radiation release events, and suitability of the site for a nuclear facility.

- *Access to electrical power*   FIRE will require input power on the order of 1000 megawatts for periods at least as long as the plasma pulse plus the ramp-up time. If an otherwise good site does not have a sufficient electrical supply, some form of energy storage could be considered. However, the high power demand and relatively long pulse could require total energy storage on the order of 20 gigajoules.
- *Access to industrial infrastructure.* Supply of construction labor and material, transportation for the delivery of tokamak and other large components, and the availability of industrial commodities such as liquid nitrogen will be factors which could effect the cost and schedule.
- *Ability to transport radioactive materials.* It *must* be acceptable to the surrounding community that the FIRE facility receives shipments of tritium and issue shipments of encapsulated radioactive waste.
- *Access to amenities for FIRE staff* . The scientists, engineers, and technicians who build and operate FIRE will require adequate schools, health care, and community infrastructure.

In the future, candidate sites will be identified and evaluated for their technical acceptability and their influence on the cost and schedule of the project.

5.15 Safety

5.15.1 Safety Philosophy and Requirements

The safety philosophy for FIRE is to use a graded approach to the mitigation of hazards. Since FIRE will utilize deuterium-tritium shots to fulfill part of its operating mission; hazards associated with the use of tritium and activation of materials from the 14 MeV fusion neutrons must be considered. In addition, the toxicity of beryllium, used as a plasma-facing component in FIRE, must also be addressed.

The DOE Fusion Safety Standard[1] was developed in 1996 to enumerate the safety requirements and to provide corresponding safety guidance related to the hazards associated with next step D-T magnetic fusion devices like FIRE. Furthermore, from a regulatory perspective, the standard also establishes the design and operational envelopes for next step fusion facilities. Given the pre-conceptual stage of FIRE design, we have focused our efforts on implementing the safety-related design requirements in the DOE Fusion Safety Standard that have the greatest impact on public safety.

The highest level requirements in the Fusion Safety Standard stem from DOE policy, namely:

- The public shall be protected such that no individual bears significant additional risk to health and safety from the operation of those facilities above the risks to which members of the general population are normally exposed.
- Fusion facility workers shall be protected such that the risks to which they are exposed at a fusion facility are no greater than those to which they would be exposed at a comparable industrial facility.
- Risks both to the public and the workers shall be maintained as low as reasonably achievable (ALARA).

In addition to these requirements, two additional fusion-specific requirements were developed:

- The need for an off-site evacuation plan shall be avoided

- Wastes, especially high-level radioactive wastes, shall be minimized

Radiological release targets for tritium, activated tungsten (e.g. tokamak dust) and activated air and nitrogen have been established to meet regulatory dose limits in the DOE fusion safety standard taking into account the ALARA principal. The design targets are presented in **Table 5.15-1**.

Table 5.15-1. Radiological Release Targets for FIRE

	Normal Operation[a]	No-evacuation Limit	
Dose Limit	0.1 mSv/yr (10 mrem/yr)	10 mSv (1 rem) per off normal event	
Meteorology	Yearly average	Best-estimate or Average Weather	
Site Boundary	1 km	1 km	1 km
Release Point	Elevated via 100 m stack	Ground	Elevated via 100 m stack
Tritium as HTO	8 g/a	150 g	1.3 kg
Activated W dust	5 kg/a	5 Mg	53 Mg
Ar-41	5 Ci/hr	b	b
N-13	8 Ci/hr	b	b
C-14	0.1 Ci/hr	b	b

a. Release targets have been reduced by a factor of ∼ 10 relative to regulatory limits as an implementation of the ALARA principle.
b. Not considered an accident hazard because of low inventory in FIRE

Radiological confinement is implemented as a key safety function to ensure that the release targets are met and that the overall high-level safety requirements are satisfied. Following the approach of the fusion safety standard, potential safety concerns that could affect the radiological confinement safety function are also examined to determine events that could lead to releases in excess of the targets. In Section 5.15.2, the methodology used to

implement radiological confinement is discussed. The potential safety concerns that could threaten radiological confinement are addressed in Section 5.15.3. An interim safety assessment is provided in Section 5.15.4.

5.15.2 Radiological Confinement

Because of the use of tritium and the presence of activated materials in FIRE, some degree of radiological confinement is needed to protect the public and the workers at the facility. Our philosophy is to minimize inventories of tritium and activated material where possible and to use a graded approach in establishing the number of confinement barriers needed for each system/component.

FIRE has as its goal to keep the total on-site tritium inventory below 30 g, so that it can be classified as a low hazard nuclear facility based on current DOE hazard classification rules.[2] Such a classification allows the greatest flexibility in applying the graded approach methodology in the management of hazards at the facility. We propose to use the graded safety approach for confinement implementation developed for ITER.[3] Thus, mobilizable inventories in excess of 100 g of tritium require at least two highly reliable (typical failure rate less than 10^{-3} per demand) confinement barriers. Mobilizable inventories, less than 1 g of tritium, require two barriers of moderate reliability (typical failure rate less than 10^{-1} per demand). Inventories between these extremes require at least one highly reliable barrier and one barrier of moderate reliability. The confinement barriers should be independent and as passive as possible with minimal dependence on new components that cannot practically be tested in the appropriate service environment before construction.

Table 5.15-2 provides a preliminary estimate of the radiological inventories in the FIRE facility. Based on these values, the vacuum vessel will be a highly reliable primary confinement barrier for the in-vessel inventories. The thermal shield will serve as a moderately reliable secondary barrier. Double confinement (e.g., a combination of

valves, windows or other barriers of moderate reliability) will be implemented in all penetrations attached to the FIRE vacuum vessel. In terms of the ex-vessel inventories, two moderately reliable barriers (e.g., the vessel, process piping, or component containing the inventory and a glovebox or other secondary boundary) will be used. Acceptable leak rates for these boundaries will be established as the design progresses.

Table 5.15.2. Radionuclide Inventories in FIRE Facility

Location	Tritium Inventory
In-vessel	
• Bred in Be	0.02 g
• Cryopumps	~ 10 g (TBD)
Ex-vessel	
• Pellet injector	TBD
• Tritium Cleanup	TBD
Location	**Activated Material Inventory**
Torus	TBD kg of W dust
Inside cryostat	**5 pCi C-14/pulse[a] 2.4 Ci N-13**
Air outside cryostat	**0.16 pCi C-14/pulse[a] 0.5 μCi N-13 5.3 μCi Ar-41**

a. Even with 10000 pulses, the inventories would be only on the order of tens of microcuries

5.15.3 Potential Safety Concerns

The DOE Fusion Safety Standard[1] identified five potential energy sources that could threaten the confinement safety function:

  a. decay heat
  b. coolant internal energy
  c. plasma energy
  d. chemical energy and combustible gas generation, and
  e. magnet energy.

We are in the process of examining each of these potential energy sources and their impact on the FIRE design. The MELCOR code was used to analyze the consequences of loss of control of these energy sources. These calculations are scoping in nature and detailed

accident event sequences with estimated probabilities have not yet been developed.

MELCOR is being developed at the Sandia National Laboratory (SNLA) to analyze severe accidents in fission reactors.[4] MELCOR tracks the flow of two-phase water during such accidents, as well as any radioactive aerosols that may exist in either water phase. Structure temperatures are determined by one-dimensional heat conduction equation solutions. Heat transfer to both phases is considered. External (walls) or internal (pipes) flow configurations are considered during forced, natural, boiling, and condensation heat transfer modes. Modifications have been made to MELCOR at the INEEL for fusion specific analyses.[5,6,7,8]

To analyze these events, a MELCOR model was developed that includes the in-vessel PFC components, the vacuum vessel, the toroidal field (TF) magnets, and the thermal shield. A detailed description of this model appears in the Appendix to this report. Cooling systems characteristics for the divertor and VV were assumed for these analyses, because design information for these cooling systems is not yet available. Plasma heating of the PFCs (particle, nuclear and decay heating) was included in this model as presented in Section 5.7. Heat transfer from the back of the FW, baffles, and inboard divertors is by radiative heat transfer to the VV. The outboard divertor cooling system has a water inventory of 31 m^3, pressure of 10 MPa, temperature of 50°C, and a pump head of 0.8 MPa. This system provides coolant through the divertor tubes at a velocity of 10 m/s.

The VV walls, shielding, and Solimide insulation were included in this model. The nuclear heating of this structure is that given in Section 5.7. The VV cooling system model has an inventory of 24 m^3, pressure of 10 MPa, temperature of 100°C, and pump head of 0.27 MPa. This system is a scaled down version (based on VV water inventory) of the model developed for ITER, and provides a loop coolant inventory transit time of about 250 s. In addition to this cooling, thermal radiation and natural convection to the TF magnets was modeled.

If no heat were added to the water jetting into the vacuum vessel during an in-vessel LOCA, the pressure would rise to that of the saturation pressure at the divertor coolant temperature. For 50°C water this pressure is only 0.0123 MPa. However, the PFC's of the vacuum vessel will superheat this water, resulting in higher pressures. Based on tests performed in the Japanese Ingress-of-Coolant (ICE) Experiments, it was estimated that for FIRE the water impingement heat transfer coefficient would be 20,000 W/m^2-K over an area of 0.8 m^2.[9] This area was assumed to be part of the inboard top divertor and outboard FW surface areas. To simulate the temperature rise following a plasma disruption produced by the injected water, 16 MJ of thermal energy was deposited on the PFCs over a 100 ms period. The partitioning of this energy among the PFCs was the same as that during a normal pulse.

We have examined the long-term thermal response of FIRE and the passive decay heat removal capability of the design under a complete loss of coolant condition. The safety concern is the mobilization of activated PFC material by oxidation in air. It is assumed that following a FIRE plasma pulse the coolant in the divertor and VV cooling systems is completely lost. The only means of heat removal that remains is the radial conduction and radiation of the decay heat to the environment. Figure 5.15.3-1 contains temperatures from different radial locations in FIRE for this event. The maximum temperature (inboard divertor) drops from 600°C to 350°C within 15 minutes after the pulse, and then steadily drops to nearly ambient temperature by ten days. By ten days, the magnet and thermal shield temperatures are still below 0°C. Since the decay heat burden has dropped to about 0.5 kW by this time, these temperatures are not likely to dramatically change beyond this time. Given these results, decay heat is not a serious concern in FIRE and oxidation of the activated PFC surfaces will not be significant.
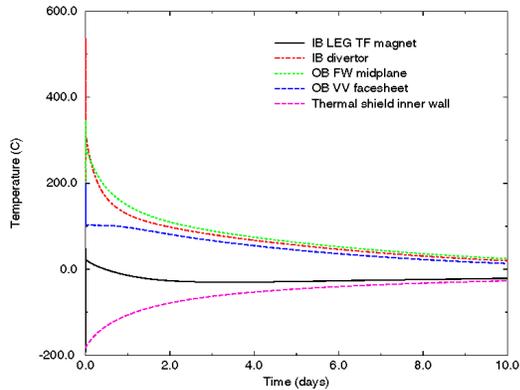
Figure 5.15.3-1 Thermal response of FIRE due to decay heating under complete loss of cooling.

The internal energy of the divertor and vacuum vessel coolants pose a potential pressurization threat to the vacuum vessel (the primary confinement boundary) if an in-vessel leak develops in these systems, either because of thermal fatigue, disruption erosion, and disruption forces. Thus, in-vessel loss-of-coolant accident (LOCA) calculations have been performed for the FIRE design. These accidents involve a break in the divertor or vacuum vessel cooling systems inside of the vacuum vessel, allowing coolant to jet into the vacuum vessel. This coolant impinges on hot plasma facing component (PFC) surfaces, producing vacuum vessel pressurization in excess of the coolant saturation pressure. The safety concerns are the possible over-pressurization of the vacuum vessel, and the production and possible combustion of hydrogen produced by the chemical reaction of first wall (FW) beryllium with the injected steam.

For divertor system breaks, the LOCA was assumed to occur at the end of a plasma pulse when PFC temperatures were at a maximum. In addition, this LOCA was assumed to induce a plasma disruption. The coolant was allowed to impinge on the inboard divertor surface (a radiatively cooled PFC) and on a portion of the outboard FW. Three different break sizes were assumed: a single cooling tube, 10 cooling tubes, and 100 cooling tubes. Figure 5.15.3-2 contains VV pressure for these events. As can be seen, the VV pressure resulting from a single tube break

gradually rises to 0.044 MPa in 60 seconds. The larger breaks give a more rapid initial pressure rises, but result in lower pressures by 60 seconds (0.025 MPa). This initial rise is primarily due to the rapid steam generation produced by coolant impingement heat transfer, that is eventually offset by VV steam condensation as additional water is injected from the divertor cooling system and PFC surfaces begin to quench. These breaks do not result in a near-term pressure that could fail the vacuum vessel. As such they do not represent safety hazards as long the long-term cooling of PFCs is provided by the VV cooling system, which operates at a temperature of 100°C. Thus, breaks in the divertor coolant system do not seriously threaten the radiological confinement integrity of the vacuum vessel.

The VV cooling system LOCA was assumed to occur at the time of maximum VV coolant temperature, and the coolant to impinge on the back of the FW (a radiatively cooled PFC) at the reactor mid-plane. An in-vessel LOCA from a 0.01 m^2 break in the vacuum vessel cooling system was analyzed for FIRE. This break size is arbitrary, but is about the same size as the 100-tube divertor break. The time of the break was established to be approximately 100 seconds, which is the time of peak VV coolant temperature for the adopted VV cooling system design. Because the FW is radiatively cooled, the temperatures of these PFCs do not change much from those at the end of the pulse. The results of VV pressure for this event in given in Figure 5.15.3-3. The maximum pressure in the VV is slightly above 0.15 MPa. This pressure is below the 0.2 MPa design pressure for the VV and is not expected to cause a failure of this structure.

In all of the events examined thus far, because of the low VV steam pressures and low FW temperatures (below 350°C), insignificant amounts of hydrogen are generated from Be-steam and W-steam interactions. Thus, the chemical energy from these reactions does not threaten the radiological confinement function of the vacuum vessel.
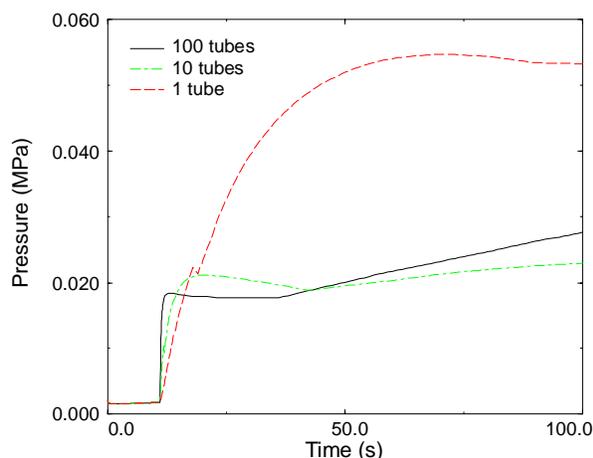
Figure 5.15.3-2 Pressure in FIRE plasma chamber for different levels of tube rupture in the divertor

Another concern with hydrogen production is deflagration and/or detonation upon mixing with air. Keeping the inventory of all hydrogenic species below the deflagration limit for the FIRE plasma chamber and extensions would reduce the threat to the radiological confinement barrier. For the 35 m^3 FIRE vacuum vessel, the deflagration limit is 60 gmoles of hydrogenic species. From the accident perspective, hydrogen from Be/steam and W/steam reactions is not the concern, however the tritium on the cryopumps must be controlled. The 30 gmoles translates into a deflagration limit of ~ 300 g DT. Regeneration will be scheduled frequently enough to stay well below this limit.
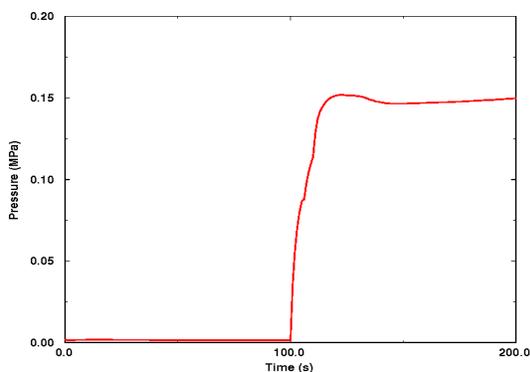

Figure 5.15.3-3 Pressure in FIRE plasma chamber resulting from an in-vessel break of the vacuum vessel cooling system

We have not yet examined the control of plasma energy, magnet energy, loss of vacuum events, or potential cryogen/water interactions as means of challenging the radiological confinement of the vacuum vessel. These events will be examined as the design evolves.

5.15.4 Interim Safety Assessment

An interim assessment of the safety of FIRE has been made relative to the project's release targets and the overall safety requirements of the DOE Fusion Safety Standard.

Examination of the inventories in Table 5.15-2 and the release targets in Table 5.15-1 indicates that none of the inventories in FIRE pose a serious concern for normal/routine effluents from the facility. Activated material inventories are orders of magnitude below the release targets. For tritium, the yearly release limit of 8 g/a is easily achievable given the modest inventories involved in FIRE and the current state of the art in tritium technology.

For off-normal events, as long as the total facility tritium inventory remains below 100 g, then complete release of that inventory would not threaten the ability of FIRE to meet the no-evacuation objective.

Implementation of the radiological confinement safety function is consistent with the overall graded approach philosophy of the Fusion Safety Standard. The use of multiple barriers improves the overall ability of FIRE to ensure that the confinement safety function is maintained over a broad range of conditions and is a good implementation of the defense-in-depth nuclear safety philosophy.

Examination of the potential safety concerns associated with the different energy sources in FIRE has not yet revealed any events that pose a serious challenge to the radiological confinement function

In terms of radioactive waste generation, the low fluence of the FIRE machine would allow all components to either be disposed of as low

level waste or recycled for other fusion experiments.

REFERENCES

[1] DOE STD 6003-96, The Safety of Magnetic Fusion Facilities, May 1996

[2] DOE STD 1027, "Hazard Categorization and Accident Analysis Techniques for Compliance with DOE Order 5480.23, Nuclear Safety Analysis Reports," DOE-STD-1027, December 1992.

[3] Technical Basis for the ITER Final Design Report, Cost Review and Safety Analysis (FDR), ITER EDA Documentation Series No. 16, IAEA, Vienna, 1998.

[4] R. M. Summers, et al., "MELCOR 1.8.0: A Computer Code for Severe Nuclear Reactor Accident Source Term and Risk Assessment Analyses," NUREG/CR-5531, Sandia National Laboratories report SAND-90-0364, January 1991.

[5] Merrill, B. J. "Initial Modifications to the MELCOR Code," ITER/US/95/TE/SA-18, US Home Team, June 30, 1995.

[6] B. J. Merrill and D. L. Hagrman, "MELCOR Aerosol Transport Module Modifications for NSSR-1," ITER/US/96/TE/SA-03, US Home Team, February 21, 1996.

[7] R. L. Moore, "Documentation of New MELCOR Flow Boiling, EOS, and Diffusion Coefficient Subroutines" ITER/US/97/TE/SA-6, US Home Team, April 24, 1997.

[8] B. J. Merrill, "An Enclosure Thermal Radiation Heat Transport Model for the MELCOR code," ITER/US/97/TE/SA-04, January 31, 1997.

[9] H.-W. Bartels, editor, "Accident Analysis Specifications for NSSR-2 (AAS)," version 2, S 81 RI 19 97-05-04 W1.1, SEHD 8.1.C-1, May 6, 1997.

6.0   Evaluation of the FY00 Design

Results of the FY00 design work continue to be very encouraging. The design meets or exceeds all of the major performance objectives that were set for FIRE at the beginning of the study in FY99: B_T=10 T; I_p=6.4 MA; minimum flat top time=10 s; minimum full power pulses=3000. The 10 T field in FIRE can be maintained for a flat-top of 18.5 s and 12 T can be achieved for a flat-top of 12 s. In addition, the toroidal and poloidal magnets are capable of extended pulse lengths at lower fields. This would allow FIRE to explore advanced tokamak modes at TPX levels (4T and 2 MA) for flat-top times up to 214 s. For pulses longer than ~25 s, however, it would be necessary to actively cool the entire divertor; for pulses longer than 2 minutes, the first wall may need active cooling .

The main features of the FIRE design are:

- LN_2 cooled, wedged TF coils with C17510 beryllium copper inner legs and C10200 OFHC copper for the balance of the TF coils
- LN_2 cooled, C10200 OFHC copper, free standing, modular central solenoid
- LN_2 cooled, C10200 copper PF coils
- A double walled vacuum vessel with integral shielding, passive stabilization system and active control coils
- Shielding with water and steel within the double walled vacuum vessel to reduce activation to allow hands-on maintenance outside the TF coils
- Plasma Facing Components using Be for the First Wall and W for the Divertor
- Double null radiative divertors

The status and assessment of specific systems is as follows:

6.1   TF Coils and Global Structure

The TF coil peak conductor membrane plus bending stresses are 469 and 689 MPa for the "baseline" wedged machine at 10 T and 12 T, respectively. This is within the static 724 MPa allowable for C17510 beryllium copper with a conductivity of 68% IACS. To investigate design margin and to quantify conductor ductility require-ments, a 13T analysis was performed. The resulting coil plastic strains and insulation stresses indicate that the TF coil would survive this overloaded condition. Preliminary fault analyses indicate acceptable results for the limited number of cases considered. Stress limits for a mission lifetime of 3,000 cycles at full field and 30,000 cycles at 2/3 field are expected to be acceptable for the TF coil since the loading in the peak stress areas is primarily compressive, which inhibits crack growth. A materials testing program will be necessary to confirm this for the large plate sizes FIRE requires. **(Conductor stress for the design is at 65% of allowable at 10 T and 95% of allowable at 12 T.).**

The TF coil temperature excursion for a 10 T, 18.5 s DT pulse or for a 26 s DD pulse is from 80K to 370K. The excursion is the same for a 12 T, 12 s DT pulse or 15 s DD pulse. The peak temperature allowable is 373K. **(TF conductor temperature rise is at the allowable**).

One of the design issues for tokamaks with highly shaped plasmas and "external" PF coils is the support for the overturning moment on the inner TF coil leg. This moment is due to the fields from the central solenoid and PF coils crossing the inner leg of the TF coil. This moment causes shearing stresses in the insulation between the turns in the inner leg. In FIRE, the maximum calculated shear in the inner leg at the mid-plane is ~50 MPa. Using a conservative coefficient of friction of 0.3 and the calculated wedging pressure of ~200 MPa, the allowable stress would be 60 MPa. **(Insulation shear stress in the throat region is at 83% of allowable).**

In wedged TF coils, the wedging pressure has a tendency to decrease at the top and bottom of the inner leg so the allowable shear stress on insulation decreases. However, the large compression rings in FIRE compensate for this effect by providing a preload and load augmentation as the TF coil temperature increases during a pulse.

Cooldown analyses indicate that cooling on the inside edge of the inboard leg of the TF coil is sufficient to achieve a pulse repetition rate of 3 hours. The space required for manifolds and cooling have been incorporated into the design, but detailed stress analyses have not been done.

A summary of operating scenarios for FIRE is given in Table 6.1-1.

FIRE could begin operation as a 10T, high Q device, studying advanced operating modes, and focusing on achieving sufficient values of Q. If such advanced physics modes were not adequate, or the expected Q could not be attained at 10T, then the 12T capability could be utilized to attain high Q, even with pessimistic physics assumptions.

If performance is as good as expected at 10 T, then very high Q modes can be investigated at 12 T and 7.7 MA. Consequently, FIRE will be constructed with high strength C17510 copper for the TF coil inner leg and somewhat larger TF compression rings than would be necessary if the machine were limited to 10 T. The primary upgrade necessary would be to provide the higher power and energy for 12 T, if they were not provided in the initial installation.

The baseline design at 10 T and 12 T has considerable capability to operate with longer pulses in D-D mode (i.e., with negligible nuclear heating). Thus, it is possible to study both high Q burning plasma physics and develop advanced operating modes in one device. The 12T design would also require a modest upgrade to the cryogenic system. These upgrades could be implemented as needed by FIRE's operating program.

Preliminary analyses in FY00 have shown that the TF could be built entirely with OFHC C102 copper, if the design were changed to bucking plus wedging and if the field were limited to 11.5 T. This would lead to substantial savings in TF coil cost and in power requirements. However, the assembly would be more complicated and a new cooling configuration design for the central solenoid would be necessary to accommodate the bucking. Detailed evaluation is planned for FY 01 to verify the preliminary results and determine if this approach should be adopted for FIRE.

FIRE Fiscal Year 2000
Status Report

Table 6.1-1 Possible FIRE Operating Modes

Operating Mode	*TF Coils : Materials and performance*	*CS Coils Materials and performance*	*PF Coils Materials and performance*	*PFCs Materials and performance*
I. Baseline : **10 T / 6.44 MA** DT Fusion Power ~200 MW P_{ext}=20 MW	BeCu , 68% IACS for inner leg; OFHC in remainder. 18 s flat top w/D-T; 26 s w/D-D	OFHC (C10200); Tmax 152 °K	OFHC (C10200); Tmax 173°K	Actively cooled divertor outer plate and baffle. Divertor inner plate and FW cooled by conduction to the Cu clad vessel.
II. Higher Field Mode 12 T / 7.7 MA P_{fusion}=250 MW P_{ext}=25 MW	Same as (I) 12 s w/ D-T; 15 s w/ D-D	Same as (I) Tmax 161 °K	Same as (I) Tmax 183 °K	Same as (I)
III. TPX-like Mode 4T / 2 MA P_{fusion}=5 MW P_{ext}=15 MW	Same as (I) ~214 s pulse duration.	Same as (I) Tmax 144°K	Same as (I) Tmax 124°K	Same as (I)
IV. AT/BP Mode 8T / 5 MA P_{fusion}=150 MW P_{ext}=150 MW	Same as (I) ~31 s w/ DT; ~46 s w/ DD.	Same as (I) Tmax TBD	Same as (I) Tmax TBD	Same as (I)

6.2   Central Solenoid and PF Coils

Stress and thermal analyses indicate that all of the CS and PF coils can use liquid nitrogen cooled OFHC copper conductor. The maximum stress conditions tend to occur in CS2 at precharge and in CS1 at EOB. The available scenarios for a 12T pulse require some adjustment and rebiasing to bring the maximum stresses within allowable levels. At present the maximum stresses are within 2% of the allowable for CS2 and 8% for CS1, hence some adjustment in the scenario is necessary. For the 10 T scenarios, all CS and PF coils operate well within allowable stress levels.

The maximum temperature in a CS or PF coil for the baseline 10 T or 12 T scenario is 183 K.

For the baseline geometry, the pulse length is expected to be limited by the temperature rise of the TF coils rather than the CS or PF coils even for the advanced physics modes - for example, B=4T and Ip=2 MA or B=8T, Ip=5 MA.

6.3 Vacuum Vessel

The double walled Vacuum Vessel has 16 sets of ports including large mid-plane ports, angled ports above and below the mid-plane, and vertical ports. The combined water and steel shielding allows hands-on maintenance outside the TF coils. Port plug shielding concepts, passive stabilization plates and active control coils have been incorporated into the vacuum vessel. Seismic and VDE loads have been estimated to allow vertical and lateral supports to be sized for the VV. Support and cooling concepts are being analyzed for the passive stabilization plates, active control coils, and PFC's. This will continue in FY01. Since the use of carbon inside the vessel is avoided, high temperature bakeout and operation is not needed. The vessel will operate at 100 C.

The vessel is fabricated in octants from Type 316 LN stainless steel. When all the octants are in place within the TF coils, they are welded together from the plasma side of the torus. The field joint for the double wall structure uses splice plates to accommodate assembly tolerances, and for accessing the coil-side, face-sheet from the plasma side of the torus. This type of joint has undergone significant, full scale testing using remote welding equipment as part of the ITER R&D program.

6.4 Divertor and Plasma Facing Components

The divertor design is required to be open to accommodate the short distances from the x-point to the plate and the spreading of the field lines. The connection lengths are short and the scrape-off layer (SOL) thickness is small.

The actively-cooled, outer divertor module design configuration builds on fabrication technologies developed for the ITER divertor and consists of 24, modular, copper-alloy "finger" plates that are mechanically attached to a stainless-steel support structure that spans the toroidal width of the module. The support structure includes machined distribution and collection pathways and manifolds that route coolant to the individual finger plates. Concepts for remotely attaching the modules to the vacuum vessel have been developed.

Passive cooling of the inner divertor plate and baffle components is sufficient for the baseline pulse lengths of 18.5 s at 10 T and 12 s at 12 T, but not sufficient for pulse lengths longer than about 25 s The first wall could be passively cooled for pulse lengths of about 2 minutes, but active cooling will be considered in FY01 to provide for longer pulse operation.

Analyses of the PFC designs have begun based on initial specifications for projected disruption and thermal loading conditions to assure that the structures and attachments are sufficient. The initial work has considered halo current loads and disruption eddy current loads on the inner and outer divertor modules. Further analyses are required to develop the attachment requirements and details of interface conditions.

In general, reliable, yet easily detachable electrical contact must be provided between the plasma facing components and / or plasma facing components and the vacuum vessel. Grounding straps and

Multilam® contacts were proposed for this in ITER, since each can accommodate thermal cycling and relative motion. Similar design concepts are being considered for FIRE.

6.5   Thermal Shield

The requirements for the thermal shield that provides the insulating environment for the liquid nitrogen cooled coils have been developed and overall design features have been selected.

The cryostat consists of a stainless steel structure with a thin shell of stainless steel covered by insulating panels and sprayed-on insulation. Penetrations will be sealed with rubber or fabric bellows that accommodate the relative motion between the VV and thermal shield. The result is a cost-effective concept that is relatively easy to maintain and modify.

6.6   Ion Cyclotron Heating

Plasma transport calculations indicate the need for 30 MW of ICRH. The preliminary design calls for a four port system with two antennas per port. With a 6 cm gap to the plasma, the 30 MW can be delivered at 150 MHz with 35 kV peak voltage. The design value for the gap is 3-4 cm and calculations indicate that 30 MW can be delivered at 100 MHz with a 3.5 cm gap.

6.7   Fueling and Vacuum Pumping

Pellet injection is used in FIRE from the outside mid-plane, vertically and also from the inside lower quadrant aimed towards the plasma center. This will be accomplished by three sets of injectors. The initial sizing and integration of the pellet injector components into the vessel has been done.

A tritium-rich pellet source will be used for core fueling and a deuterium-rich gas source for edge fueling. The fueling system includes: a conventional gas puffing system, using all-metal electro-magnetic valves, (four toroidal stations at two poloidal locations at each divertor level), and a pellet injection system using two identical (redundant) injectors. The technology to deliver intact pellets at the highest possible speeds around curved surfaces (guide tubes) is under development.

The design vacuum pumping speed is 200 torr-liter/s for a 20 s pulse length. The base pressure prior to discharge is 10^{-7} torr for fuel gases (H, D, T) and 10^{-9} torr for impurities; operating pressure is $\sim 10^{-4}$ to 10^{-3} torr. There will be a total of 16 cryopumps with 8 each on the top and bottom (at alternate divertor ports), close coupled to the torus in the pumping duct directly from the double null divertor. The interface issues for these elements will continue to be addressed together with the impact on the requirements for other possible operating scenarios.

6.8   Tritium

The on-site tritium inventory has been set at 30 g to allow sufficient operational flexibility without introducing additional restrictions. However, the inventory can be reduced if a tritium reprocessing system is added to recycle the tritium daily.

6.9 Neutronics and Shielding

Nuclear heating has been computed for the major components (e.g., magnets and PFC's) as input to the cooling design. The largest nuclear heating values in the different components were calculated for the 200 MW fusion power DT pulses. During these pulses the average neutron wall loading is 3 MW/m^2 with values at the outboard (OB) midplane, inboard (IB) midplane, and divertor being 3.6 MW/m^2, 2.7 MW/m^2, and 1.8 MW/m^2, respectively. Radiation damage estimates have also been done to size shields and estimate lifetime for sensitive components.

The insulation dose is computed to be 1.3-1.5 x 10^{10} rads for 3000 full power DT pulses (fusion energy of 5 TJ) and 30, 000 DD pulses (fusion energy of 0.5 TJ). This is the peak, end of life, value and occurs at the magnet surface at the inboard mid-plane. This value drops to 9.8x10^8 rads in the divertor region and 7-12.6 x 10^6 rads in the outboard region at mid-plane.

The commonly accepted dose limit for epoxies is 10^9 rads. Polyimides and bismaleimides are more radiation resistant with experimental data showing only a small degradation in shear strength at dose levels in excess of 10^{10} rads. However, they are difficult to process due to their high viscosity and requirement for high temperatures to fully cure. Newly developed insulations, such as cyanate esters, should provide radiation resistance with easier processing requirements. The avail-ability, properties, and manufacturing impact of using these insulations will be investigated. For example, it will be necessary to confirm that the mechanical properties are sufficient.

The vacuum vessel jacket/shield thickness has been sized so that it, in conjunction with the shielding provided by the TF coils and port plugs, will permit "hands on" ex-vessel maintenance. This will require further consideration of shielding details.

6.10 Activation, Decay Heat and Radiation Exposure

The plasma facing components, first wall on the inboard and outboard sides and the divertor, experience the highest levels of specific activity and decay heat. However, the operational schedule allows short-lived radionuclides to decay between pulses resulting in low levels of activity and decay heat at shutdown.

The biological dose rates behind the vacuum vessel and the divertor remain high during the first year following shutdown, however, the dose rates outside the magnet and at the mid-plane are acceptable for hands on maintenance within a few hours after shutdown. At the top of the machine the dose rate drops to an acceptable level within one day after shutdown.

Dose rate calculations have indicated that port plugs 1.1 m long would provide adequate shielding and have led to the addition of shielding outside the magnets on the top and bottom of the machine.

At the end of the machine life, calculations indicate that all components would qualify for disposal as Class C low level waste.

6.11 Remote Maintenance

The strategy is to employ hands-on maintenance to the fullest extent possible in order to minimize remote handling operations and equipment while achieving acceptable machine availability. Activation levels outside the vacuum vessel are low enough to permit hands-on maintenance in the ex-vessel region. Remote handling (RH) is required for in-vessel components including the divertor, FW and limiter modules, and the port mounted systems including heating, diagnostics and cryopumping systems.

When in-vessel maintenance or modification is required, the affected components are removed from the vessel and transferred to the hot cell where they are refurbished or processed as waste. Divertor, FW and limiter modules are accessed through the midplane ports and are handled with an articulated boom equipped with a specialized end-effector. The boom can access the complete in-vessel region from 4 of the 16 midplane ports. Port mounted system assemblies are located in both the mid-plane ports and the upper and lower auxiliary ports and are removed by a vehicle and manipulator system operating at the closure plate of the related port

RH operations are performed from sealed transfer casks that dock to the ports via a double door system to contain and prevent the spread of in-vessel contamination. Casks carry components between the reactor and the hot cell and are transported by a vehicle or the facility overhead

Components have been classified according to their required maintenance frequency and their designs will be standardized and optimized for RH. Preliminary time estimates to complete the more frequent maintenance tasks are consistent with the required machine availability. Replacement of a port assembly requires approximately 3 weeks of maintenance operations. A complete divertor changeout, 32 modules, is completed in about 6 months. Individual divertor, limiter and first wall modules can be replaced in about one month. The time target to perform a complete changeout of the divertor and FW components is one year.

Studies have begun and will continue in FY01 on kinematics and end-effector design for the in-vessel manipulator to assure that sufficient space has been allocated in ports and around the machine. Analysis shows that the 800 kg combined divertor module (32 module configuration) can be supported and transported through the vessel and ports. Studies will also continue in FY01 on the port assembly and handling equipment design, cell layout and cask design to assure adequate building size and layout for component transport for repair or disposal.

6.12 Power Supplies

The conceptual design of power supplies for FIRE magnet systems seeks to minimize capital cost by leveraging existing capabilities of the local electric utility, which are assumed to be robust. Therefore, all of the FIRE device's time-varying power (peak demand of 800MW) for TF and PF magnets as well as the RF systems are provided directly by the utility's "stiff grid" without

requiring any power demand ramp rate limiting equipment, or energy storage equipment, at the FIRE device site. However, provision for reactive power (MVA) support up to 300MVA is included in the design baseline. The grid's ability to supply the required time varying active and reactive power demand will be evaluated when a specific FIRE site is chosen and the above assumptions adjusted as necessary.

If the local electric utility is not capable of powering the pulsed load directly from its ac power line, MG energy storage devices could still be installed, but at additional cost.

We plan to survey grid capabilities to determine if direct pulsing from the grid would seriously restrict site selection options before choosing between direct grid powering or combined grid/MG set powering.

Power equipment for TF and CS/PF magnets includes thyristor rectifiers, resistor banks, and switching/interrupter circuits. The required total pulse rating of the rectifier complement is approximately 1000 MVA for the 10 T pulse. For the DD long-pulse scenario at 4 T, 2 MA the total 243 second long-pulse rectifier rating required is 345 MVA. By way of comparison, these total rectifier MVA ratings are similar to the total ratings of existing rectifiers, that were used to operate the TFTR magnets. Resistor banks and interrupter switching circuits are used in FIRE for plasma initiation in a fashion similar to TFTR and JET. Some of the magnets require current reversal during a pulse and therefore incorporate dc polarity

switching in their rectifier circuits, as done for TFTR.

For the 12 T, 7.7 MA scenario, it would be necessary to upgrade the power supplies. An additional 200 MVA of thyristor rectifiers would provide a short-pulse 12T 7.7MA capability. An extended flattop pulse duration at 12T could be obtained by inserting additional rectifiers in series to boost the TF charging voltage, bringing the FIRE total rectifier rating to 1850 MVA. If this were too much for the local utility, one possible option would be to power the additional 650 MVA of TF voltage-boosting rectifiers from a local MG storing at least 1.7 GJ of energy.

A preliminary assessment of a FIRE machine using an all OFHC TF coil set indicates that a 46 % peak TF power reduction and twice as long pulse durations would be possible. The engineering and cost ramifications of this option will be studied in FY01.

6.13 Cryoplant

The FIRE cryoplant and nitrogen distribution system is a modified form of the design developed for CIT and BPX.

Major design features of the cryoplant:

- Large liquid nitrogen storage tanks are used on site. The FY99 concept for nitrogen deliveries by truck has been replaced by pipeline delivery from a new on-site or near site air liquefaction plant. Commercial suppliers recommended the latter.
- The amount of radioactive N^{13} generated in FIRE is

small and would be within allowables for most site boundaries. A helium purge has been added before each pulse to displace any remaining nitrogen in the passage prior to the pulse, thus eliminating N^{13} generation and the need for a gas holdup circuit.

- FIRE uses the Alcator C-Mod method of one pump and cool down and which has proven to be very reliable.
- A subcooler is used to provide 80 K liquid nitrogen to the coils.

The magnets are kept cold overnight and weekends, and only warmed up to room temperature during maintenance periods. This provides considerable flexibility for adjusting shot scenarios.

The cost of nitrogen is substantial and is dominated by the 30,000 partial power pulses; therefore, the mission specification will be reviewed and the cryoplant configuration will be evaluated further in FY01. In particular, because of the cost uncertainties in component and gas prices, an alternative scenario with a nitrogen gas purge before and after each shot will be considered.

6.14 Facilities and Siting

A conceptual layout and building design has been developed for a "green field" site. For example, the deletion of the central tie rod system from the tokamak has allowed a decrease in the test cell height. In the future, candidate sites should be identified and evaluated for their technical acceptability and their influence on the cost and schedule of the

project since significant savings may be available in the form of "site credits".

The test cell size is determined by space required to maneuver and dock remote handling casks at ports. Because of the length of the port inserts, remote handling casks are expected to be approximately 8 m in length and about 1.9 m in width. There are several strategies under consideration for the design of remote handling cask vehicles. A tentative routing for the vehicles to other parts of the facility has been selected.

Some components, for example port inserts ("plugs"), will require enough shielding to make it impractical for the casks and remote handling vehicles to include shielding. Therefore, transfer of objects of this type are planned as remote handling activities. The special requirements on the facility for routing and storage of these items are being evaluated.

The hot cell concept is based on the expectation that some port mounted objects can be repaired and returned to the tokamak. The extent and nature of these hot cell processes are not yet well developed, but it is expected that they will include divertor repair, tritium recovery from beryllium, size reduction by sawing or cutting, and encapsulation of radioactive material for subsequent shipment to a waste repository.

Some building requirements are not yet well developed, but a preliminary allowance has been made. For example, the cryogenics systems building is used to house indoor parts of the liquid nitrogen system for the FIRE magnets. It also houses a liquid helium

refrigerator that provides liquid helium to cryopumps in the tokamak vacuum vessel and in the diagnostic neutral beam, and to the isotopic separation system in the fuel process.

6.15   Safety

Radiological release targets for tritium, activated tungsten (e.g. tokamak dust) and activated air and nitrogen have been established to meet regulatory dose limits in the DOE fusion safety standard taking account of the ALARA principle.

A goal for the FIRE design is to keep the total on-site tritium inventory below 30 g, so that it can be classified as a low hazard nuclear facility based on current DOE hazard classification rules. For off-normal events, as long as the total facility tritium inventory remains below 100 g, then complete release of that inventory would not threaten the ability of FIRE to meet the no-evacuation objective.

The vacuum vessel will be a highly reliable primary confinement barrier for the in-vessel inventories. The thermal shield will serve as a moderately reliable secondary barrier. Double confinement (e.g. a combination of valves, windows or other barriers of moderate reliability) will be implemented in all penetrations attached to the FIRE vacuum vessel. Acceptable leak rates for these boundaries will be established as the design progresses.

Examination of the potential safety concerns associated with the different energy sources in FIRE has not yet revealed any events that pose a serious challenge to the radiological

confinement function. A preliminary analysis has been done for:

- Long term thermal response and passive decay heat removal capability under a complete loss of coolant condition for the divertor and VV following a pulse-- Results indicate that decay heat is not a serious concern and that oxidation of the activated PFC surfaces will not be significant.

- Break in the divertor or VV cooling lines inside of the VV—Results indicate that pressure within the VV does not rise to a level expected to compromise its radiological confinement integrity. Furthermore, because of the low VV steam pressures and low FW temperatures (below 350°C), insignificant amounts of hydrogen are generated from Be-steam and W-steam interactions. Thus, the chemical energy from these reactions does not threaten the radiological confinement function of the vacuum vessel.

- Deflagration and/or detonation of hydrogen upon mixing with air. From the accident perspective, hydrogen from Be/steam and W/steam reactions was not of concern, however the tritium on the cryopumps must be controlled. The deflagration limit of 30 g-moles translates into a deflagration limit of ~ 300 g DT. Regeneration will be scheduled frequently

enough to stay well below this limit.

The control of plasma energy, magnet energy, loss of vacuum events, and potential cryogen/water interactions has not yet been analyzed. As the design matures, this examination will continue such that confinement is adequately ensured in FIRE.

In summary, all of the major subsystems for FIRE have been addressed to a level that provides confidence that the mission requirements can be achieved. Several design improvements have been incorporated to produce greater physics flexibility or resolve engineering issues. First round cost estimates have been completed and are being reviewed to determine design changes which can reduce costs.

6.16 Bucked and Wedged TF Coil Design Option

Preliminary studies indicate that an alternative configuration employing combined bucking and wedging for the TF coils would reduce stresses and allow them to be made entirely of OFHC copper. If these results are confirmed, this configuration offers a number of very significant advantages:

- The lower TF system resistance will the TF power requirements from 490 MW for a 10T, 20 s pulse to 267 MW. This, in turn, will greatly reduce capital equipment costs and operating costs in the power subsystem (one of the major cost subsystems) and cryogenic

subsystem. The lowered peak power demands will also broaden the number of potential sites for FIRE.

- The higher conductivity of the OFHC copper will significantly reduce the TF temperature rise and thermal stress excursions at the currently planned FIRE pulse durations. Alternatively, the temperature margin could be used for ~ 2 times longer pulses at a given field.

- Research and development costs will be reduced, since it will not be necessary to develop OFHC-BeCu joining processes.

- TF coil manufacturing costs may be less since OFHC copper is much less costly to procure and process than BeCu.

On the negative side, the bucked and wedged configuration will probably require the peak field to be limited to 11.5 T and the CS/TF assembly will be more difficult to manufacture and assemble due to the need to maintain precise fit up tolerances to achieve the proper balance between wedging and bucking. The benefits are expected to outweigh the negatives; consequently, more in-depth studies are planned to permit a complete evaluation.